IMPINGEMENT AIR COOLED PLATE FIN HEAT SINKS

ZHIPENG DUAN

NOTE TO USERS

Your file Votre référence
ISBN: 0-612-93024-6
Our file Notre référence
ISBN: 0-612-93024-6

Impingement Air Cooled Plate Fin Heat Sinks

by

© Zhipeng Duan

A thesis submitted to the
School of Graduate Studies
in partial fulfillment of the
requirements for the degree of
Master of Engineering

Faculty of Engineering and Applied Science
Memorial University of Newfoundland

September 2003

St. John's Newfoundland

Abstract

The performance of impingement air cooled plate fin heat sinks differs significantly from that of parallel flow plate fin heat sinks. The present work addresses impingement air cooled plate fin heat sinks for electronic components. Simple impingement flow pressure drop and thermal resistance models based on developing laminar flow in rectangular channels are proposed. Both models are constituted from simple momentum and energy balances and utilize fundamental solutions from heat transfer and fluid dynamics to predict their constitutive components. To test the validity of the models' predictions, experimental measurements of pressure drop and thermal resistance are performed with heat sinks of various impingement inlet widths, fin spacings, fin heights and flow velocities. The models are expected to achieve accuracies within 20% for pressure drop and within 20% for thermal resistance at channel Reynolds numbers less than 1200. The simple models are suitable for impingement air cooled heat sink parametric design studies.

Acknowledgments

I would like to express my appreciation to my supervisor Dr. Yuri Muzychka for his enthusiastic guidance and support of this work. He has opened my eyes to the art of heat transfer and fluid dynamics through many enlightening discussions. He nucleated my interests in electronic cooling and provided many useful insights over the duration of my exciting graduate research. The experience of working with him has been more than rewarding.

I am also appreciative of the technical assistance in lab work provided by Craig Mitchell. I could not complete the experimental measurements without his support.

I would also like to thank Dr. Kelly Hawboldt and Dr. Neil Hooky who reviewed this thesis, and did it in a short period. Their feedback helped me in improving the quality of the thesis.

Table of Contents

List of Tables

List of Figures

Nomenclature

A_b	base plate area, m^2
A_c	cross-section area, m^2
A_{duct}	plenum chamber area, m^2
A_{inlet}	heat sink impingement inlet area, m^2
A_{outlet}	heat sink outlet area, m^2
A_s	heat source area, m^2
b	fin spacing, m
c_p	specific heat of air, J/kg K
D_h	hydraulic diameter, m
f, f_{app}	friction factor and apparent friction factor, respectively
h	heat transfer coefficient , W/m^2 K
h_c	contact conductance, W/m^2 K
h_{eff}	effective heat transfer coefficient , W/m^2 K
h_l	head loss, m
H	fin height, m
I	current, A
j	Colburn facter, = $St\ Pr^{2/3}$
k	thermal conductivity of heat sink, W/m K
k_a	thermal conductivity of air, W/m K
K	pressure loss coefficient for impingement flow
K_c, K_e	contraction and expansion loss coefficient, respectively
K_{90}	loss coefficient due to 90° bend in air flow
L	length of heat sink base, m
L^*	dimensionless fin length
L_{eff}	effective length

L_s	length of heat source, m
m	fin parameter $\approx (hP/kA_c)^{1/2}$, 1/m
N_f	number of fins
Nu	Nusselt number, $= hD_h/k_f$
P	perimeter, m
P_{inlet}	static pressure of heat sink impingement inlet, Pa
P_{outlet}	static pressure of heat sink outlet, Pa
ΔP	pressure drop, Pa
Pr	Prandtl number
Q	total electrical power input, W
Q	air volume flow rate, m^3/s
Q_{loss}	ambient heat loss, W
R	thermal resistance, K/W
R_{1D}	one-dimensional thermal resistance, K/W
R_{bare}	prime surface thermal resistance, K/W
R_{base}	conduction thermal resistance of heat sink base, K/W
R_{eff}	heat sink effective thermal resistance, K/W
R_{fins}	fin surface thermal resistance, K/W
R_{rad}	radiation thermal resistance, K/W
R_{sink}	overall heat sink thermal resistance, K/W
R_{sp}	spreading thermal resistance, K/W
R_{total}	total thermal resistance, K/W
Re_b*	modified channel Reynolds number $= (bV_{ch}/v)(b/L)$
Re_{Dh}	channel Reynolds number, $= D_h V_{ch}/ v$
s	impingement inlet width, m
St	Stanton number, $= Nu/(Re\ Pr)$
t	fin thickness, m
t_b	base plate thickness, m
T	temperature, °C

T_s	heat source temperature, K
T_{amb}	ambient temperature, K
$\bar{T}_{source}$	mean heat source temperature, K
$\bar{T}_{base}$	mean heat sink base temperature, K
U	voltage, V
V	velocity, m/s
V_{ch}	channel velocity, m/s
V_d	velocity in the plenum chamber, m/s
V_{inlet}	heat sink impingement inlet velocity, m/s
V_{outlet}	heat sink outlet velocity, m/s
V_{loss}	flow rate leakage loss, m^3/s
W	width of heat sink base, m
W_s	width of heat source, m
x_f	flow development length
x_t	thermal development length

Greek symbols

$\beta_{m,n}$	eigenvalues, $=(\delta_m^2+\lambda_n^2)^{1/2}$
δ_m	eigenvalues, $=m\pi/c$
ε	emission coefficient
ε	heat exchanger effectiveness
ζ	dummy variable, m^{-1}
η	fin efficiency, $= \tanh(mH)/(mH)$
λ_n	eigenvalues, $= n\pi/d$
μ	dynamic viscosity of air, Ns/m^2
ν	kinematic viscosity, m^2/s
ρ	density, kg/m^3
σ	Stefan-Boltzman number, $W/m^2 K^4$
σ	fraction of frontal free flow area

ϕ	spreading function

Subscripts

1	based upon vertical channel
2	based upon horizontal channel
amb	ambient
app	apparent
b	base
D_h	based upon hydraulic diameter
eff	effective
f	fin
fd	fully developed
s	heat source

Chapter 1

Introduction

1.1 Motivation

With advances in the performance of modern computers, the electric power dissipated in electronic devices is increasing. Furthermore, the structure of these computers is becoming ever more compact. These trends lead to difficulties in heat dissipation from these electronic devices and in the design of air-flow cooling systems for the computers. Impingement air cooling with heat sinks is one attractive solution to these problems. Figure 1.1 shows the impingement air cooled heat sink found in portable computer.

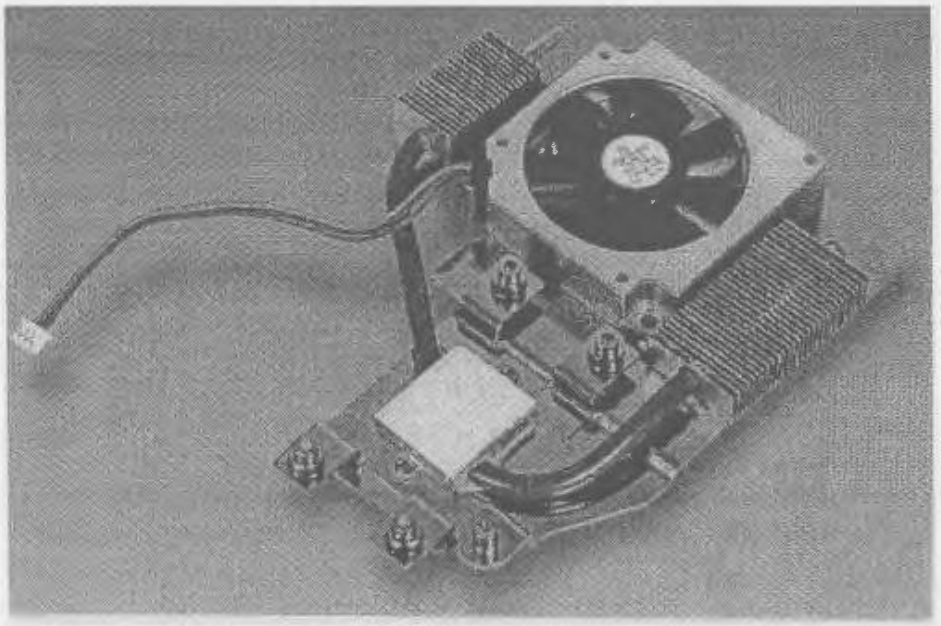

Figure 1.1 Impingement air cooled heat sink system for a portable computer.

The primary motivation stems from the needs of the computer industry to cool compact, high power electrical components. An incessant drive towards increased processor performance has produced burgeoning power densities. For example, the Pentium IV 2.0 GHz (478 pins, 0.17 μm technology) dissipates 75.3 W (Intel, 2001). Furthermore, the power dissipation of these CPUs is expected to increase, approaching 100 W in the near future. A great deal of industry effort has gone into preparing advanced technologies providing the requisite high heat transfer rates. While much attention has been devoted to exotic techniques such as liquid immersion and multi-phase cooling owing to high effective heat transfer coefficients, air cooled heat sinks operating under modest pressure drops can readily achieve impressive heat transfer rates from the surface of a processor module substrate.

Despite relatively poor thermal conductivity and heat capacity when compared to liquids, air has economic advantages as a coolant for computer systems. From a practical standpoint, a limitless supply of ambient air is available from the surroundings; there are no coolant material costs; the cost of transporting air is low; and the use of air in an open loop system is environmentally safe. Furthermore, for most systems, air is the ultimate thermodynamic reservoir to which heat will be rejected, accordingly, heat dissipation into air is a feature of most electronic cooling systems, and its direct use in heat removal from the chip or package can greatly simplify the thermal management system.

Parallel plate heat sinks are commonly used today and also rank among the most promising types of heat sinks for future high performance air cooling. Aluminum heat sinks with small axial fans mounted on them are usually used to dissipate the processor module generated heat. Rapid development in packaging technology allows portable electronics to gain faster processing speed and enhanced capabilities, however, thermal management in the portable electronics environment is becoming increasingly difficult due to high heat load and dimensional constraints. Further, the major thermal resistance in the thermal circuit for cooling processor modules is the heat sink resistance. It is important to understand the thermal and hydraulic behaviour of heat sinks. The present work concentrates on the impingement flow plate fin heat sink geometry, shown schematically in Figure 1.2.

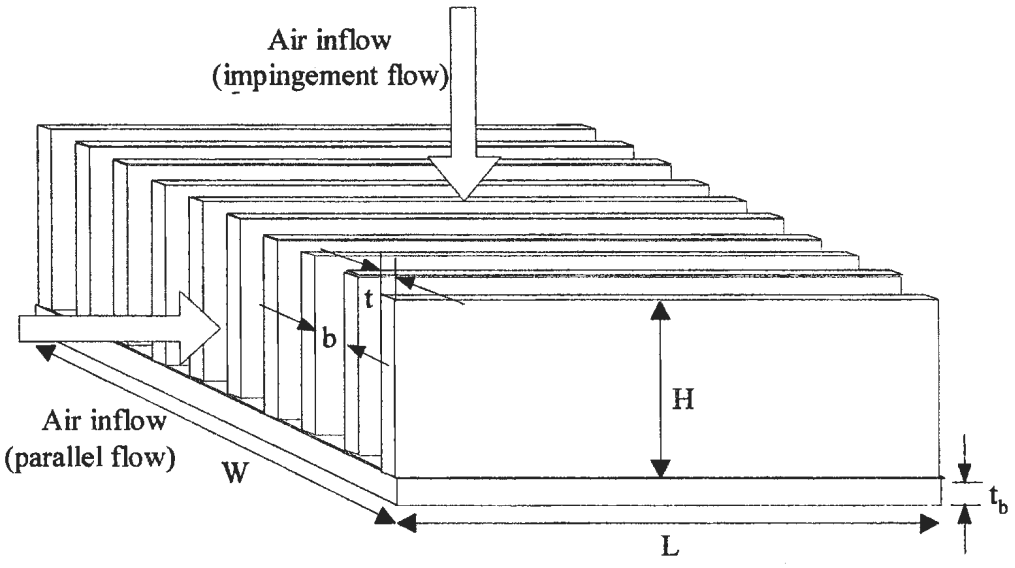

Figure 1.2 Schematic of a plate fin heat sink.

Nottage (1945) suggested that the heat sink fin and channel may be thought of as a type of heat exchanger in which the hot fluid stream is replaced with the solid fin. One of the goals in the field of heat exchangers is to determine the overall effectiveness of heat transfer, by comparing the actual rate of heat transfer to the maximum thermodynamically possible rate of heat transfer. The flowstream direction relative to heat flow direction plays a significant role in determining the heat transfer effectiveness of a fin-fluid arrangement. Three basic one dimensional heat exchanger flow arrangements of counter-flow, cross-flow and parallel-flow are shown in Figure 1.3.

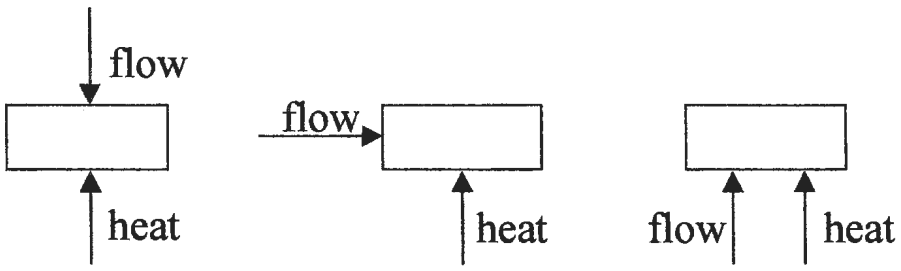

Figure 1.3 One dimensional flow arrangements for a rectangular fin.

In the field of compact heat exchanger design, Kays and London (1984) have developed a comprehensive design procedure. They parameterized heat transfer performance using effectiveness, defined as $\varepsilon = q_{actual}/q_{max}$, and a dimensionless number of heat transfer units, NTU, based on the heat exchanger area, overall conductance, and heat transfer rate capacity. Figure 1.4 shows the effect of flow arrangement on effectiveness as a function of the number of transfer units. The plots are for the case in which the hot and cold fluids

have equal heat transfer capacity rates ($C_{min}/C_{max}=1$). This case illustrates the maximum difference in performance due to relative fluid flow direction when all other parameters are equal.

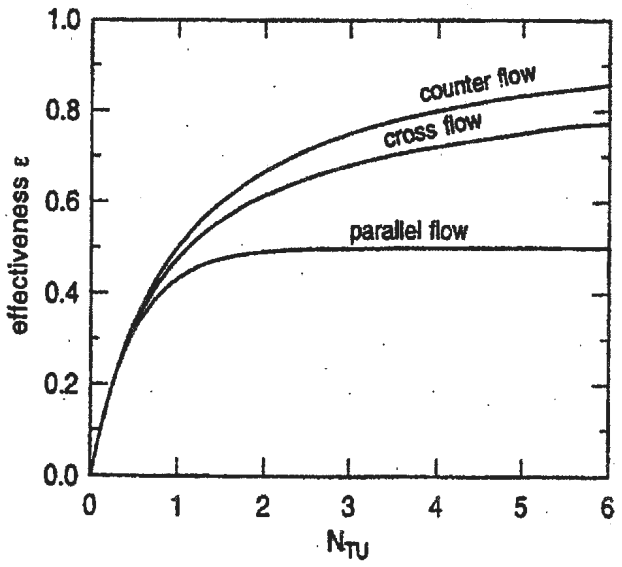

Figure 1.4 Effect of fluid flow direction on heat exchanger effectiveness (Kays and London, 1984).

The counterflow arrangement has greatest potential to achieve high effectiveness, followed by cross-flow. Both of these exhibit $\varepsilon \rightarrow 1$ as NTU$\rightarrow\infty$. The parallel-flow arrangement has the lowest effectiveness. From an implementation standpoint in electronics cooling, this would require an airflow direction normal to the heat sink base, however, heat sinks with air flow directed normal to the base have received little attention. Since the impingement air flow pattern in a heat sink is intermediate between counterflow and crossflow, its thermal performance is expected to exceed that of a purely

crossflow heat sink. This implicit advantage in thermal performance provided the impetus for developing an impingement air cooled heat sink for the present multichip module cooling application.

1.2 Heat Dissipation Problem

The primary function of a heat sink is to reject heat through a finite temperature difference. The performance of a heat sink is frequently specified by the thermal resistance: defined as the temperature difference between the heat sink base and the ambient air, resulting from a given heat dissipation and measured in units K/W. The objective of heat sink thermal design is to minimize the thermal resistance. The major thermal resistance in the thermal circuit for cooling electronic devices is the heat sink resistance, therefore, the thermal-hydraulic behavior of heat sinks must be understood.

A heat sink design must take into account the environmental temperature extremes, and the allowable chip or transistor junction temperatures for the semiconductor technology. The ambient air reservoir temperature of office and computer room environments is typically 21 to 24 °C, with worst case extremes of 32 to 40 °C. Typical junction temperature limits are 85 to 100 °C, therefore, the allowable chip temperature excursion above ambient is limited to 60 °C

A heat sink is characterized by the pressure drop and heat transfer for a given flow rate. Modelling a heat sink involves identifying appropriate equations to predict the air heat transfer coefficient and friction factor. The airflow configuration can be either parallel to the base or impingement, see Figure 1.2. Heat sink models typically assume a uniform airflow at the heat sink inlet. The flow in typical plate fin heat sinks used in cooling processor modules is laminar, because of the small fin spacing and low air flow rates produced by the attached axial fans. It should be noted that for the type of heat sink under investigation here, there is no concern with flow bypass since all heat sinks are assumed to be ducted or shrouded.

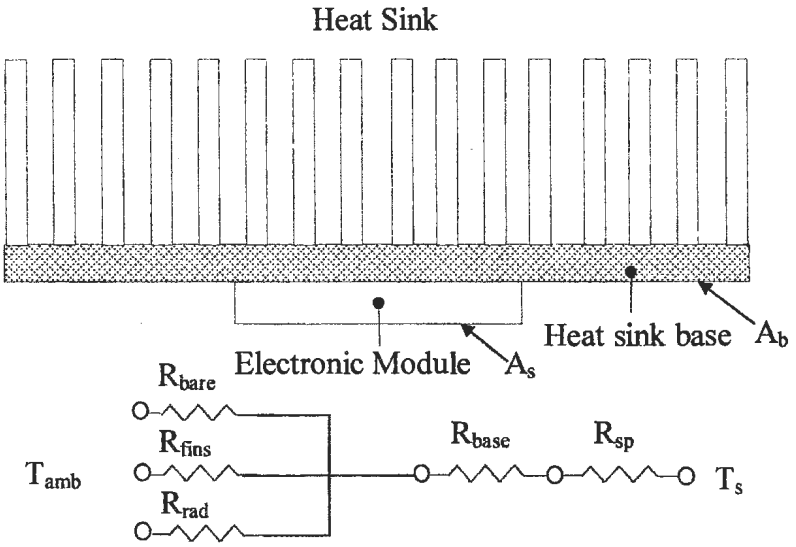

Figure 1.5 Thermal resistance circuit.

Heat generated from a processor module can be approximated as constant heat flux over area A_s. The thermal resistance network for heat flow from the processor module surface temperature (T_s) to ambient temperature (T_{amb}) is depicted in Figure 1.5. The processor module surface area (A_s) is usually too small to dissipate the required heat, so a heat sink is typically required. A heat sink is attached to the processor module surface (the heat source). Since heat sink base area (A_b) is usually larger than A_s, heat spreads from A_s to A_b in the heat sink base. Spreading thermal resistance (R_{sp}) occurs when heat leaves a heat source of finite dimensions (A_s) and enters into a larger region (A_b). Heat flux is assumed uniform over the base of fins. Heat is conducted from the base to the tip of the fins and it is convected from the fin surface (R_{fins}), and heat is convected from the prime surface (the exposed portion of the base) (R_{bare}). The fin conduction resistance must account for the fin efficiency. The thermal resistance from the fins and prime surface to the ambient air is the total convection resistance of heat sink. The heat sink total convection resistance is usually the dominant thermal resistance in the thermal circuit for the cooling processor module, therefore, the present work concentrats on understanding this component.

1.3 Space and Noise Constraints

The heat removal from a processor module can not be treated as an isolated design problem. The thermal solution is constrained to space and noise limits. The movement of air through restricted duct spaces gives rise to significant dynamic and frictional losses in pressure, therefore, it is desirable to keep the heat sink flow rate down to the minimum

necessary for thermal performance in order to reduce pressure losses. Heat sink design with high pressure requirements will increase costs.

The acoustical noise level is of crucial importance in the design of computer. In many microcomputer systems the fans and blowers used to move air are the dominant noise sources. Heat sink design affects the acoustic output of the turbomachines used to cool it.

A high performance heat sink influences the package acoustic level most directly by its requirements for volumetric flow and static pressure differential. The hydraulic load of the heat sink is normally met by some type of turbomachine device located within the system. This device may be an axial fan or centrifugal blower, and it may act singly or in multiples using parallel and series arrangements. The actual noise is generated by mechanisms which take place within the turbomachine, but the noise level at the air moving device is commensurate with the hydraulic loading requirements of the heat sink. Other acoustic factors might add to the overall system noise level, however, under the majority of circumstances, only the hydraulic loading added by the heat sink is important.

Space limits may vary based on computer chassis size. The channel width of the inter-fin gaps is limited by fabrication constraints, for example, an aluminum extrusion process may be limited to a maximum height/channel width ratio. The fin height may be limited by packaging layout space requirements or fabrication constraints.

1.4 Objectives

The generic problem in thermal management of computers is to find increasingly better cooling solutions. The present work is focused on the impingement flow plate fin geometry. The research objectives are to develop robust models for predicting thermal resistance and pressure drop of plate fin heat sinks for impingement air cooling. To test the validity of the model, experimental measurements of pressure drop and thermal resistance are performed with heat sinks of various dimensions and flow velocities.

1.5 Outline of the Thesis

This chapter presents an introduction to the problem investigated. Chapter 2 presents a comprehensive literature review on impingement flow in plate fin heat sinks. A brief review of parallel flow plate fin heat sinks, spreading resistance and optimization of heat sinks is also given. Chapter 3 presents an analytic pressure drop model and an analytic heat transfer model. Chapter 4 describes the experimental apparatus and procedures for obtaining experimental data on heat sinks. The uncertainty analysis is also discussed. Chapter 5 presents the results of the experiments and provides comparisons with analytical model predictions. Chapter 6 summarizes the important findings of the present work. Detailed experimental data are given in Appendix A.

Chapter 2

Literature Review

This chapter presents a brief review of parallel flow plate fin heat sink studies, spreading resistance, optimization of heat sinks, and a literature review on impingement flow plate fin heat sink studies.

2.1 Parallel Plate Heat Sink

A parallel plate heat sink consists of closely spaced, parallel, thin rectangular plates, as shown in Figure 2.1. Air cooled parallel plate heat sinks have been widely applied and are the subject of much study, because they combine some fundamental advantages: high convective heat transfer coefficients, large fin area in a compact layout, low pressure drop and ease of fabrication. In comparison with the other simple internal duct geometries, parallel plates are thought to offer the best combination of high heat transfer and low pressure drop for high performance heat sinks.

The channel surface-to-fluid convection rate is a limiting factor in the heat transfer performance of a heat sink. For fully developed (thermal and hydraulic boundary layers) laminar flows, the Nusselt number and friction factor have been established for a variety of internal duct shapes. The Nu and fRe values for these configurations are based on the

hydraulic diameter of the flow passage, D_h=4A/P, in which A is the cross-sectional flow area and P is the wetted perimeter. The heat transfer coefficient for a given geometry scales inversely with hydraulic diameter:

$$h = \frac{Nu \cdot k}{D_h} \tag{2.1}$$

where the Nusselt number is based on the hydraulic diameter D_h. The pressure drop for a given duct geometry varies proportionally with mean velocity V and duct length L in the direction of the flow, and inversely with the square of the hydraulic diameter D_h:

$$\Delta P = 4f \frac{L}{D_h} \frac{1}{2} \rho V^2 = \frac{2\mu (fRe) LV}{D_h^2} \tag{2.2}$$

For a given duct shape and fully developed laminar flow, fRe is a constant, where Re is based on hydraulic diameter.

For the shapes considered, the highest thermal transfer that can be obtained for a given pressure drop is that of infinite parallel plates (Incropera, 1996). In practice, due to the presence of a base and fin tip shroud ducting, implementations of parallel plate heat sinks more closely resemble high aspect rectangular channels, which rank a close second in heat transfer and pressure performance.

A variety of flow arrangements are possible with a generic parallel plate heat sink attached to a processor module. Two flow arrangements: parallel flow and impingement flow will be discussed.

2.2 Parallel Flow

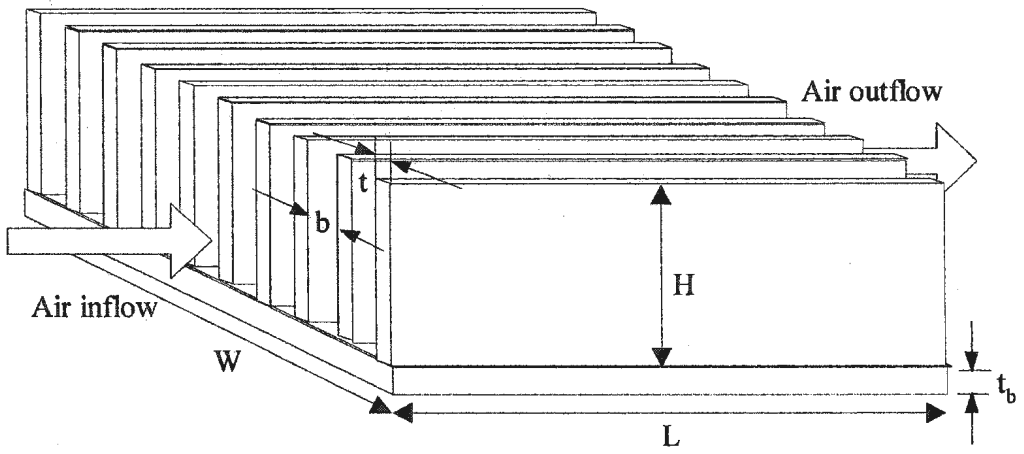

Figure 2.1 Geometry of a plate fin heat sink in parallel flow.

A plate fin heat sink in parallel flow is shown schematically in Figure 2.1. Heat sinks in which the flow enters one end, flows transversely through the channels, and exits through the opposite end, are termed "SISE", for *side inlet side exit*. This flow arrangement is probably the most common for plate fin heat sinks. Parallel flow modeling in a plate fin heat sink is essentially a simultaneously developing hydraulic and thermal boundary layer problem in a rectangular duct. The flow may become fully developed if the heat sink is sufficiently long in the flow direction or with small fin spacing, however, this is very unlikely for electronic cooling heat sinks. The friction factor and Nusselt number in rectangular channels depends on the aspect ratio (b/H) of the channel, Reynolds number (Re) and hydrodynamic and thermal entrance lengths.

Beavers et al. (1970) performed a comprehensive experimental investigation of laminar flow development in rectangular ducts, encompassing the range of cross section aspect ratios from 1:1 to 51:1 (i.e. near approximation to a parallel plate channel). The Reynolds numbers of the experiments ranged from 400 to 3000.

Shah and London (1978) present numerical solutions from various researchers for rectangular ducts and show that the effect of aspect ratio is more prominent on Nusselt number than on friction factor.

The microchannel heat sink, as first proposed by Tuckerman and Pease (1981), was seen as a means of cooling integrated circuits using water as the coolant. The convective heat transfer coefficient h between the substrate and the coolant was found to be the primary impediment to achieving low thermal resistance. For laminar flow in confined channels, h scales inversely with channel width, making microscopic channels desirable. The use of high-aspect ratio channels to increase surface area will further reduce thermal resistance. Based on these considerations, a new, very compact, water-cooled integral heat sink for silicon integrated circuits has been designed and tested. Accepting a coolant temperature rise of 71 °C, a heat flux of 790 W/cm^2 could be dissipated.

Ashiwake et al. (1983) used channel-averaged heat transfer coefficients in conjunction with fin efficiencies to model transverse air cooled heat sinks.

Narrow channel forced air heat sinks have also been designed, built, and tested (Goldberg, 1984). Each heat sink had a different fin thickness but the b/t ratio was kept at unity. The air flow for each heat sink was adjusted to provide a rate of 30 liters/minute. As expected, the design with largest pressure drop and smallest channel width yielded the smallest thermal resistance.

Googman (1993) reviewed some works published on microchannel heat exchangers using both air and liquid in laminar and turbulent flows. The majority of these studies are limited to the assumption of one dimensional transverse flow direction.

Biber and Belady (1997) compared previously published fully developed, developing flow friction factor correlations, and Computational Fluid Dynamics (CFD) results with experiments on five heat sinks. The test heat sink was placed in a duct with small gaps on three sides which are equivalent to the fin spacing. They found that the fully developed prediction methods give results within 7% of the experimental data. The developing flow correlation, however, is nearly 50% over the test data, therefore, they suggested correlations specially for heat sinks should be developed. The test data is doubtful, however, since flow in heat sinks is not fully developed.

Linton and Agonafer (1995) conducted CFD studies of a plate fin heat sink using a coarse and a fine grid. The fine grid showed better match to test data than the coarse grid.

Sasao et al. (1997) numerically investigated flow and heat transfer for plate fin heat sinks in parallel flow configurations. In this model, all the fins of an individual heat sink were replaced with a single uniform element having the appropriate flow resistance and thermal conductivity. The convective heat transfer coefficient between the air and the elements was calculated as for the heat transfer in a rectangular duct. Calculations and experiments were carried out with different heat sinks. The estimated error was found to be within ±15 % for the total pressure drop, and within ±20% for the heat sink temperature, as compared to the experimental results.

Loh et al. (2002) conducted thermal tests on eight heat sinks and obtained an optimization point. In addition, the experimental results were compared with a theoretical pressure drop model developed by Copeland (2000) and a thermal model by Teerstra et al. (1999). The chosen thermal model predicted the heat sink thermal resistance to an average error of 6-10 %.

Culham and Muzychka (2001) proposed a heat sink model in parallel flow using the apparent friction factor model developed by Muzychka and Yovanovich (1998) and the heat transfer model developed by Teertstra et al. (1999). The friction model is asymptotic between developing and fully developed flow. The friction factor correlation is for developing laminar flow.

$$f_{app}Re = \left[\left(\frac{3.44}{\sqrt{L^*}}\right)^2 + \left(fRe_{D_h}\right)^2\right]^{1/2} \tag{2.3}$$

where

$$L^* = \frac{L}{D_h Re_{D_h}} \tag{2.4}$$

and fRe_{D_h} is for fully developed flow friction factor Reynolds number group and depends on b/H only for laminar flow. A polynomial form is suggested for fRe_{D_h} by Shah and London (1978),

$$fRe_{D_h} = 24 - 35.527\left(\frac{b}{H}\right) + 46.721\left(\frac{b}{H}\right)^2 - 40.829\left(\frac{b}{H}\right)^3 + 22.954\left(\frac{b}{H}\right)^4 - 6.089\left(\frac{b}{H}\right)^5 \tag{2.5}$$

Muzychka and Yovanovich (1998) validated the model with most of the developing flow data and found the estimation error was within ±12 % for a wide range of duct shapes but within ±3 % for the rectangular channel.

The inlet and exit loss coefficient (K_c and K_e) which are functions of the degree of contraction and expansion of the flow (σ) were computed using the simple expressions for a sudden contraction and a sudden expansion from White (1986).

$$K_c = 0.42\left(1 - \sigma^2\right) \tag{2.6}$$

$$K_e = \left(1 - \sigma^2\right)^2 \tag{2.7}$$

where

$$\sigma = 1 - \frac{N_f \cdot t}{W} \tag{2.8}$$

The heat transfer coefficient, h, is computed using the model proposed by Teertstra et al. (1999), and the Nusselt number is a function of the heat sink geometry and fluid velocity.

$$Nu_b = \frac{\tanh\sqrt{2Nu_i \frac{k_a}{k}\frac{H}{b}\frac{H}{t}\left(\frac{t}{L}+1\right)}}{\sqrt{2Nu_i \frac{k_a}{k}\frac{H}{b}\frac{H}{t}\left(\frac{t}{L}+1\right)}} Nu_i \tag{2.9}$$

where

$$Nu_i = \left[\left(\frac{Re_b Pr}{2}\right)^{-3} + \left(0.664\sqrt{Re_b^*}\,Pr^{1/3}\sqrt{1+\frac{3.65}{\sqrt{Re_b^*}}}\right)^{-3}\right]^{-1/3} \tag{2.10}$$

$$Nu_b = h \cdot b / k_a \tag{2.11}$$

$$Re_b^* = Re_b \cdot (b/L) \tag{2.12}$$

The model is asymptotic between two limiting cases - fully developed and developing flow in parallel plate channels. Teertstra et al. (1999) validated the model with experiments and found 2.1% RMS error and 6% maximum error.

Copeland (2000) suggested using laminar flow pressure drop and heat transfer models for parallel flow in isothermal rectangular channels (b/H) to model the heat sink in Figure 2.1. The friction factor data for developing laminar flow was taken from Shah and London (1978) and fitted to an equation of the Churchill-Usagi form:

$$f_{app}Re = \left[\left(\frac{3.2}{(L^*)^{0.57}}\right) + \left(fRe_{D_h}\right)^2\right]^{1/2} \tag{2.13}$$

The model is asymptotic between developing and fully developed flow and similar to the Culham and Muzychka (2001) model described above, however, near the inlet of any non-circular duct, the leading term should be $3.44(L^*)^{(-0.5)}$, Muzychka (1999). The Nusselt

number data was also taken from Shah and London (1978) and fitted to an equation of the same form

$$Nu = \left\{ \left[2.22 \left(\frac{L^*}{Pr} \right)^{-0.33} \right]^3 + \left(Nu_{fd} \right)^3 \right\}^{1/3} \tag{2.14}$$

in which fRe_{D_h} and Nu_{fd} are solutions for fully developed flow and the following relations were used

$$fRe_{D_h} = 19.64G + 4.7 \tag{2.15}$$

$$Nu_{fd} = 8.31G - 0.02 \tag{2.16}$$

in which G is a function of the channel aspect ratio

$$G = \frac{1 + \left(\frac{b}{H} \right)^2}{\left(1 + \frac{b}{H} \right)} \tag{2.17}$$

Data for pressure loss was taken from Kays and London (1984). The inlet and exit loss coefficients (K_c and K_e) are fitted to

$$K_c = 0.8 - 0.4\sigma^2 \tag{2.18}$$

$$K_e = (1 - \sigma)^2 - 0.4\sigma \tag{2.19}$$

It is noted that the heat transfer model is for an isothermal boundary condition and must be further modified by a fin efficiency correction. The friction factor and heat transfer models were not validated experimentally by Copeland (2000).

2.3 Impingement Flow

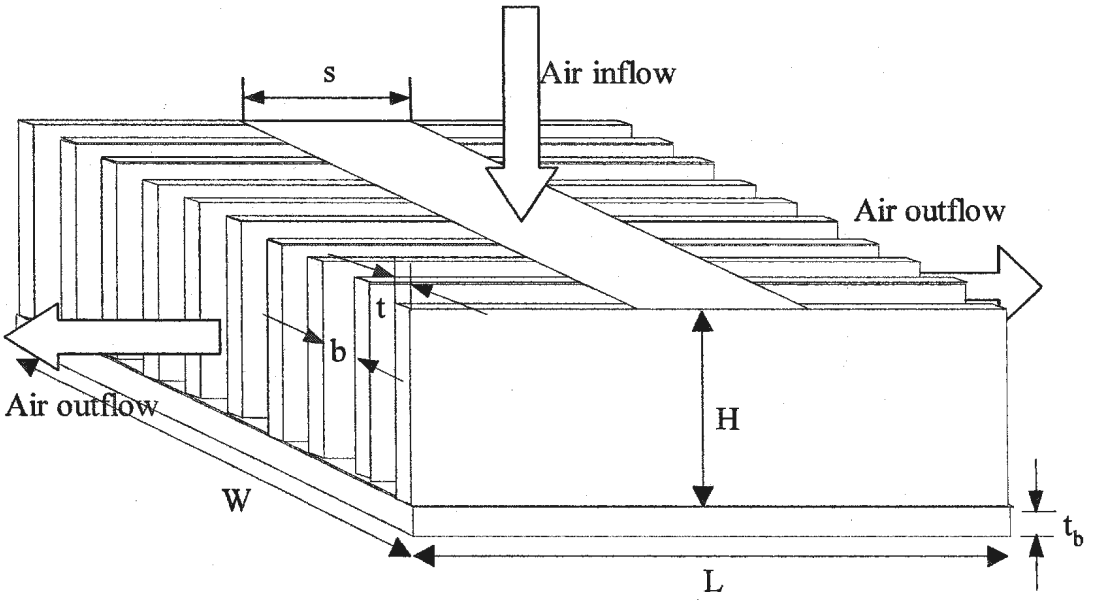

Figure 2.2 Geometry of a plate fin heat sink in impingement flow.

The geometry of a heat sink in impingement flow is shown schematically in Figure 2.2. In this flow arrangement the air enters at the top and exits out the sides, i.e. TISE (*top inlet side exit*). The physics of impingement flow in a plate fin heat sink is as follows: flow enters through a finite area (sW) and impinges on the heat sink base, turns, and flows along the rectangular channels formed by the base of the heat sink and the plate fin sidewalls. One boundary layer develops along the heat sink walls (plate fin surfaces), and another boundary layer develops along the base of the heat sink. These boundary layers will interact close to where base and sidewalls meet. A simple two-dimensional

stagnation flow can be analyzed easily; the results of an exact numerical solution can be found in Schlichting (1979). The present case is three dimensional, however, due to the presence of the sidewalls. Only the center plane of the channel, owing to the symmetry in geometry and flow, is two-dimensional.

Although there has been a wide range of research reporting on impingement air cooling, there have been few studies specifically on impingement cooling with heat sinks.

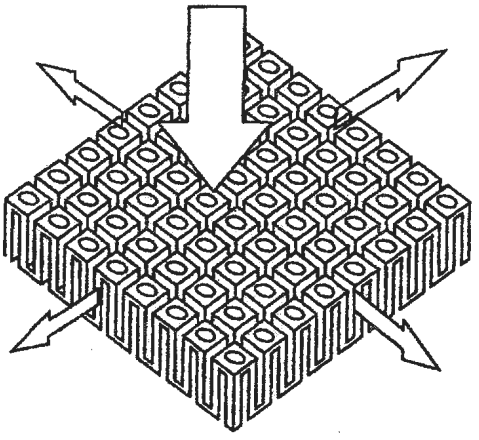

Figure 2.3 Serpentine pattern impingement flow heat sink (Biskeborn et al., 1984).

Biskeborn et al. (1984) reported experimental results for a TISE design using unique "serpentine" square pin fins, shown in Figure 2.3, designed to accommodate a thermal expansion mismatch between the aluminum sink and the ceramic cap. This design was implemented in the IBM 4381 processor, which cooled up to 22 modules in parallel on a single board using individual inlet nozzles. With this device, and the planar impingement jet, an external thermal resistance of less than 8 °C/W was achieved.

Sparrow et al. (1985) performed heat transfer experiments on (an isothermal) TISE type single channel passage, pictured in Figure 2.4, and showed that the average heat transfer coefficient increased by about 40% in response to a halving of the interwall spacing for the unshrouded passage. Shrouding of half the inlet produced 25-40% higher heat transfer coefficients and a 150% higher pressure drop at higher Reynolds number, and side shrouding of half the exit passage produced 10-15% higher heat transfer coefficients at low Reynolds numbers and a 70% higher pressure drop than the unshrouded passage. The objective of the shrounding was to encourage the flow to penetrate into the downstream portion of the passage and, thereby, to promote the streamwise uniformity of the local heat transfer coefficient.

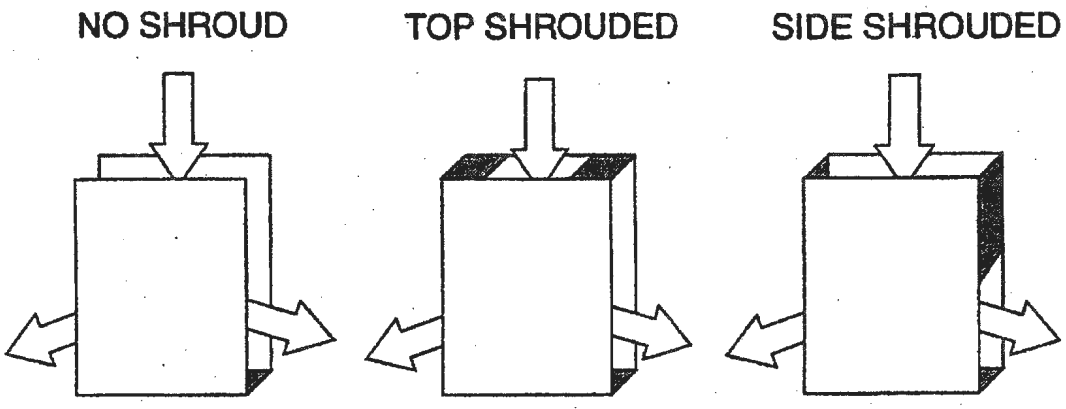

Figure 2.4 Impingement flow passage configuration (Sparrow et al., 1985).

Jet impingement cooling has also been studied in use with a 3.1 cm square 0.15 cm thick silicon heat sink (Mahalingham and Andrew, 1987). They considered an air flow rate of 2 ft^3/min and a maximum available junction to ambient temperature difference of 60 °C.

The lowest thermal resistance was found to be 1 °C/W for the impingement type assembly.

A novel laminar-flow heat sink with two sets of triangular or trapezoidal shaped fins on the two inclined faces of a base has been reported by Hilbert et al. (1990), as shown in Figure 2.5. Although air flow is directed from above towards the base of the heat sink, the incoming air divides into two streams which flow between the two sets of fins in a direction that is transverse to the direction of heat transport in the fins. The design is, therefore, akin to two separated transverse flow heat sinks on each of the inclined faces of the base, however, this design is more efficient because the downward flow at the inlet increases the air speed near the base of the fins where the fin temperatures are highest. Furthermore, by dividing the total surface area among two sets of fins, the length of the fins in the flow direction is reduced so that frictional pressure drop is decreased while the heat transfer coefficient is increased. The heat sink, which had a volume of less than 1 cm^3, showed a thermal resistance of less than 1.7 °C/W at an air-flow rate of 2 ft^3/min, with a pressure drop of 750 Pa. On the other hand, another design offered a similar thermal performance at a much reduced pressure drop of 50 Pa. Pressure requirements were reduced by sacrificing compactness. This design demonstrated the capability to remove in excess of 600 W from a multi-chip module with a quiet 10 W tube-axial fan. The volume of the complete module including the plenum and the fan is only about 1 l. The chips were held to a maximum temperature rise of 55 °C. This technology extends

the applicability of air cooling to power levels traditionally considered to lie in the domain of complex liquid cooled modules.

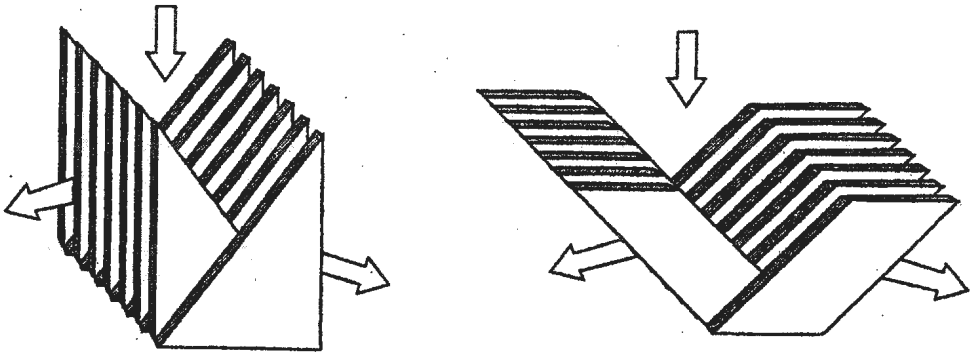

Figure 2.5 Fin designs employing impingement flow patterns (Hilbert et al., 1990).

Sathe et al. (1995) conducted a numerical and experimental study of a TISE parallel plate heat sink that was notched in the center to reduce flow stagnation, as shown in Figure 2.6. This high performance heat sink was designed to meet the stringent pressure drop and thermal performance criteria using a novel fin design. The design was achieved using numerical simulation of the conjugate fin-fluid problem under impingement condition. Factors leading to the high performance design were careful selection of fin and channel dimensions and a judicious removal of the central stagnation zone near the base of the heat sink using unique fin shapes. In the study, a rectangular jet impinges on a set of parallel fins and then turns into cross-flow. The effect of the fin thickness and gap, nozzle width and fin shape on the heat transfer and pressure drop were investigated. It was found that the pressure drop was reduced by cutting the fins in the central impingement zone without sacrificing the heat transfer, due to a reduction in the extent of the stagnant zone.

A combination of fin thickness of the order of 0.5 mm and channel gaps of 0.8 mm with appropriate central cut-out yielded heat transfer coefficients over 1500 W/m^2K at a pressure drop of less than 100 Pa.

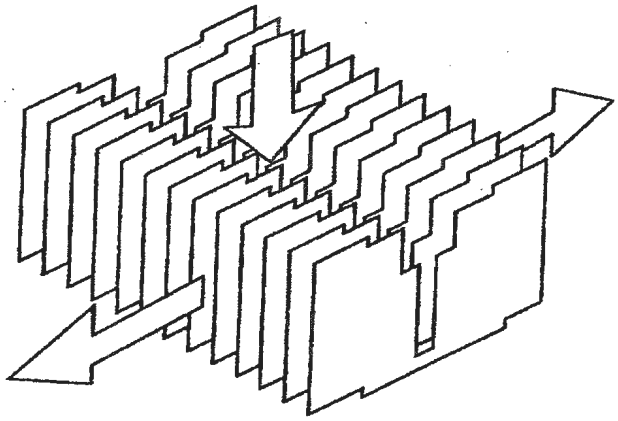

Figure 2.6 Center-notched heat sink design (Sathe et al., 1995).

In one of the few studies of microchannel heat sinks involving a non-transverse flow direction, Copeland (1995) performed theoretical, experimental and numerical analyses on a manifold microchannel heat sink having multiple top inlets alternated with top outlets, as shown in Figure 2.7. The design differs from a traditional microchannel heat sink in that the flow length is greatly reduced to a small fraction of the total length of the heat sink. Alternating inlet and outlet channels guide the coolant to and from the microchannels. At a given pumping power, increasing the number of inlet/outlet channels (a traditional microchannel heat sink has one channel) requires an increase in the volume

flow rate, but permits higher flow velocity, provides lower thermal resistance, and produces significantly lower pressure drops.

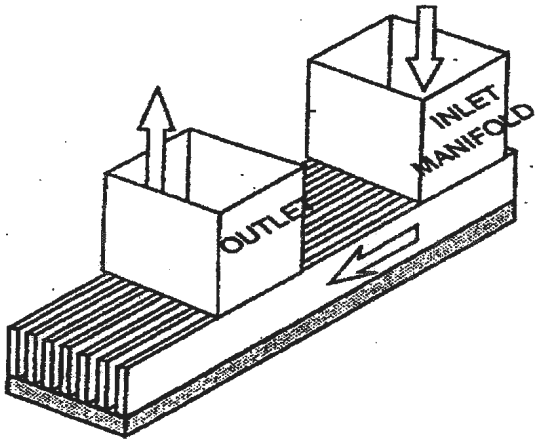

Figure 2.7 Manifold microchannel heat sink (Copeland, 1995).

A one dimensional model of air cooled parallel plate impingement heat sinks was developed to understand how the heat sink performance depends on the different geometry variables (Kang and Holahan, 1995), see Figure 2.8. The one dimensional model was used to develop an initial design for the heat sink and to develop expressions to correlate R and ΔP versus Q. The simplification introduced by assuming a pure counterflow with the heat sink is expected to lead to an overprediction of the heat transfer performance. The resulting equation for the thermal resistance is

$$R = \frac{H(b+t)}{ktWL} \cdot \left[\frac{\frac{e^{A}}{A} + \frac{e^{-B}}{B}}{e^{-A} - e^{B}} \right] \tag{2-20}$$

where,

$$A = \frac{hH}{2C} \cdot \left(\sqrt{\frac{4C^2}{hkt} + 1} - 1 \right) \tag{2.21}$$

$$B = \frac{hH}{2C} \cdot \left(\sqrt{\frac{4C^2}{hkt} + 1} + 1 \right) \tag{2.22}$$

$$C = \rho U c_p \cdot (b + t) \tag{2.23}$$

This pressure drop model has assumed a flow length of $H+L/2$ to estimate the frictional pressure drop. In the interest of simplicity, important details such as the effect of flow turning and the exit area being smaller or larger than the inlet area have been completely ignored. The resulting expression for pressure drop is

$$\Delta P = \frac{H + \frac{1}{2}L}{b^2} 12\mu U + 0.9 \frac{t}{b+t} \rho U^2 \tag{2.24}$$

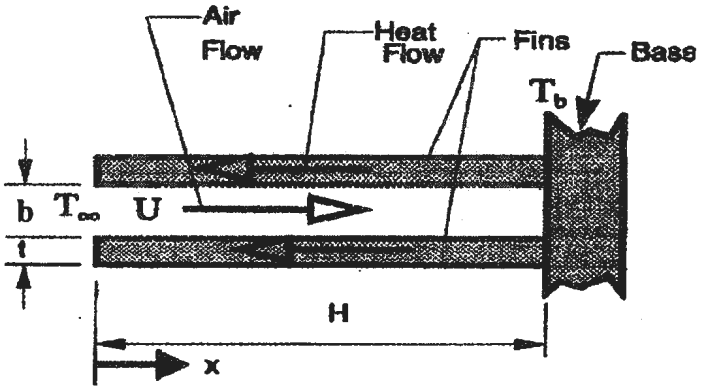

Figure 2.8 One dimensional model of a counterflow heat sink (Kang and Holahan, 1995).

These simple models are intended to provide only an order of magnitude estimate of the thermal resistance and pressure drop to aid in the identification of heat sink geometries. One further outcome of the analytical study was that the thermal resistance could be correlated well with the air flow rate in the form (R~C_1+C_2/Q) and the pressure drop could be correlated with the form (ΔP~C_3Q+C_4Q^2).

Holahan & Kang (1996) modeled the flow field in the channel between the fins as a Hele-Shaw flow. Conduction within the fin is modeled by superposition of a kernel function derived from the method of images. Convective heat transfer coefficients are adapted from existing parallel plate correlations. They described the following more accurate pressure drop model compared with the above one dimensional model:

$$\Delta P = \frac{1}{2}\rho(a\alpha L)^2\left[\left(\frac{b}{b+t}\right)\left(K_c + \frac{K_e}{\alpha^2}\right) + \left(0.64 + \frac{38\nu}{2a\alpha bL}\right)\right] + 6\mu a\left(\frac{L}{b}\right)^2\left(\alpha^2 + 1\right) \qquad (2.25)$$

where

$$a = \frac{Q}{bsW} \qquad (2.26)$$

$$\alpha = \frac{H}{L} \qquad (2.27)$$

Kondo et al. (1995) reported on a semi-empirical development of a pressure drop prediction for impingement cooling of heat sinks with plate fins. The flow region is divided into five parts. Values were predicted for pressure drops with plate fins for a variety of impingement inlet widths, gaps, fin heights, and the number of fins. These predictions agree with the experimental data within ±30%.

Later, Kondo et al. (1996) described an experimental study on the impingement cooling characteristics of heat sinks with plate fins of 0.2 mm thickness, which are spaced with a fin spacing in the range 0.5 mm to 2.0 mm. The air cooling of the heat sink comes from a slot-shaped orifice positioned above the heat sink center. The breadth of the gap between the fin tops and the inlet orifice is in the range 0 mm to 10 mm. The thermal resistance of the thin plate fins used is about 50% to 57% that of the thick plate fins now in commercial use. The cooling performance of the thin-plate fins is almost the same as that of optimally arranged pin-fins with the same total surface area. A maximum value of six times the heat transfer rate of a single flat plate having the same base area was observed for the thin-plate fins. A comparison of cooling performance between impingement and parallel flow systems was also conducted. The performance of the impingement cooled systems is almost unaffected by the height of the gap between the fin tops and the inlet orifice.

Furthermore, they completed another experimental study and reported a zonal model of a thermal resistance prediction for impingement cooling heat sinks with plate fins. The impingement flow over the plate fins was divided into six regions. The experiments were performed with a variety of different fins. To enhance impingement cooling, one long rectangular inlet orifice over the center of the heat sink was found to offer the best structure. The optimum orifice width is about 1/6 of the base width of the heat sink. The thermal resistance at a fixed volumetric flow rate and orifice width varies little with size of the gap between the fin tops and the inlet orifice. A set of correlations are proposed

between the thermal resistance of the heat sink and the geometry of the plate fins. The accuracy of the predicted thermal resistance was found to be within ±25% of the experimental data.

Finally, Kondo et al. (1998) summarized and modified the above semi-empirical models for impingement flow in plate fin heat sinks. This zonal model divides the total area into six air-cooling sections, and the flow region into five sections. Each section is modeled by different heat transfer models or pressure drop models. Dividing the heat sink into sections requires a large number of equations and makes the model very complicated. Experiments were performed to test the validity of the model. The thermal resistance was predicted within ± 25 % and the pressure drop within ± 20 % of the experimental data.

Aranyosi et al. (1997) conducted parametric studies and revealed the weight of individual variables in the design of micro channel and woven wire screen heat sinks. Five novel heat sinks are tested, each proven to be suitable for cooling of high-power electronics components. The results demonstrate that confined ducting of laminar or low-Reynolds-number turbulent flows through compact structures of the presented types, combined with central feeding of air, provides greatly improved thermal performance (up to removable base plate heat flux of about 20 W/cm^2) compared to conventional forced air cooling schemes, along with reasonable pressure drops, power requirements and acoustic noise.

Tanaka et al. (1997) performed a turbulent heat transfer and flow calculation based on the two-equation model of turbulence for the problem of impingement air cooling of LSI Packages with large plate fins. The calculated velocity vectors show good agreement with the results of flow visualization. The calculated temperature distributions also agree well with experimental values. This kind of simulation is helpful for the research and development of new cooling methods.

Sathe et al. (1997) presented a computational analysis for three dimensional flow and heat transfer in the IBM 4381 heat sink. This heat sink uses forced convection cooling of air over an array of fins to achieve the desired cooling. The flow is observed to be very strong in the region of the fin array below the nozzle. The temperature of the center region is low and uniform and it increases in the outward direction. The predicted values of temperature and pressure drop agree well with the experimental values.

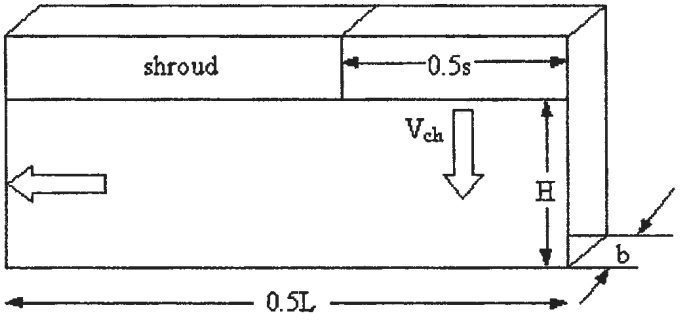

Figure 2.9 Geometric configuration of an impingement flow channel.

Biber (1997) carried out a numerical study and analytical scaling to determine the pressure drop and thermal performance of a single isothermal channel with variable width

impingement flow. She modeled one fourth of a channel for a uniform flow entering through a rectangular slot as shown in Figure 2.9. The parameters used in this study are summarized in Table 2.1. Fin thickness was not a parameter in the model, since only one channel was modeled.

Table 2.1 Variable ranges of Biber model.

Parameter	Variable	Range
Length (mm)	L	100-200
Fin height (mm)	H	25-50
Fin spacing (mm)	b	10-50
Inlet width (mm)	s	20-100
Channel velocity (m/s)	V_{ch}	1-5
Reynolds number	Re_{ch}	25-5200

She numerically studied 43 different combinations of channel parameters and presented the correlations for pressure loss coefficient and total heat transfer in a channel with impingement flow. The correlations for pressure loss coefficient, K, and Nu are suggested as

$$K\left(\frac{H}{W}\right)^2 = \left[\left(8.5x_f^{\,0.25}\right)^7 + \left(75x_f^{\,1.05}\right)^7\right]^{\frac{1}{7}} \quad \text{valid for } 0.001 < x_f < 2 \tag{2.28}$$

$$\text{with} \qquad x_f = \left(\frac{0.5(L-s)+H}{D_h Re}\right)\frac{H}{0.5s} \tag{2.29}$$

$$Nu = \left[\left(6.05x_t^{\,-0.22}\right)^{-3/4} + \left(0.20x_t^{\,-1.05}\right)^{-3/4}\right]^{-4/3} \quad \text{valid for } 0.001 < x_t < 3 \tag{2.30}$$

$$\text{with} \qquad x_t = \left(\frac{L}{D_h Re}\right)\frac{H}{0.5s} \tag{2.31}$$

where K accounts for frictional pressure drop and pressure change due to flow acceleration / deceleration from inlet to exit areas. Inlet and exit pressure loss coefficients are not included in the model. These correlations were used to predict thermal performance for 10 different heat sinks in impingement flow. The test cases covered a size range from approximately 3 cm to 21 cm in length, with fin height ranging from 0.7 cm to 3.6 cm. The accuracy of the predicted thermal resistance was found to be within ±20% of the experimental data. The pressure drop model was not validated experimentally by Biber (1997). The correlation of *Nu* is doubtful since *Nu* is constant when impingement inlet width changes for the same flow rate.

Sasao et al. (1999) developed a numerical method for simulating impingement air flow and heat transfer in plate-fin type heat sinks. In this method, all the fins of an individual heat sink and the air between them are replaced with a single, uniform element having an appropriate flow resistance and thermal conductivity. With this element, fine calculation meshes adapted to the shape of the actual heat sink are not needed, so the size of the calculation mesh is much smaller than that of conventional methods. Simulations and experiments were carried out with flat-fin heat sinks of various dimensions. They did not give any correlations for design purposes. The purpose of this research was to validate the concept with experiments. The thermal resistance was predicted within ±15 % and pressure drop within ± 20 % of the experimental data.

Soodphakdee et al. (2001) compared performance of TISE (*Top Inlet Side Exit or impinging flow*) and SITE (*Side Inlet Top Exit or suction flow*) for plate fin heat sink-fan combinations. The fins and base were taken as isothermal and the fin efficiency developed by Iwasaki and Ishizuka (2000) was applied later to the numerical results. It was shown that such treatment of fin efficiency correction yields results in good agreement with the CFD results. They found that the TISE configuration outperformed SITE and performance was quite sensitive to fin spacing. The empirical correlations of the CFD solutions for friction factor and heat transfer were not provided.

Saini and Webb (2002) proposed a model for parallel flow based on developing laminar flow in rectangular channels, and validated this model by experiments. The test pressure drop data are higher than the predicted values by nearly 20%. The model under predicts thermal resistance within 8% RMS error. They also described a modified Biber (1997) model and validated this model by experiments. The predicted measured pressure drop is 13-31% lower than the experimental values, and underprediction increases with increasing flow rate. The thermal resistance is over predicted by approximately 11% in the typical operating range of the heat sinks in impingement flow. and overprediction increases with increasing flow rate.

The theoretical models for impingement flow in plate fin type heat sinks are summarized as follows: Holahan & Kang (1996) described an approximate pressure drop model; Biber (1997) developed a pressure drop and heat transfer model of a single isothermal

channel with variable width; and Kondo et al. (1998) provided a lengthy set of equations that constitute their proposed zonal model. The zonal model is given in Appendix B. Since the model involves a large number of equations, it is not convenient in practice, therefore, it is necessary to develop a concise and accurate model specially for impingement flow plate fin heat sinks.

2.4 Optimization of Heat Sinks

There have been only a few studies of the optimization of heat sink geometries. In one of these, Azar et al. (1992) used correlations for fully developed laminar flow between parallel plates to predict thermal and hydraulic performance of small (25 mm square) heat sinks. At a moderate pressure drop of 15 Pa, optimum fin thickness was below 0.2 mm and fin spacing below 1mm.

The thermal performance of three designs of air cooled aluminum fin array containing 5, 8, and 11 fins, respectively, were compared by Knight et al. (1992). The best thermal performance was obtained with the 8 fin design. They extended previous analyses of microchannel heat sinks for turbulent flow.

Bejan and Sciubba (1992) reported the optimal spacing between parallel plates in forced convection. The analysis was performed for isothermal and constant heat flux boundary conditions. Correlations for developing flow were taken from Shah and London (1978).

They found that the maximum total heat transfer rate is proportional to $(\Delta P)^{1/2}$, the total thickness of the stack, and the maximum allowable temperature difference between the board and the coolant inlet. It was shown that the surface thermal boundary condition has a minor effect on the optimal spacing and the maximum heat transfer rate. The maximum heat transfer rate for air ($Pr = 0.72$) is achieved for $L^* \cong 0.04$. They also showed that the ratio of heat transfer rate and pumping power monotonically decreases as the spacing between plates increases.

Boesmans et al. (1994) analyzed heat sinks of different geometries using a new design criterion which involves both the effects of heat transfer performance and pressure drop. It is shown that, when pressure drop is taken into account, plate fin heat sinks have a better cooling performance than offset-strip fin or pin fin heat sinks. The dimensions of a plate-fin heat sink are optimized using an analytical model. The optimal plate-fin has a cooling performance comparable to what is normally achieved by integral water cooling. This fin structure should allow a multi-chip module to dissipate up to 4 W/cm^2 (at a junction temperature of 80 °C and an ambient temperature of 40 °C).

Mansuria and Kamath (1994) performed numerical and experimental studies of three fin geometries (plate, pin and radial) for impingement and suction flow. Impingement cooling generates lower thermal resistance than suction through the fins. Numerical simulation of 12 geometries (4 each of pin, plane and radial fins) showed that the plate

fin geometry had the minimum convection thermal resistance. For the plate fin geometry, there was a significant increase in the pressure drop when the number of fins increased.

Copeland (1995) modified previous analyses for developing flow and calculated optimum fin thickness and spacing for silicon heat sinks cooled by fluorocarbon liquid. As channel length decreased, optimum fin spacing and thickness decreased.

Lee (1995) proposed to use "*f*" and "*j*" factors from Kays and London (1984) to model plate fin heat sinks in parallel flow. He analyzed flow through parallel fin heat sinks in fully ducted and partially ducted flows. Unlike a fully ducted configuration, in a partially ducted configuration at a fixed approach velocity, an optimum fin thickness and fin spacing exists. When the bypass path is eliminated, thermal performance improves monotonically as fin spacing is decreased.

Aranyosi et al. (1997) performed experimental and numerical studies and produced isocurves of pressure drop and fan/blower power at fixed thermal resistance in addition to isocurves of thermal resistance at fixed pressure drop and fan power. As pressure drop or fan/blower power increased, optimum fin spacing and thickness decreased, resulting in reduced thermal resistance.

Kondo et al. (1997) considered two types of heat sink: plate fins and pin fins. They optimized the heat sink geometries by evaluating sixteen parameters simultaneously,

including fin thickness, spacing and height. For the plate fins, the optimal thickness was found to be 0.12-0.15 mm. For the pin fins, optimal pin diameters were 0.39-0.40 mm. Under the conditions of constant pumping power, the optimal thermal resistance of the plate fins was about 60% of that of the pin fins.

Furthermore, Kondo et al (1998) utilized the previous complicated zonal approach on the design and optimization of plate fin heat sinks cooled by impingement. Using this model, a method was proposed for optimizing heat sink geometry by applying the univariate search technique. For a 60 by 60 mm LSI, the optimum fin geometry was: fin thickness of 0.15 mm; fin spacing of 0.54 mm; number of fins: 87; fin height of 14.5 mm; and impingement inlet width of 30 mm.

Biber and Fijol (1999) performed a thorough study of the optimization of a fixed size heat sink using an actual fan curve as the hydraulic operating condition. Variation of the base thickness was also considered.

Copeland (2001) performed parallel flow analysis using analytic equations for an ideal heat sink with infinite thermal conductivity and zero fin thickness (fully developed flow) and practical heat sink with finite thermal conductivity and fin thickness (developing flow). The effect of fan power and fin height was studied for typical ranges of fin spacing and thickness. He found that each fin spacing value has a single best fin thickness.

Increasing fin height was shown to decrease thermal resistance faster than by increasing fan power.

Iyengar and Cohen (2001) performed a least material optimization and proposed a number of performance metrics for comparing heat sinks. These metrics are array heat transfer coefficient ($q/(LW\Delta T)$), mass specific heat transfer coefficient ($q/(\rho_{fin}V_{fin}\Delta T)$), volumetric efficiency of the heat sink ($q/(LWH\Delta T)$ and coefficient of performance (COP $= q/P_{pump}$). Cohen and Iyengar (2002) used a laminar developing flow heat transfer model provided by Kakac et al. (1987) and a pressure drop model developed by Holahan et al. (1996) to carry out plate fin heat sink optimization for least material and maximum heat transfer. The test optimization was carried out based on a heat sink coefficient of performance.

Culham and Muzychka (2001) presented a heat sink optimization technique that allows simultaneous optimization of heat sink design parameters based on entropy generation minimization. The optimization used a parallel flow model developed by Muzychka and Yovanovich (1998) for pressure drop and Teertstra et al. (1999) for heat transfer. All design parameters for plate fin heat sinks, including geometric parameters, heat dissipation, material properties and flow conditions can be simultaneously optimized to characterize a heat sink. In addition, a fan performance curve was used to find the system operating point and optimized design parameters.

Loh et al. (2002) investigated eight plate fin heat sinks in parallel flow under two fans and two blowers for different fin spacing length ratios. The optimization point between the different types of fans or blowers under certain fin spacing/length was obtained. They predicted heat sink performance using the Copeland (2000) model for pressure drop and the Teertstra et al. (1999) model for heat transfer. The heat transfer model over predicted the optimum geometries by 6-10 %.

Saini and Webb (2002) addressed the heat rejection limits for a fan-heat sink combination within a fixed volume. Analytical models are used to predict the optimum geometry for plate fins with parallel and impingement flow. Experiments are done to validate the predictions. They also performed optimization for an offset-strip fin geometry in parallel flow and found that the plate fin outperformed the offset-strip fin geometry.

Heat sink optimization involves many different considerations: thermal, mechanical, fluid, system environment and manufacturing variables. Most of the research on heat sink optimization was focused on minimizing of fin mass, minimizing pumping power, or finding optimum geometries. Most studies have concentrated on parallel flow rather than impinging flow.

2.5 Spreading Resistance

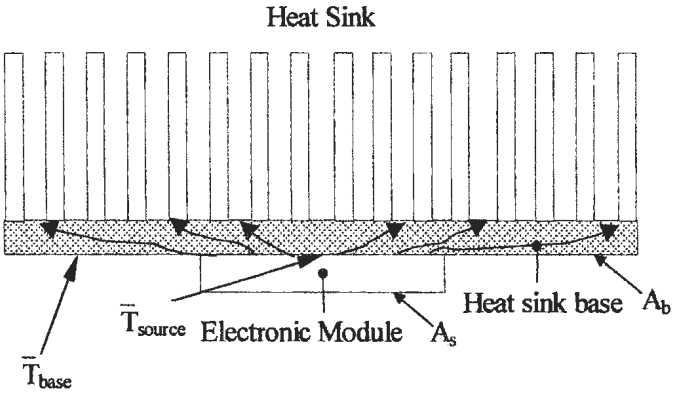

Figure 2.10 Schematic view of spreading thermal resistance.

Thermal spreading resistance occurs whenever heat leaves a heat source of finite dimensions and enters into a larger region, as shown in Figure 2.10. Typical applications include cooling of electronic devices, both at the package and system level, and cooling of power semiconductors using heat sinks. In the electronic module cooling problem, heat flows from the electronic module surface (source area A_s) to the heat sink base (area $A_b > A_s$) which is convectively cooled. The definition proposed by Mikic and Rohsenow (1966) can be used to define the spreading resistance:

$$R_{sp} = \frac{\bar{T}_{source} - \bar{T}_{base}}{Q} \tag{2.32}$$

In heat sink applications the convective film resistance can be replaced by an effective extended surface film coefficient.

Lee et al. (1995) developed an analytical model for predicting spreading thermal resistance in a plate with a uniform heat flux on one surface and a convective boundary condition over the other surface. Dimensionless expressions in the form of infinite series are provided for computing spreading thermal resistance as a function of contact size, plate thickness and the Biot number. It was found that the spreading resistance is insensitive to changes in both the plate thickness and the Biot number, and is solely dependent on the contact size of the heat source. Lee et al. (1998) suggested the following expressions as an approximation to the infinite series solution for determining spreading resistance in heat sink applications. R_0 is the average heat sink resistance.

$$R_{sp} = \frac{\sqrt{A_b} - \sqrt{A_s}}{k\sqrt{\pi A_b A_s}} \times \frac{\lambda k A_b R_0 + \tanh(\lambda t)}{1 + \lambda k A_b R_0 \tanh(\lambda t)} \tag{2.33}$$

where

$$\lambda = \frac{\pi^{3/2}}{\sqrt{A_b}} + \frac{1}{\sqrt{A_s}} \tag{2.34}$$

The above correlations were reported to agree with the analytical infinite series solution within 10% over the range of parameters commonly found in microelectronics applications.

Yovanovich et al. (1998) reviewed the previously published spreading resistance models and presented simple correlation equations for ease of computation. They showed that a number of particular solutions were special cases of a more comprehensive model developed for a circular heat source in perfect thermal contact with a compound disk which consists of two isotropic layers (thermal conductivities k_1 and k_2) in perfect

thermal contact with each other. The top surface of the compound disk was subjected to uniform cooling or constant heat transfer coefficient. The Lee et al. (1995) solution is then a special case of this solution for $k_1 = k_2$ and constant heat flux over a circular heat source.

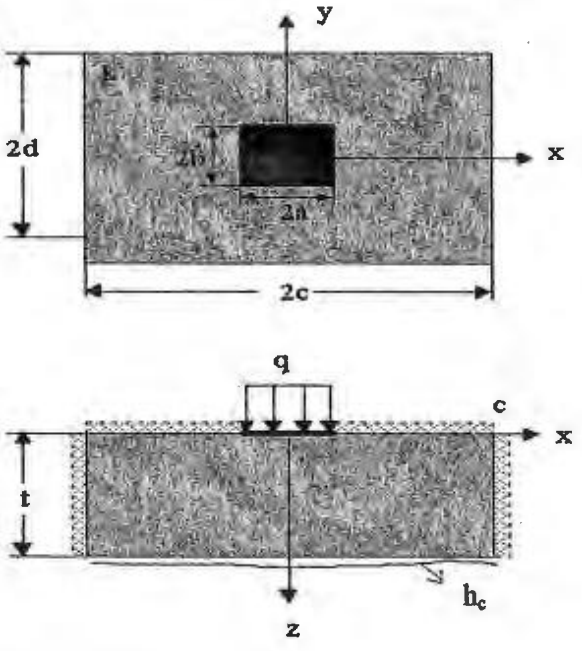

Figure 2.11 Finite isotropic channel with central heat source.

Yovanovich, Muzychka and Culham (1999) presented the thermal spreading resistance of an isoflux, rectangular heat source on a two layer rectangular flux channel with convetive or conductive boundary conditions at one boundary. They showed that the dimensionless spreading resistance depends on several dimensionless geometric and thermal parameters.

For the present heat sink applications, heat dissipated by electronic devices is conducted through electronic packages into the heat sink base plate which is convectively cooled. A

planar rectangular heat source situated on one end of a finite isotropic rectangular flux channel that has thickness t and thermal conductivity k is considered. The heat flux channel is cooled along the bottom surface through a uniform contact conductance h_c. The heat source area is rectangular, having dimensions $2a$ by $2b$. The dimensions of the heat flux channel (heat sink base) are $2c$ by $2d$, as shown in Figure 2.11. The lateral boundaries of the heat flux channel are adiabatic. The general expression for the spreading resistance of central heat source on finite isotropic rectangular flux channel with convective cooling at one boundary is presented by Yovanovich, Muzychka and Culham (1999).

$$R_{sp} = \frac{1}{2a^2cdk}\sum_{m=1}^{\infty}\frac{\sin^2(a\delta_m)}{\delta_m^{\,3}}\cdot\phi(\delta_m)+\frac{1}{2a^2cdk}\sum_{n=1}^{\infty}\frac{\sin^2(b\lambda_n)}{\lambda_n^{\,3}}\cdot\phi(\lambda_n)$$
$$+\frac{1}{a^2b^2cdk}\sum_{m=1}^{\infty}\sum_{n=1}^{\infty}\frac{\sin^2(a\delta_m)\sin^2(b\lambda_n)}{\delta_m^{\,2}\lambda^2\beta_{m,n}}\cdot\phi(\beta_{m,n}) \tag{2.35}$$

where

$$\phi(\zeta) = \frac{(e^{2t\zeta}+1)\zeta-(1-e^{2t\zeta})h_c/k}{(e^{2t\zeta}-1)\zeta-(1+e^{2t\zeta})h_c/k} \tag{2.36}$$

In all summations, $\phi(\zeta)$ is evaluated in each series using $\zeta=\delta_m$, λ_n, and $\beta_{m,n}$. The general expression depends on several geometric and thermal parameters (a, b, c, d, t, k, h_c). The eigenvalues are $\delta_m=m\pi/c$, $\lambda_n=n\pi/d$, $\beta_{m,n}=(\delta_m^{\,2}+\lambda_n^{\,2})^{1/2}$. The eigenvalues δ and λ, corresponding to the two strip solutions, depend on the flux channel dimensions and the indices m and n, respectively. The eigenvalues $\beta_{m,n}$ for the rectangular solution are functions of the other two eigenvalues.

Muzychka et al. (2000) analytically studied the spreading resistance of eccentric heat sources on a rectangular flux channel for both isotropic and compound flux channels. It was shown that the solution could be used to model any number of discrete heat sources on a compound or isotropic flux channel using superposition. Also, the solution for a central heat source can be used to compute the spreading resistance for corner and edge heat sources using the method of images.

2.6 Summary

This chapter presented a literature review pertinent to the present research. Heat sink modelling research was reviewed for parallel and impingement flow geometries. Parallel flow geometry is more clearly understood in the literature than the impingement flow geometry, as more research on parallel flow has been reported than for impingement flow. A review of research on heat sink optimization was also presented. Finally, a brief review of literature on thermal spreading resistance in heat sink applications was also provided. A simple approximate solution and an exact analytical infinite series solution were presented to calculate spreading resistance.

Chapter 3

Theoretical Modelling

This chapter presents pressure drop and heat transfer models for developing impingement flow in plate fin heat sinks. Both models are constituted from simple momentum and energy balances and utilize fundamental solutions from heat transfer and fluid dynamics to predict their constitutive components.

3.1 Pressure Drop Model

The pressure drop model for the impingement plate fin heat sink will be based on correlations for laminar duct flows, which are essentially one-dimensional. We need only study one half of the heat sink since the flow field, temperature contours and pressure fields on the other half are a mirror image due to symmetry. Half of the impingement cooled heat sink channel is considered as two connected rectangular channels; one is vertical and the other is horizontal. Their effective lengths are L_{eff1} and L_{eff2}, as illustrated in Figure 3.1. This consideration is justifiable if one imagines a typical streamline, for example near the middle of the impingement slot. This streamline length is better approximated by the L-shaped path of height $0.5H$ and length $0.5L$-$0.25s$ after a 90° turn.

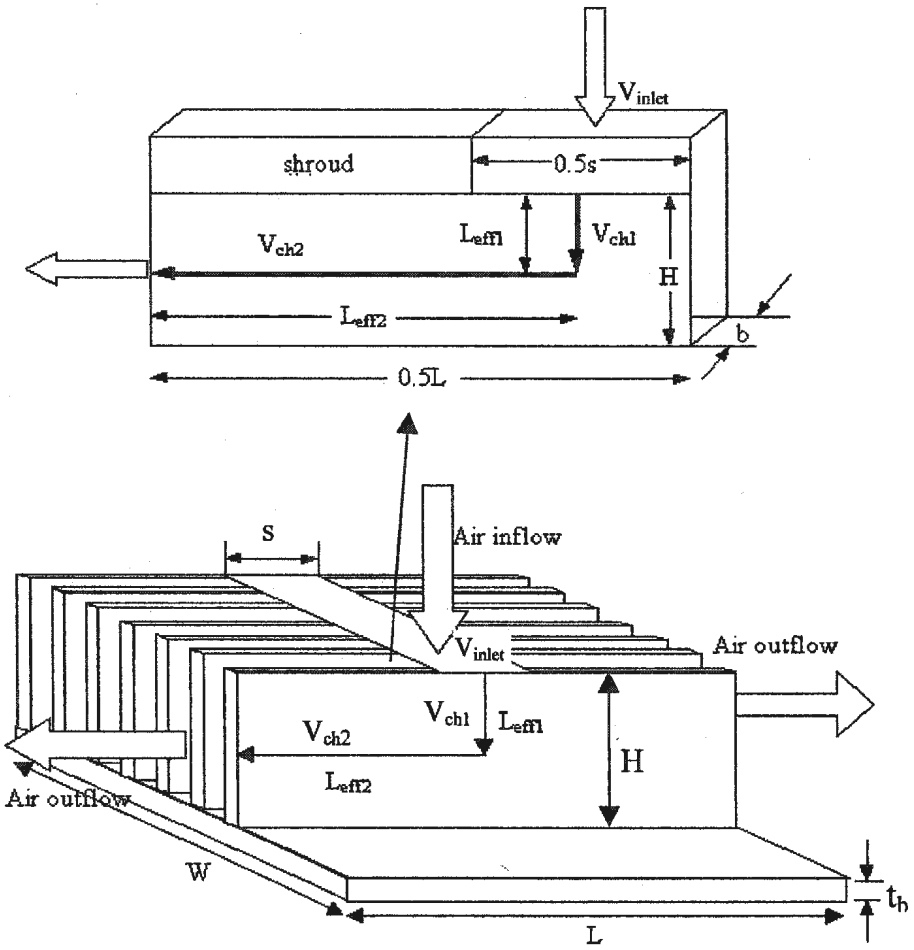

Figure 3.1 Impingement flow geometric configuration.

Summing all of the frictional and dynamic losses, the total pressure drop model function is given in terms of Bernoulli's equation,

$$\Delta P = K_c \frac{1}{2}\rho V_{ch1}^{\ 2} + K_{90}\frac{1}{2}\rho V_{ch1}^{\ 2} + 4f_{app1}\frac{L_{eff1}}{D_{h1}}\frac{1}{2}\rho V_{ch1}^{\ 2} + 4f_{app2}\frac{L_{eff2}}{D_{h2}}\frac{1}{2}\rho V_{ch2}^{\ 2} + K_e\frac{1}{2}\rho V_{ch2}^{\ 2} \qquad (3.1)$$

or $$\Delta P = \left[\left(K_c + K_{90} + 4f_{app1}\frac{L_{eff1}}{D_{h1}}\right)\frac{4H^2}{s^2} + 4f_{app2}\frac{L_{eff2}}{D_{h2}} + K_e\right]\frac{1}{2}\rho V_{ch2}^{\ 2} \qquad (3.2)$$

The average velocity in the channel can be obtained from mass conservation,

$$V_{ch1} = V_{inlet} \frac{W}{W - tN_f} \tag{3.3}$$

$$V_{ch1} \frac{s}{2}(W - tN_f) = V_{ch2}(WH - tN_fH) \tag{3.4}$$

$$V_{ch1} = V_{ch2} \frac{2H}{s} \tag{3.5}$$

3.1.1 Frictional Pressure Losses

Impingement flow modeling in a plate fin heat sink is essentially a simultaneously developing hydraulic and thermal boundary layer problem in rectangular ducts. The flow may become fully developed if the heat sink channel is sufficiently long in the flow direction or with small fin spacing, however, this is very unlikely for electronic cooling application heat sinks. The apparent friction factor, f_{app}, for a rectangular channel may be computed using a form of the model developed by Muzychka and Yovanovich (1998) for developing laminar flow:

$$f_{app}\,\mathrm{Re}_{D_h} = \left[\left(\frac{3.44}{\sqrt{L^*}}\right)^2 + \left(f\,\mathrm{Re}_{D_h}\right)^2\right]^{1/2} \tag{3.6}$$

$$L^* = \frac{L}{D_h\,\mathrm{Re}_{D_h}} \tag{3.7}$$

The fRe_{D_h} term is the fully developed flow friction factor Renolds number group and depends on b/H only for laminar flow. A single term from the exact series is suggested by Muzychka and Yovanovich (2002).

$$fRe_{D_h} = \frac{24}{\left[1+\left(\frac{b}{H}\right)^2\right]\left[1-\frac{192b}{\pi^5 H}\tanh\left(\frac{\pi H}{2b}\right)\right]} \tag{3.8}$$

They validated the model with most of the available developing flow data and found the estimation error was within ±3% for rectangular channel.

For vertical channel 1,

$$L_1{}^* = \frac{L_{eff1}}{D_{h1}Re_{D_{h1}}} \tag{3.9}$$

$$L_{eff2} = \frac{H}{2} \tag{3.10}$$

$$D_{h2} = \frac{2sb}{s+2b} \tag{3.11}$$

$$Re_{D_{h1}} = \frac{V_{ch1}D_{h1}}{\nu} \tag{3.12}$$

For horizontal channel 2,

$$L_2{}^* = \frac{L_{eff2}}{D_{h2}Re_{D_{h2}}} \tag{3.13}$$

$$L_{eff2} = \frac{L}{2} - \frac{s}{4} \tag{3.14}$$

$$D_{h2} = \frac{2Hb}{H+2b} \tag{3.15}$$

$$Re_{D_{h2}} = \frac{V_{ch2} D_{h2}}{\nu} \tag{3.16}$$

If the flow is turbulent, the Churchill equation (Burmeister, 1993) can be used to compute f_{app}

$$f = 2\left[\left(\frac{8}{Re_{D_h}}\right)^{12} + \left(\frac{1}{(A+B)^{3/2}}\right)\right]^{1/12} \tag{3.17}$$

$$A = \left\{2{,}457 \ln\left[\frac{1}{\left(\frac{7}{Re_{D_h}}\right)^{0.9} + 0.27\left(\frac{e}{D}\right)}\right]\right\}^{16} \tag{3.18}$$

$$B = \left(\frac{37530}{Re_{D_h}}\right)^{16} \tag{3.19}$$

where e/D represents relative roughness.

3.1.2 90° Bend Pressure Loss

The 90° bend pressure loss coefficient data is taken from Idelchik (1993) and curve fitted to the following relation for $0 < H/s \leq 1$

$$K_{90} = 3.64 - 9.15\frac{H}{s} + 10.87\left(\frac{H}{s}\right)^2 - 4.29\left(\frac{H}{s}\right)^3 \tag{3.20}$$

If $H/s > 1$, the 90° bend pressure loss coefficient from Kondo (1996) can be used

$$K_{90} = 0.5\left(\frac{1+V_{ch2}/V_{ch1}}{2}\right)^2 \tag{3.21}$$

This accounts for loss in momentum due to the turning of the fluid in the channel.

3.1.3 Inlet and Exit Pressure Losses

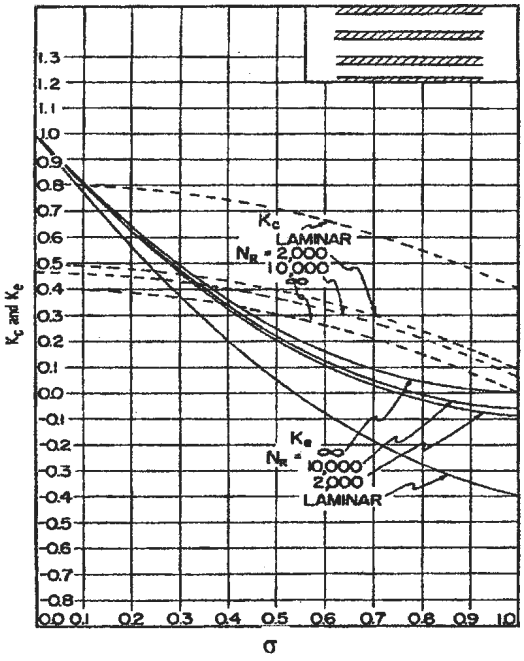

Figure 3.2 Entrance and exit pressure loss coefficient (Kays and London, 1984).

For the inlet and exit pressure losses for a heat sink, Kays and London (1984) provide loss coefficients in the form $\Delta P=K(\rho V^2/2)$ as a function of the ratio of free-flow area to frontal area $\sigma=b/(b+t)$. The graphs for laminar flow in that reference, as shown in Figure 3.2, have been curve fit here to second order equations:

$$K_c = 0.79685 + 0.04174\sigma - 0.43765\sigma^2 \tag{3.22}$$

$$K_e = 1.00008 - 2.38627\sigma + 0.98718\sigma^2 \tag{3.23}$$

The concise expression for laminar flow parallel plate channels from Kays and London (1984) can also be used

$$K_c = 0.4(1-\sigma^2) + 0.4 \tag{3.24}$$

$$K_e = (1-\sigma)^2 - 0.4\sigma \tag{3.25}$$

If the flow is turbulent, the expansion and contraction loss coefficients may be computed using simple expressions for a sudden contraction and a sudden expansion (White, 1986).

$$K_c = 0.42(1-\sigma^2) \tag{3.26}$$

$$K_e = (1-\sigma^2)^2 \tag{3.27}$$

3.2 Heat Sink Thermal Circuit Analysis

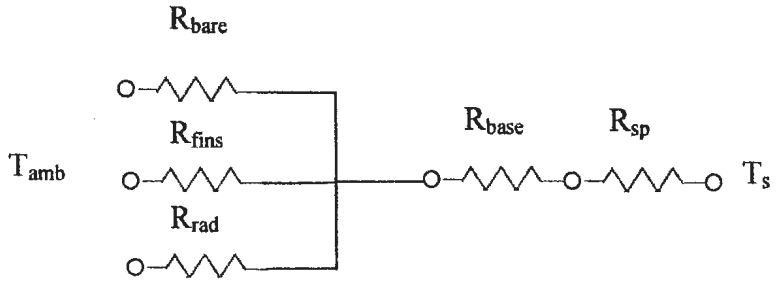

Figure 3.3 Heat sink thermal circuit.

Figure 3.3 illustrates the thermal circuit corresponding to the heat transfer from a plate fin heat sink. The total heat sink thermal resistance is

$$R_{total} = \frac{T_s - T_{amb}}{Q} \tag{3.28}$$

It can be expressed as

$$R_{total} = R_{sp} + R_{base} + \frac{1}{\frac{1}{R_{bare}} + \frac{1}{R_{fins}} + \frac{1}{R_{rad}}} \tag{3.29}$$

The effective thermal resistance is defined as:

$$R_{eff} = \frac{1}{\frac{1}{R_{bare}} + \frac{1}{R_{fins}} + \frac{1}{R_{rad}}} \tag{3.30}$$

where R_{eff} is an effective resistance that accounts for heat flow paths by conduction, convection and radiation in the fins, and by convection and radiation from the exposed portion of the base area.

The conduction resistance in the base of the heat sink is:

$$R_{base} = \frac{t_b}{kA_b} \tag{3.31}$$

$$A_b = LW \tag{3.32}$$

The convection resistance for the exposed base area is:

$$R_{bare} = \frac{1}{hA_{bare}} \tag{3.33}$$

$$A_{bare} = (N_f - 1)bL \tag{3.34}$$

The assumption of one-dimensional conduction in a fin with uniform properties, constant cross-section, and adiabatic tip gives the following expression for fin resistance:

$$R_{fin} = \frac{1}{\sqrt{hPkA_c}\tanh(mH)} \tag{3.35}$$

$$R_{fins} = \frac{R_{fin}}{N_f} \tag{3.36}$$

The radiation thermal resistance is given by:

$$R_{rad} = \frac{1}{h_{rad}A_{rad}} \tag{3.37}$$

$$h_{rad} = \varepsilon\sigma(T_s + T_{amb})(T_s^{\,2} + T_{amb}^{\,2}) \tag{3.38}$$

$$A_{rad} = 2(LH + WH) + LW \tag{3.39}$$

where σ and ε are Stefan-Boltzmann constant and the surface emissivity, respectively.

The overall heat sink resistance is given by

$$R_{\sin k} = \frac{1}{\frac{N_f}{R_{fin}} + h(N_f - 1)bL + h_{rad}A_{rad}} + \frac{t_b}{kLW} \tag{3.40}$$

The spreading thermal resistance for the present research is obtained from the following expression developed by Yovanovich, Muzychka and Culham (1999).

$$R_{sp} = \frac{8}{L_s^{\,2}LWk}\sum_{m=1}^{\infty}\frac{\sin^2(\delta_m L_s/2)}{\delta_m^{\,3}}\cdot\phi(\delta_m) + \frac{8}{L_s^{\,2}LWk}\sum_{n=1}^{\infty}\frac{\sin^2(\lambda_n W_s/2)}{\lambda_n^{\,3}}\cdot\phi(\lambda_n)$$
$$+\frac{16}{L_s^{\,2}W_s^{\,2}LWk}\sum_{m=1}^{\infty}\sum_{n=1}^{\infty}\frac{\sin^2(\delta_m L_s/2)\sin^2(\lambda_n W_s/2)}{\delta_m^{\,2}\lambda^2\beta_{m,n}}\cdot\phi(\beta_{m,n}) \tag{3.41}$$

where $$\phi(\zeta) = \frac{(e^{2t_b\zeta} + 1)\zeta - (1 - e^{2t_b\zeta})h_{eff}/k}{(e^{2t_b\zeta} - 1)\zeta - (1 + e^{2t_b\zeta})h_{eff}/k} \tag{3.42}$$

In all summations $\phi(\zeta)$ is evaluated in each series using $\zeta=\delta_m$, λ_n, and $\beta_{m,n}$.

The general expression for spreading resistance consists of three terms. The single summations account for two-dimensional spreading in the x and y directions, respectively, and the double summation term accounts for three-dimensional spreading from the rectangular heat source. The eigenvalues are $\delta_m=2m\pi/L$, $\lambda_n=2n\pi/W$, $\beta_{m,n}=(\delta_m^2+\lambda_n^2)^{1/2}$. The eigenvalues δ and λ, corresponding to the two strip solutions, depend on the flux channel dimensions and the indices m and n, respectively. The eigenvalues $\beta_{m,n}$ for the rectangular solution are functions of the other two eigenvalues.

3.3 Heat Transfer Model

The problem of interest in this study involves forced convection heat transfer for a plate fin heat sink, a parallel array of N_f plate fins mounted to a conductive base plate, as shown in Figure 3.1. This analysis will assume a uniform velocity through the channels formed between the fins. No leakage of air through the top edges of the channels is achieved by placing a shroud on top of the fins.

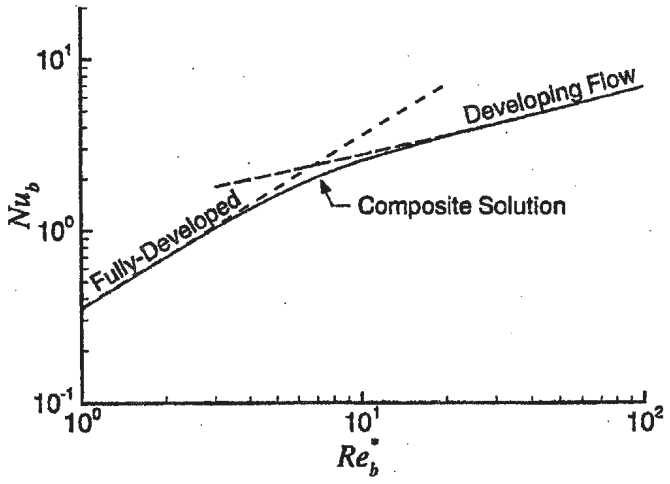

Figure 3.4 Proposed solution behaviour (Teertstra et al., 1999).

The heat transfer coefficient, h, will be computed using the following model developed by Teertstra et al. (1999). This model is applicable to both fully developed and developing flows. Figure 3.4 shows the behavior of these two asymptotes, along with the composite model for the full range of Re_b^* from developing to fully developed flow. Teertstra et al. validated the model with experimental and numerical data and found 2.1% RMS error and 6% maximum error. The development of a heat transfer model will be similar to the development of the pressure drop model.

$$Nu_b = \left[\left(\frac{Re_b^* Pr}{2} \right)^{-3} + \left(0.664 \sqrt{Re_b^*} Pr^{1/3} \sqrt{1 + \frac{3.65}{\sqrt{Re_b^*}}} \right)^{-3} \right]^{-1/3} \tag{3.43}$$

$$Nu_b = \frac{h \cdot b}{k_a} \tag{3.44}$$

$$Re_b^* = Re_b \cdot \left(\frac{b}{L} \right) \tag{3.45}$$

For vertical channel 1,

$$Nu_{bch1} = \frac{h_{ch1} \cdot b}{k_a} \tag{3.46}$$

$$Re_{bch1}{}^{*} = Re_{bch1} \cdot \left(\frac{b}{L_{eff1}} \right) \tag{3.47}$$

For horizontal channel 2,

$$Nu_{bch2} = \frac{h_{ch2} \cdot b}{k_a} \tag{3.48}$$

$$Re_{bch2}{}^{*} = Re_{bch2} \cdot \left(\frac{b}{L_{eff2}} \right) \tag{3.49}$$

The average heat transfer coefficient for the heat sink is suggested as

$$h = h_{ch1} \frac{s}{L} + h_{ch2} \frac{L - s}{L} \tag{3.50}$$

Since the heat transfer model assumes isothermal boundary conditions i.e., the fin temperature is equal to that of the base plate, it must be further modified by a fin efficiency which quantifies the ratio of actual to ideal heat transfer. Assuming an adiabatic condition at the fin tip, the efficiency can be determined as follows:

$$\eta = \frac{\tanh(mH)}{mH} \tag{3.51}$$

where m is defined as

$$m = \sqrt{\frac{hP}{kA_c}} \tag{3.52}$$

The perimeter P and cross sectional area A_c of the fins are given by: $P=2t + 2L$, $A_c=tL$.

3.4 Effective Heat Transfer Coefficient

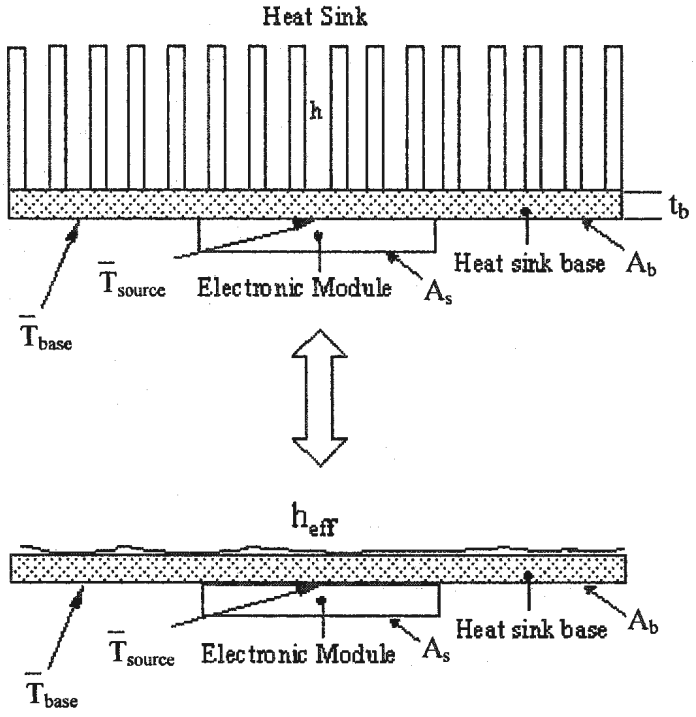

Figure 3.5 Schematic showing the effective heat transfer coefficient.

In heat sink applications, the value of h_{eff} is an effective value which accounts for both the heat transfer coefficient on the fin surface and the increased surface area, as shown in Figure 3.5.

$$h_{eff} = \frac{1}{A_b R_{eff}} \tag{3.53}$$

The total thermal resistance of the system is defined by the relation

$$R_{total} = R_{1D} + R_{sp} \tag{3.54}$$

where R_{1D} is the one dimensional resistance of the system given by

$$R_{1D} = \frac{t_b}{kA_b} + \frac{1}{h_{eff} A_b} \tag{3.55}$$

The spreading thermal resistance will depend on several geometric and thermal parameters

$$R_{sp} = f(L, W, L_s, W_s, t_b, k, h_{eff}) \tag{3.56}$$

The spreading resistance vanishes when the heat flux is distributed uniformily over the entire heat sink base surface.

The R_{total} is known from experimental measurements, therefore, the effective heat transfer coefficient h_{eff} can be calculated from Eq.(3.54). In the present heat sink research, h_{eff} can utilized to obtain the actual heat sink heat transfer coefficient, h, which can be used to examine the proposed heat transfer model.

Chapter 4

Experimental Facility

4.1 Introduction

The aim of the experimental part of this study was to reproduce the impingement airflow and heat transfer phenomena that occur in high performance parallel plate heat sinks. The phenomena had to be produced in such a way that they could be quantitatively measured, to permit a comparison with the analytical models described in Chapter 3.

The experimental facility was used to measure the hydraulic and thermal performance of the heat sinks. The hydraulic performance of the heat sink is expressed as pressure drop across the heat sink versus flow rate. While the thermal performance of the heat sinks is expressed as R_{total}, and is given by

$$R_{total}=\frac{T_s-T_{amb}}{Q} \tag{4.1}$$

Calculation of R_{total} involves measurement of the temperature difference between the heat sink base and ambient conditions, and the heat flow across the heated surface to the heat sink. This thermal resistance includes a spreading resistance, R_{sp}. The experimental facility has two main parts - flow bench for pressure drop and airflow velocity

measurements, and a thermal tester for measurement of temperature difference and heat flow applied to the heat sink base. The two parts were integrated to facilitate simultaneous measurements of pressure drop and thermal resistance at a known airflow velocity. The experimental facility is shown in Figures 4.1 and 4.2.

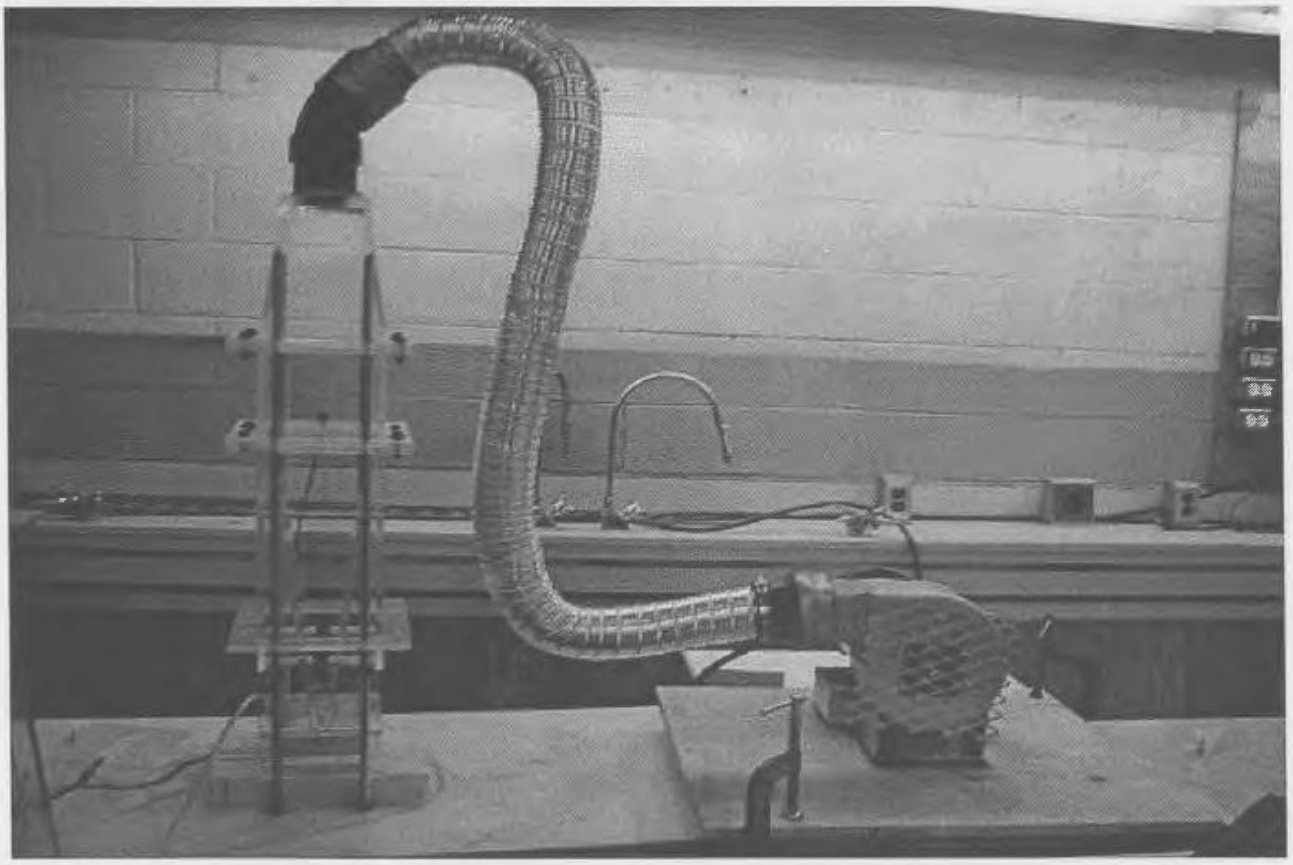

Figure 4.1 Experimental facility for impingement flow test.

4.2 Flow Bench

The flow bench was designed to measure the air velocity and pressure drop for different airflow rates. A schematic of the flow bench is presented in Figure 4.2. The air was discharged from a blower into the test section. The height of the test section could be varied to allow the use of different fin height heat sinks. Furthermore, the impingement inlet width of the test section could be adjusted from 0-100% of the heat sink length.

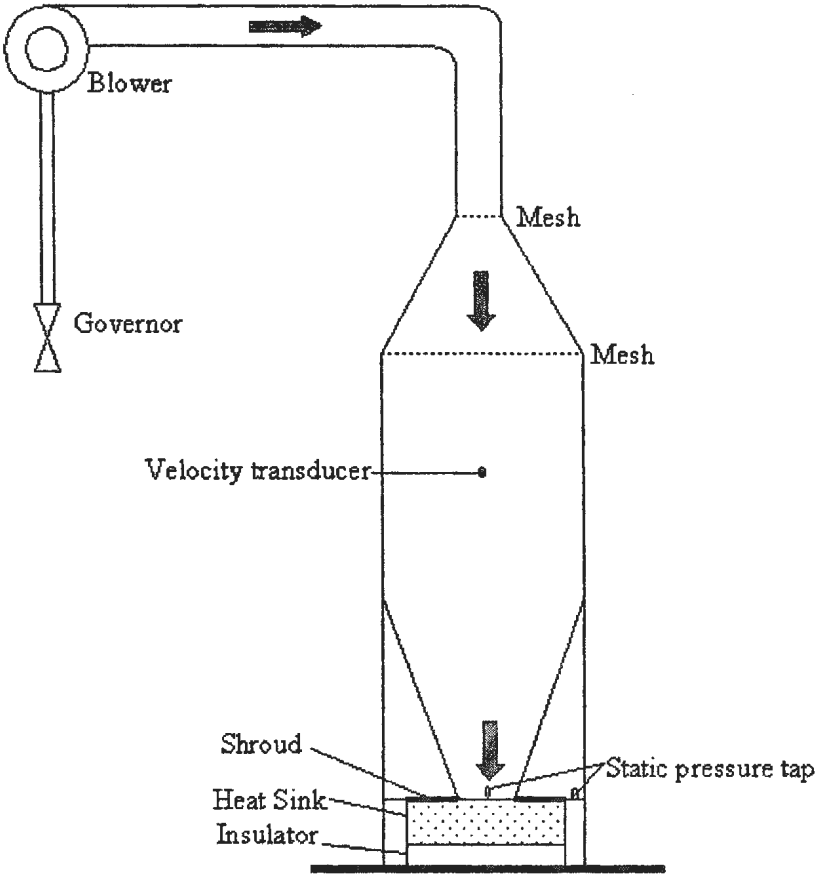

Figure 4.2 Schematic of experimental facility for impingement flow test.

4.2.1 Measurement of the Air Flow Rate

Air entering the test section was passed through two screens before reaching a plenum chamber. The square cross-section plenum chamber had dimension of 152.4 mm. A TSI air velocity transducer is mounted to measure airflow velocity in the plenum chamber (V_d) as shown in Figure 4.3. The impingement inlet velocity (V_{inlet}) and outlet velocity (V_{outlet}) can be calculated from mass conservation. The experimental measurements were carried out at seven different velocities (V_d), 0.4 m/s-1.0 m/s. The air velocity transducer indicates the velocity at standard conditions of 21.1 °C and 101.4 kPa, and its accuracy is ± 2.0% of reading and ± 0.5% of full scale.

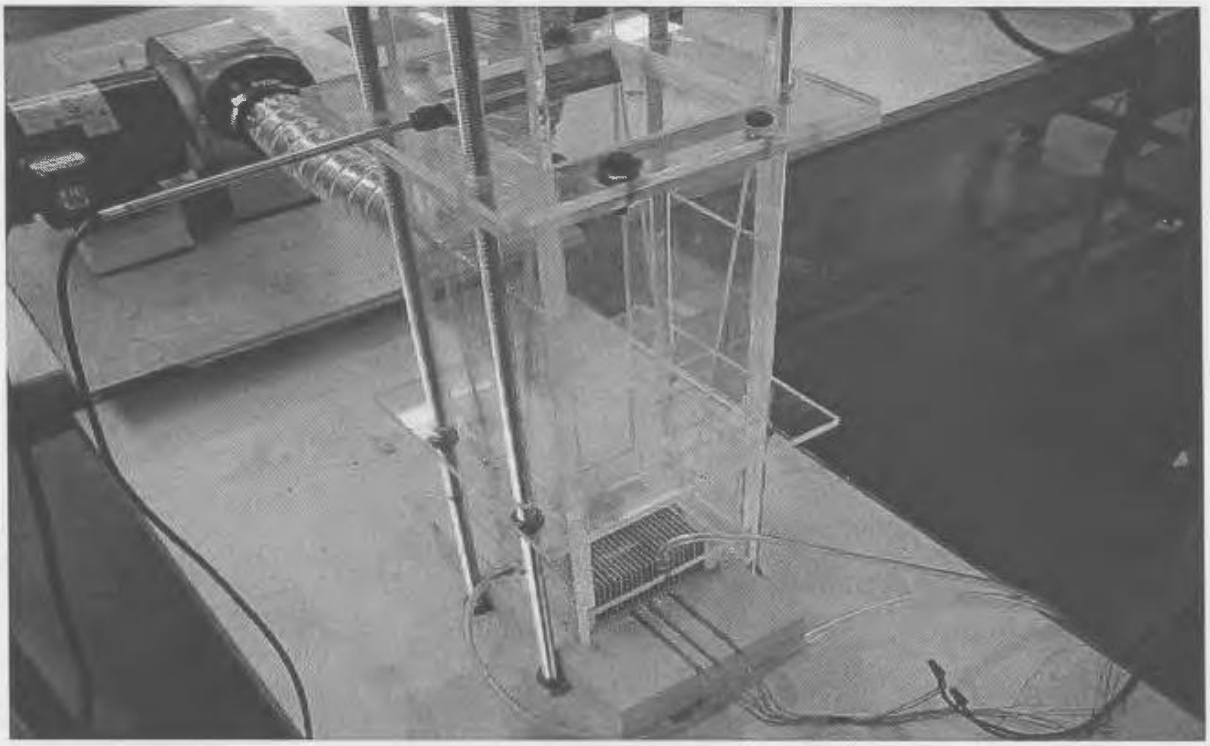

Figure 4.3 A velocity transducer to measure air velocity (V_d).

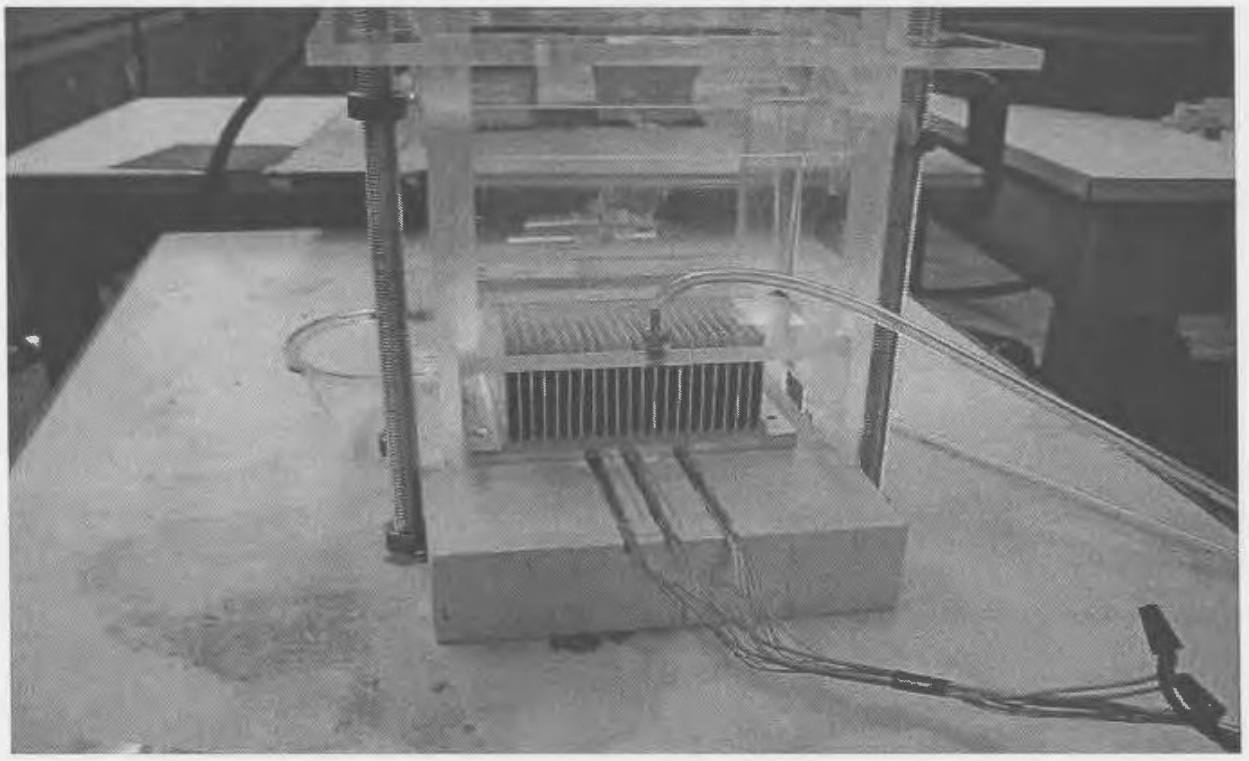

Figure 4.4 Static pressure taps to measure pressure drop.

4.2.2 Measurement of the Heat Sink Air Pressure Drop

The goal of the pressure measurement was to obtain static pressure drop data to compare against the analytical model. The exit air from the plenum chamber passes through an inverted trapezoid duct, which can be used to adjust impingement inlet width, and impinges onto the heat sink. Two static pressure holes are drilled through the inlet duct wall and heat sink outlet wall. The pressure difference between the impingement inlet static pressure (P_{inlet}) and the heat sink outlet static pressure (P_{outlet}) is measured with a calibrated differential pressure transmitter, which is connected to the static pressure taps

as shown in Figure 4.4. A differential pressure transmitter with a range of 25.4 mm of water column is used for this purpose.

The experimental total air pressure drop for impingement flow can be found in terms of Bernoulli's equation

$$\frac{P_{inlet}}{\rho g}+\frac{1}{2}\frac{V_{inlet}^{\ 2}}{g}+z_{inlet}=\frac{P_{outlet}}{\rho g}+\frac{1}{2}\frac{V_{outlet}^{\ 2}}{g}+z_{outlet}+\sum h_l \tag{4.2}$$

Since both pressures are measured in the same plane (z_{inlet}=z_{outlet}), total head loss can be obtained

$$\sum h_l=\frac{P_{inlet}-P_{outlet}}{\rho g}+\frac{1}{2}\left(\frac{V_{inlet}^{\ 2}-V_{outlet}^{\ 2}}{g}\right) \tag{4.3}$$

The average impingement inlet and outlet velocities can be calculated from mass conservation.

$$V_d A_{duct}-V_{loss}=V_{inlet}A_{inlet}=V_{outlet}A_{outlet} \tag{4.4}$$

where V_{loss} is the flow rate leakage loss.

The total pressure loss is thus given by

$$\Delta P=\rho g\sum h_l \tag{4.5}$$

4.3 Thermal Tester

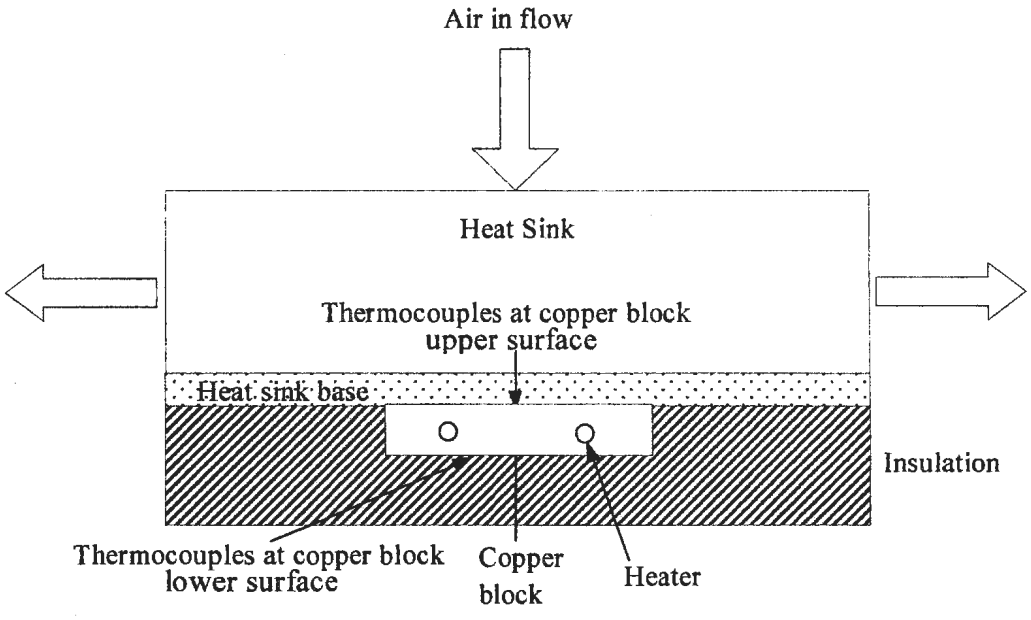

Figure 4.5 Schematic of the thermal tester.

Figure 4.5 shows a schematic of the thermal tester. Two electrical heaters were used to simulate an electronic module. These heaters were connected to a XANTREX XFR series power supply by lead wires. This power supply provides low noise, precisely regulated, variable DC output at 1200 Watts (MAX) of output power. Over voltage protection and thermal shutdown are standard. There are several remote control choices: standard analog programming, optional isolated programming or readback, and optional GPIB programming or RS-232 control. The available voltage and current ranges are 0-150 V and 0-8 A, respectively. These electrical heaters were put into a 76.2 mm square cross

section 12 mm high copper block. Insulation was placed under the copper block. This heat loss through the bottom of the block was estimated to be less than 5 % of the heat input, and a correction was applied in the data reduction. Insulation was also applied to the periphery of the copper block and the heat loss from the periphery of the copper block was estimated to be a maximum of 0.5 % of the total heat input, and a correction was applied in the data reduction. The estimation of heat losses assumes fixed thermal conductivity of the insulation and one-dimensional conduction though the insulation surrounding the copper block. The heat input to the heat sink was determined at the time of test by the product of measured voltage and current (UI) corrected for ambient heat loss (Q_{loss}).

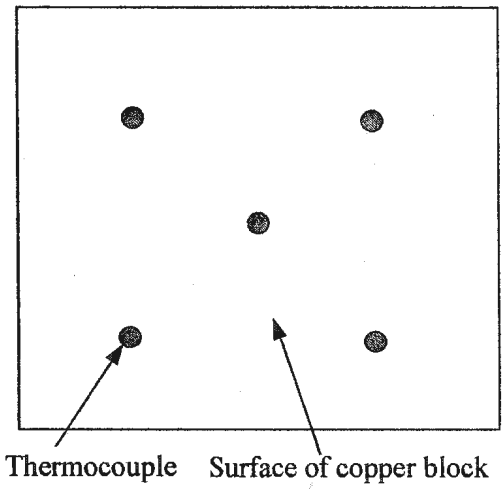

Figure 4.6 Thermocouple locations on upper and lower surface of the copper block.

Five copper-constantan thermocouples were attached, in grooves with thermal epoxy, to the upper surface of the copper block to measure the upper surface average temperature. Another five copper-constantan thermocouples were attached to the lower surface of

copper block to measure the lower surface average temperature. The upper and lower surfaces are divided into four equal areas. The five thermocouples are placed at the centroids of the four equal areas and the center of the whole surface, respectively, as shown in Figure 4.6. The mean temperature of the heat sink base was represented as the average of the ten readings of thermocouples. The ambient temperature was measured with three other thermocouples. The three thermocouple readings were averaged to give the average ambient temperature. The temperature drop, ΔT, from the heat sink base to ambient can thus be calculated directly.

Electrical energy input (UI) to the heater was measured by a DC power supply with high resolution. The tests were conducted with 72.6-104.2 W of input power. The measured thermal resistance is given by $R_{total} = \Delta T/(UI\text{-}Q_{loss})$. Note that the heat sink base area is larger than the heat input area, so the measurement includes the spreading resistance.

4.4 Data Acquisition System

Data acquisition is fully automated using a KEITHLEY Model 2700 Multimeter/Data Acquisition System connected to a personal computer. Real time monitoring of all measurements is displayed at all times. Data collection is user initiated and a total of 50 data points are collected over a 12 minute interval for each set data. Average values of the 50 data points are then used in the data reduction procedures.

4.5 Description of Experiments

Experiments were conducted to validate the analytical heat sink models. Tests were conducted for four heat sink geometries for impingement flow. Heat sink pressure drop and thermal resistance data were taken for different flow rate conditions and different impingement inlet widths. For each heat sink, the experimental measurements were carried out at seven different velocities in the plenum chamber (V_d), 0.4 m/s, 0.5 m/s, 0.6 m/s, 0.7 m/s, 0.8 m/s, 0.9 m/s, 1.0 m/s, and six different impingement inlet widths, 5%L, 10%L, 25%L, 50%L, 75%L, 100%L, respectively. In total, 168 data points were collected for thermal resistance and pressure drop. The details of the heat sinks used for the tests are summarized in Table 4.1.

Table 4.1 Geometry of the heat sinks used in the experiments.

Configuration	Heat Sink #1	Heat Sink #2	Heat Sink #3	Heat Sink #4
L (mm)	127	127	127	127
W (mm)	122	122	116	116
t_b (mm)	12.7	12.7	12.7	12.7
t (mm)	1.2	1.2	1.2	1.2
b (mm)	2.25	2.25	4.27	4.27
H (mm)	26.5	50.0	34.0	50.0
N_f	36	36	22	22

4.6 Experimental Data Collection Procedure

The procedure for collecting a set of data was as follows:

a. Start the Data Acquisition System.

b. Turn on and adjust the fan such that the prescribed velocity was obtained.

c. DC power supply was turned on.

d. Thermocouple readings were monitored until they stablizied.*

e. Collect a set of data.

f. Adjust to next prescribed velocity to collect another set of data.

* The data were taken at steady state conditions, defined by less than ± 0.1°C temperature variation over a period of at least one minute.

4.7 Uncertainty Analysis

4.7.1 Introduction

This section describes the uncertainty analysis for airflow velocity, pressure drop and thermal resistance measurements. The uncertainty analysis for the test data was determined using the root sum square method described in Moffat (1988) and Holman (1994). A brief description of the method is given here. The result R of the experiment is assumed to be calculated from a set of independent measurements $X_1, X_2, \ldots X_N$,

$$R = f(X_1, X_2, \ldots X_N) \tag{4.6}$$

Consider a variable, which has a known uncertainty δX_i. The form for representing this variable and its uncertainty is

$$X_i = X_i(measured) \pm \delta X_i \tag{4.7}$$

The result R can take values $R \pm \delta R$ and the uncertainty of δR is given by

$$\delta R = \left[\left(\frac{\partial R}{\partial X_1} \delta X_1 \right)^2 + \left(\frac{\partial R}{\partial X_2} \delta X_2 \right)^2 + \left(\frac{\partial R}{\partial X_3} \delta X_3 \right)^2 + \ldots + \left(\frac{\partial R}{\partial X_N} \delta X_N \right)^2 \right]^{1/2} \tag{4.8}$$

In many applications, the uncertainty estimate is desired as a fraction of reading, rather than in engineering units. The percent uncertainty in R is then given by $(\delta R / R) \times 100$.

4.7.2 Uncertainties Due to Measurement Error and Fluid Property

Table 4.2 Uncertainties in Measurements and Fluid Property.

Measurement & Property	Uncertainty
Temperature- T (°C)	±0.1
Pressure- P (Pa)	±0.1%
Velocity- V (m/s)	±2.0%
Voltage- U (mV)	±0.35
Current- I (mA)	±0.1
Dimension- l (mm)	±0.1
Density- ρ (kg/m^3)	0.5%

The uncertainty in the experimental measurements and fluid property are summarized in Table 4.2.

4.7.3 Uncertainty in Velocity Measurements

From mass conservation

$$V_{inlet} = \frac{V_d A_{duct} - V_{loss}}{A_{inlet}} \tag{4.9}$$

The uncertainty in impingement inlet velocity measurement is determined from

$$\frac{\delta V_{inlet}}{V_{inlet}} = \left[\left(\frac{\delta (V_d A_{duct} - V_{loss})}{(V_d A_{duct} - V_{loss})} \right)^2 + \left(\frac{\delta A_{inlet}}{A_{inlet}} \right)^2 \right]^{1/2} \tag{4.10}$$

where

$$\delta (V_d A_{duct} - V_{loss}) = \left[(A_{duct} \delta V_d)^2 + (V_d \delta A_{duct})^2 + (\delta V_{loss})^2 \right]^{1/2} \tag{4.11}$$

where δA_{duct} and δA_{inlet} are the uncertainties in duct area and impingement inlet area estimates. The side length of the duct is measured with uncertainty of 0.1 mm and all dimensions are known so δA_{duct} and δA_{inlet} can be obtained. The calibration certificate of the velocity transducer indicates the percent uncertainty of the average velocity in the plenum chamber (V_d) to be $\delta V_d / V_d$ =2.0%. The flow rate leakage losses (V_{loss}) are estimated to be approximately 3 % of total flow rate. The $\delta V_{loss} / V_{loss}$ is assumed to be 50%. The percent uncertainty in impingement inlet velocity is calculated using Eq. (4.10). The percent uncertainty is estimated to be 2.5% in the validation tests.

Using the same method, we have

$$V_{outlet} = \frac{V_d A_{duct} - V_{loss}}{A_{outlet}} \tag{4.12}$$

$$\frac{\delta V_{outlet}}{V_{outlet}} = \left[\left(\frac{\delta (V_d A_{duct} - V_{loss})}{(V_d A_{duct} - V_{loss})} \right)^2 + \left(\frac{\delta A_{outlet}}{A_{outlet}} \right)^2 \right]^{1/2} \tag{4.13}$$

The percent uncertainty in outlet velocity is estimated to be 2.5 % in the validation tests.

4.7.4 Uncertainty in the Pressure Drop Measurements

The total pressure drop is given by

$$\Delta P = P_{inlet} - P_{outlet} + \frac{1}{2}\rho\left(V_{inlet}{}^2 - V_{outlet}{}^2\right) \tag{4.14}$$

The uncertainty in pressure drop measurement is determined from

$$\delta\Delta P = \left[\left(\delta(P_{inlet} - P_{outlet})\right)^2 + \left(\rho V_{inlet}\delta V_{inlet}\right)^2 + \left(\rho V_{outlet}\delta V_{outlet}\right)^2 + \left(\frac{1}{2}(V_{inlet}{}^2 - V_{outlet}{}^2)\delta\rho \right)^2 \right]^{1/2} \tag{4.15}$$

The uncertainty in the static pressure drop measurement ($\delta(P_{inlet}$-$P_{outlet})$) is 0.1% of one inch of water column (≈0.25 Pa). The minimum and maximum measured total ΔP in validation tests was 1.28 and 60.18 Pa, respectively, from Appendix A, therefore, the uncertainties in pressure drop measurement were 19 % (for minimum ΔP) and 0.7 % (for maximum ΔP), respectively.

4.7.5 Uncertainty in Thermal Resistance Measurements

The measured total thermal resistance is given by

$$R_{total} = \frac{T_s - T_{amb}}{Q} = \frac{T_s - T_{amb}}{UI - Q_{loss}} \tag{4.16}$$

The uncertainty in thermal resistance measurement is determined from

$$\frac{\delta R_{total}}{R_{total}} = \left[\left(\frac{\delta(T_s - T_{amb})}{(T_s - T_{amb})} \right)^2 + \left(\frac{\delta(UI - Q_{loss})}{(UI - Q_{loss})} \right)^2 \right]^{1/2} \tag{4.17}$$

where

$$\delta(T_s - T_{amb}) = \left[(\delta T_s)^2 + (\delta T_{amb})^2 \right]^{1/2} \tag{4.18}$$

$$\delta(UI - Q_{loss}) = \left[(I\delta U)^2 + (U\delta I)^2 + (\delta Q_{loss})^2 \right]^{1/2} \tag{4.19}$$

According to the analysis, the primary contributor to the uncertainty is the heat losses. The voltage and current readings are less significant. The heat losses (Q_{loss}) are estimated to be approximately 3-5 % of UI. The estimation of heat losses assumes fixed thermal conductivity of the insulation and one-dimensional conduction through the insulation surrounding the copper block. The $\delta Q_{loss}/Q_{loss}$ is assumed to be 50%. The uncertainty in the total measured thermal resistance (R_{total}) was then computed, using Eq. (4.17), to be a maximum of 2.6 % for the validation test data.

Chapter 5

Results and Discussion

5.1 Introduction

This chapter presents and discusses results of the present research. The models described in Chapter 3 are validated with the experimental data taken on four heat sinks in the experimental facility described in Chapter 4, and other experimental data from the published literature. The comparisons of experimental data with the predictions from the models are given first. The differences between experimental data and model predictions are discussed. The thermal resistance network is reexamined and each of the thermal resistances is analyzed.

The results of the experiments are presented as pressure drop and thermal resistance as a function of channel velocity (V_{ch2}). The model predictions are shown in the figures along with the experimental data for comparison. The ambient temperature for the tests was 21± 2 °C, and the heat source temperature was 50-65 °C, therefore, air properties at 40 °C were used in making predictions, and 200 W/mK was used for the thermal conductivity (k) of the aluminum.

The models used for the impingement plate fin study are experimentally validated in Section 5.2 and 5.3. The major assumptions in applying the model predictions are:

(i) Uniform airflow at the heat sink impingement inlet is assumed. Fan induced airflow will actually be non-uniform.

(ii) The copper block and heat sink base will form an interface. The interface is bonded and offers negligible thermal resistance. A zero interface thermal resistance is assumed for the present work.

(iii) The flow is assumed uniform over the entire channel.

(iv) A uniform heat transfer coefficient is assumed over the heat sink surface for calculation of the thermal resistance.

(v) The air properties and thermal conductivities of the copper heat block and aluminum heat sink are assumed constant.

(vi) The fin spacing for each channel is precisely equal.

5.2 Validation of the Pressure Drop Model

5.2.1 Comparison of the Pressure Drop Model with the Experimental Data

To check the validity of the model predictions, tests were conducted on four heat sinks. In this section, the values of pressure drop predicted by the analytical model described in Chapter 3 will be compared with the values obtained experimentally. Please refer to Table 4.1 for the heat sink geometry.

Figure 5.1 shows the measured and model predicted air pressure drop of Heat Sink #1 for different impingement inlet widths. The test data errors between the measured and analytical values are summarized in Table 5.1. The highest Reynolds number in the experimental data was 1020, which is in the laminar regime. The differences between predictions and test results increase slightly with increasing flow rate.

Figure 5.2 illustrates the measured and model predicted air pressure drop of Heat Sink #2 for various impingement inlet widths. The test data errors are presented in Table 5.2. The highest Reynolds number in the experimental data was 526, which is in the laminar regime. The differences between predictions and test results increase slightly with increasing flow rate.

Figure 5.3 depicts the measured and model predicted air pressure drop of Heat Sink #3 for different impingement inlet widths. The test data errors are summarized in Table 5.3. The highest Reynolds number in the experimental data was 1270, which is in the laminar regime. The differences between predictions and test results increase slightly with increasing flow rate.

Figure 5.4 demonstrates the measured and model predicted air pressure drop of Heat Sink #4 for varied impingement inlet widths. The test data errors are presented in Table 5.4. The highest Reynolds number in the experimental data was 820, which is in the laminar regime. The differences between predictions and test results increase gradually with increasing flow rate.

The uncertainty in static pressure drop measurement ($\delta(P_{inlet}-P_{outlet})$) is 0.1% of one inch of water column (≈0.25 Pa), therefore, the uncertainty in total pressure drop measurement increases when total pressure drop is small in terms of Eq. (4.15). This explains the relatively large difference in test data and predicted values when total pressure drop is small.

Table 5.1 The pressure drop test errors of Heat Sink #1.

s	10% L	25% L	50% L	75% L	100% L
error	2.2-12.6 %	0.7-15.2 %	1.2-12.4 %	0.5-16.0 %	4.5-20.9 %
RMS	7.3 %	8.7 %	10.0%	9.1%	12.8 %

Table 5.2 The pressure drop test errors of Heat Sink #2.

s	10% L	25% L	50% L	75% L	100% L
error	2.1-10.1 %	0.7-19.2 %	4.2-20.4 %	4.1-17.3 %	5.6-20.5 %
RMS	8.1 %	12.9 %	13.2%	11.8%	12.6 %

Table 5.3 The pressure drop test errors of Heat Sink #3.

s	10% L	25% L	50% L	75% L	100% L
error	6.9-12.1 %	1.0-15.8 %	0.4-7.6 %	3.9-15.5 %	0.2-18.8 %
RMS	9.6 %	12.5 %	5.5%	12.9%	13.5 %

Table 5.4 The pressure drop test errors of Heat Sink #4.

s	10% L	25% L	50% L	75% L	100% L
error	1.0-13.6 %	1.4-11.6 %	0.8-17.4 %	3.5-16.8 %	7.3-20.1 %
RMS	11.3 %	10.8 %	12.1%	12.5%	16.3 %

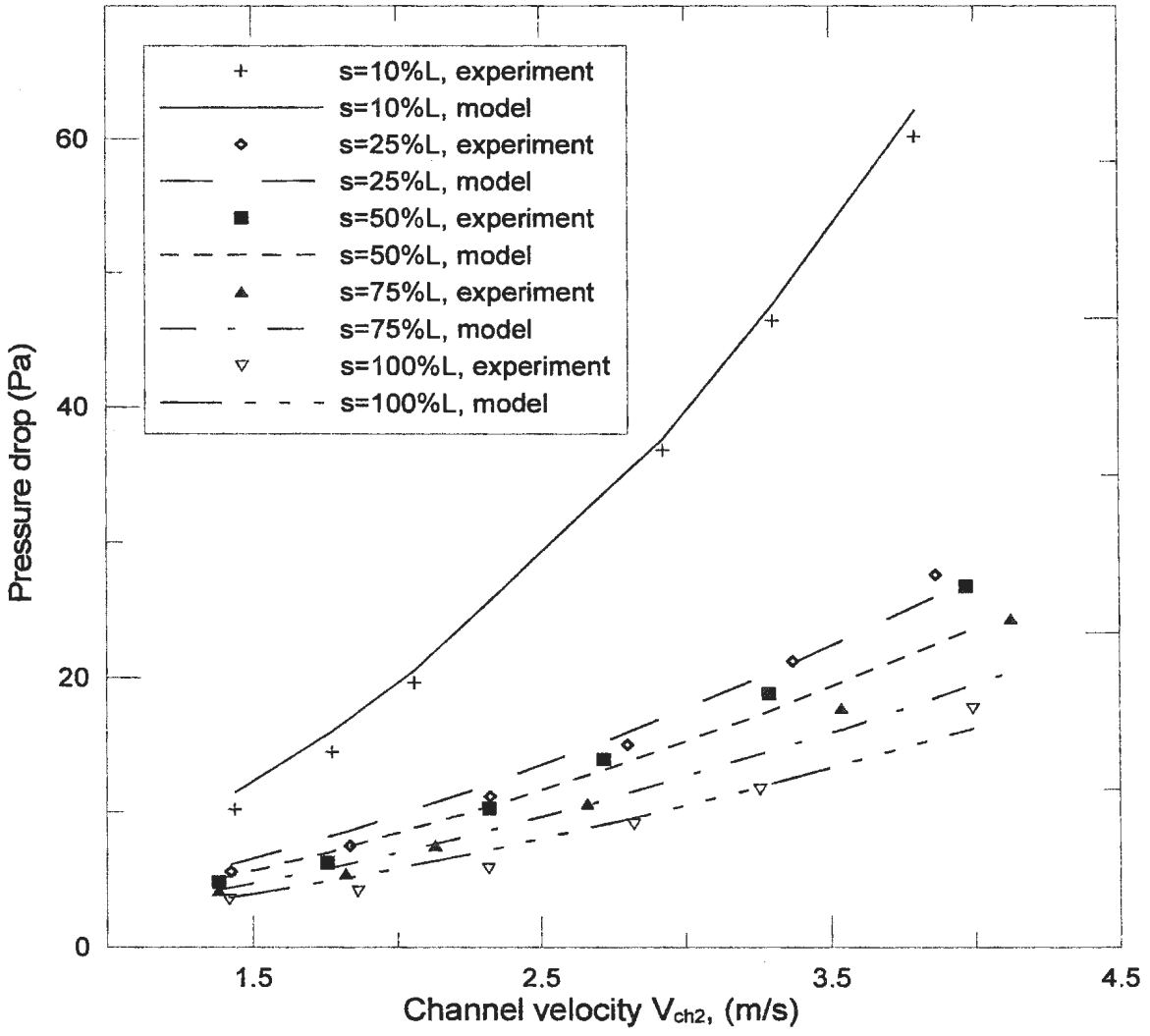

Figure 5.1 Pressure drop comparison for Heat Sink #1.

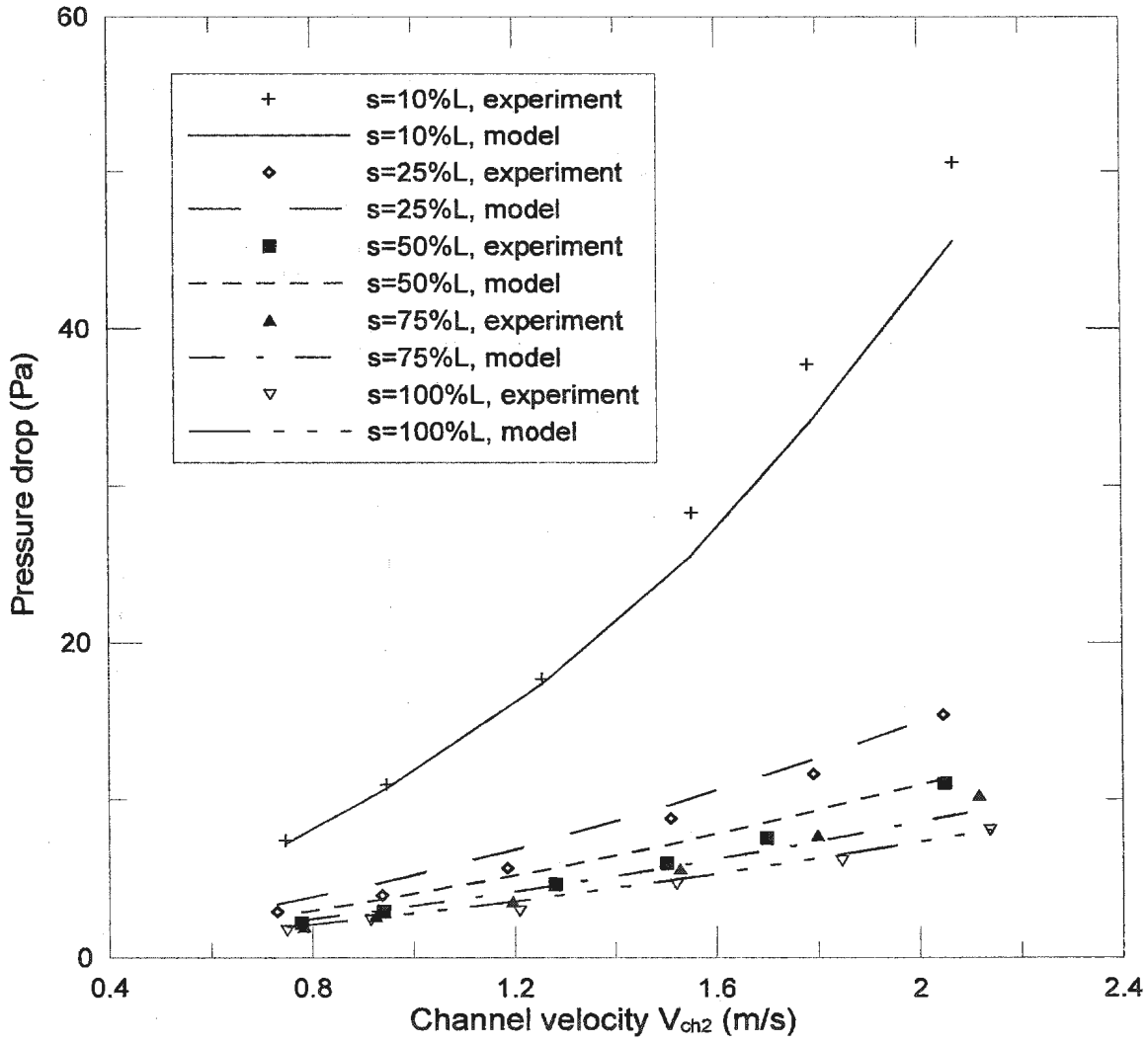

Figure 5.2 Pressure drop comparison for Heat Sink #2.

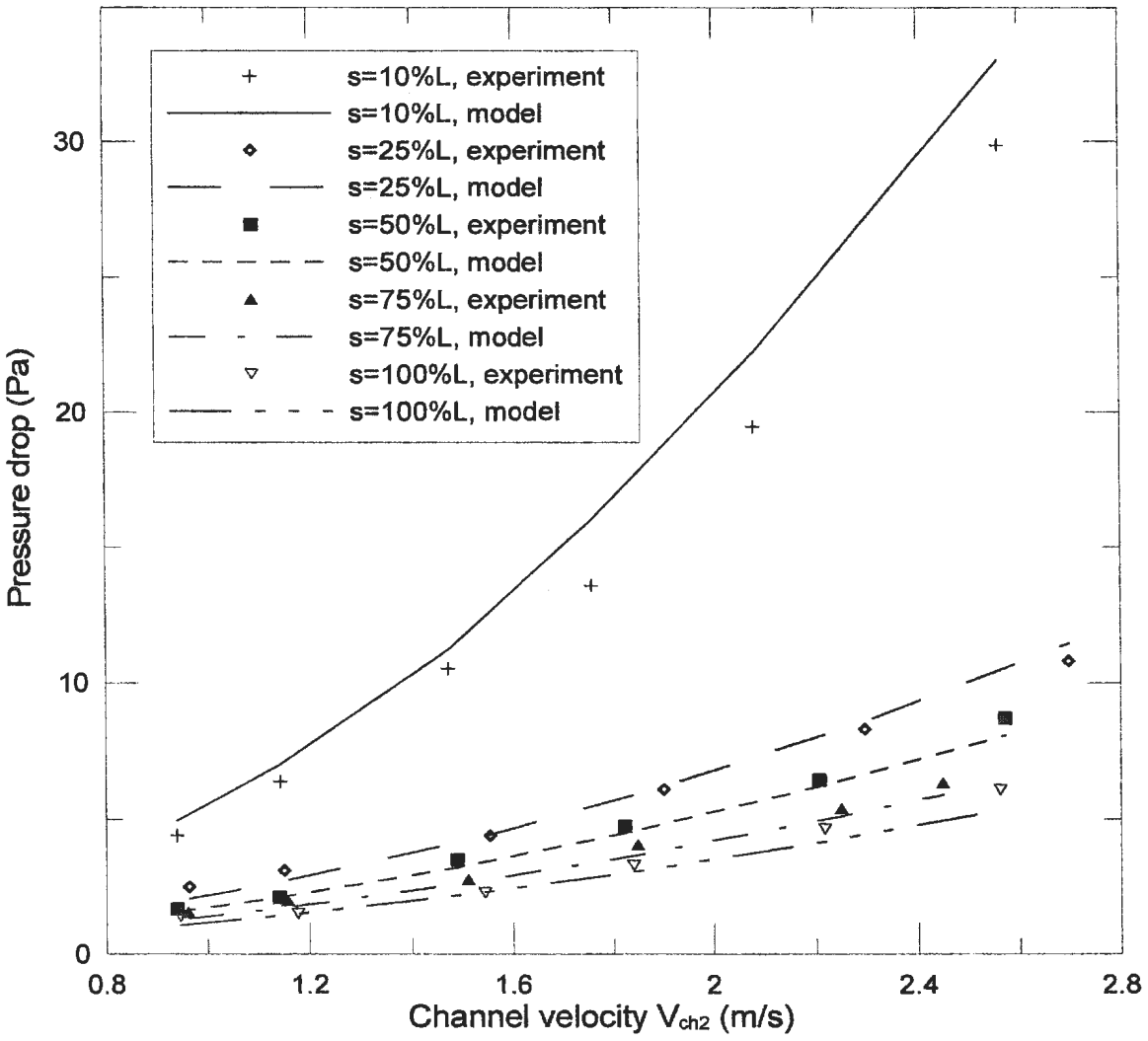

Figure 5.3 Pressure drop comparison for Heat Sink #3.

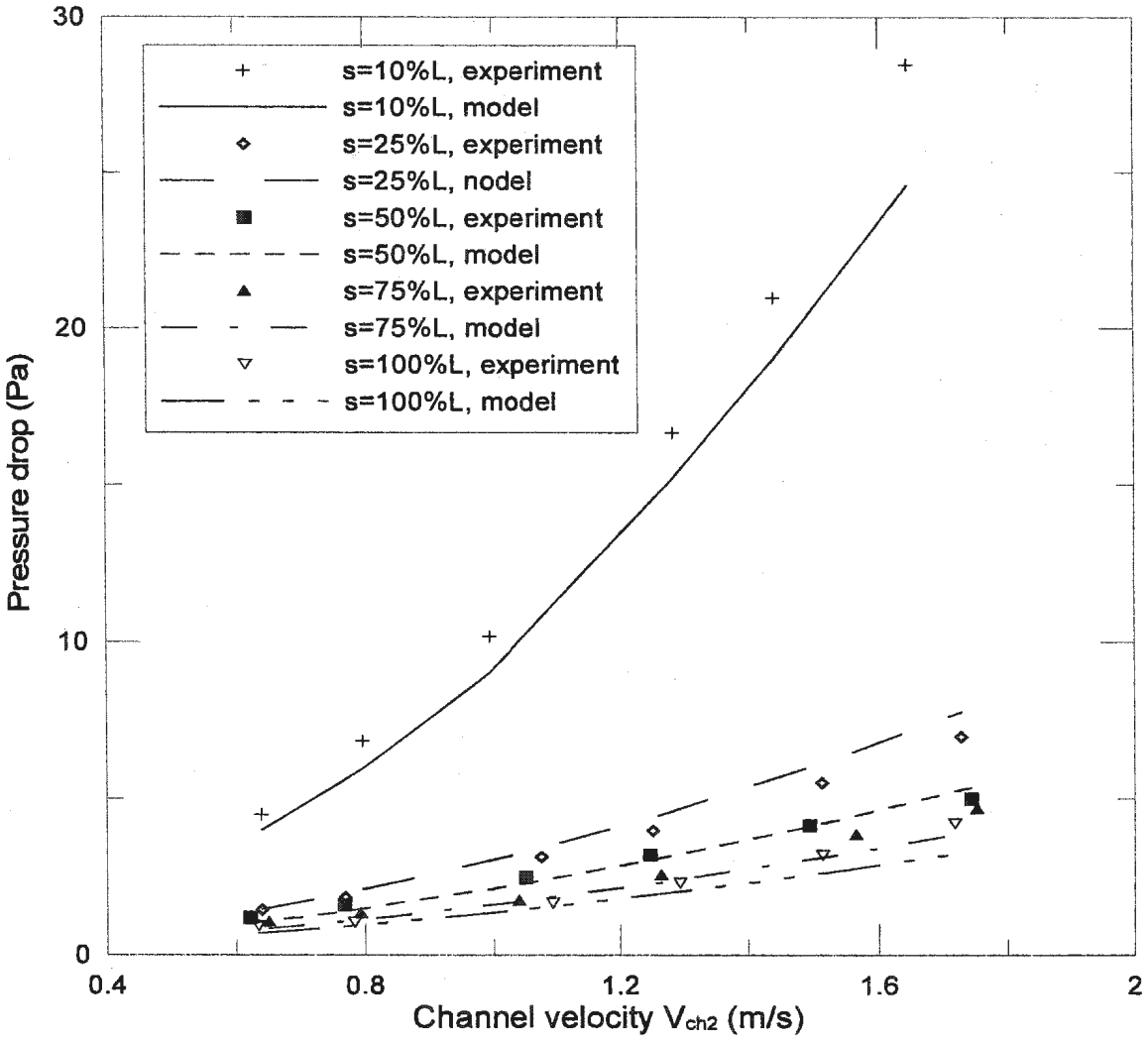

Figure 5.4 Pressure drop comparison for Heat Sink #4.

5.2.2 Comparison of the Model with Other Experimental Data

Figure 5.5 shows the comparison between the Saini and Webb (2002) experimental data and the analytical model predictions of total pressure drop. The details of the heat sink used for the test are summarized in Table 5.5. These test data are consistently lower than the predictions by 5.9% to 20.3 % with an RMS error of 15.1 %. The over prediction decreases from 20.3 % to 5.9 % with increasing flow rate. Overall, the trend is very good.

Table 5.5 Geometry of the heat sink used in Saini and Webb (2002) experiment.

s (mm)	L (mm)	W (mm)	t_b (mm)	t (mm)	b (mm)	H (mm)	N_f
31.5	76	59.5	4.9	0.5	1.5	29	30

Figure 5.6 demonstrates the comparison between the Holahan (1996) experimental data and the analytical model predictions of total pressure drop. The geometry of the heat sink used for the test is detailed in Table 5.6. These test data errors are 1.0-12.5 % with an RMS error of 8.0 %. The differences between predictions and test results increase slightly with increasing flow rate.

Table 5.6 Geometry of the heat sink used in Holahan (1996) experiment.

s (mm)	L (mm)	W (mm)	t_b (mm)	t (mm)	b (mm)	H (mm)	N_f
50	75	145	10	1.01	0.9	34	74

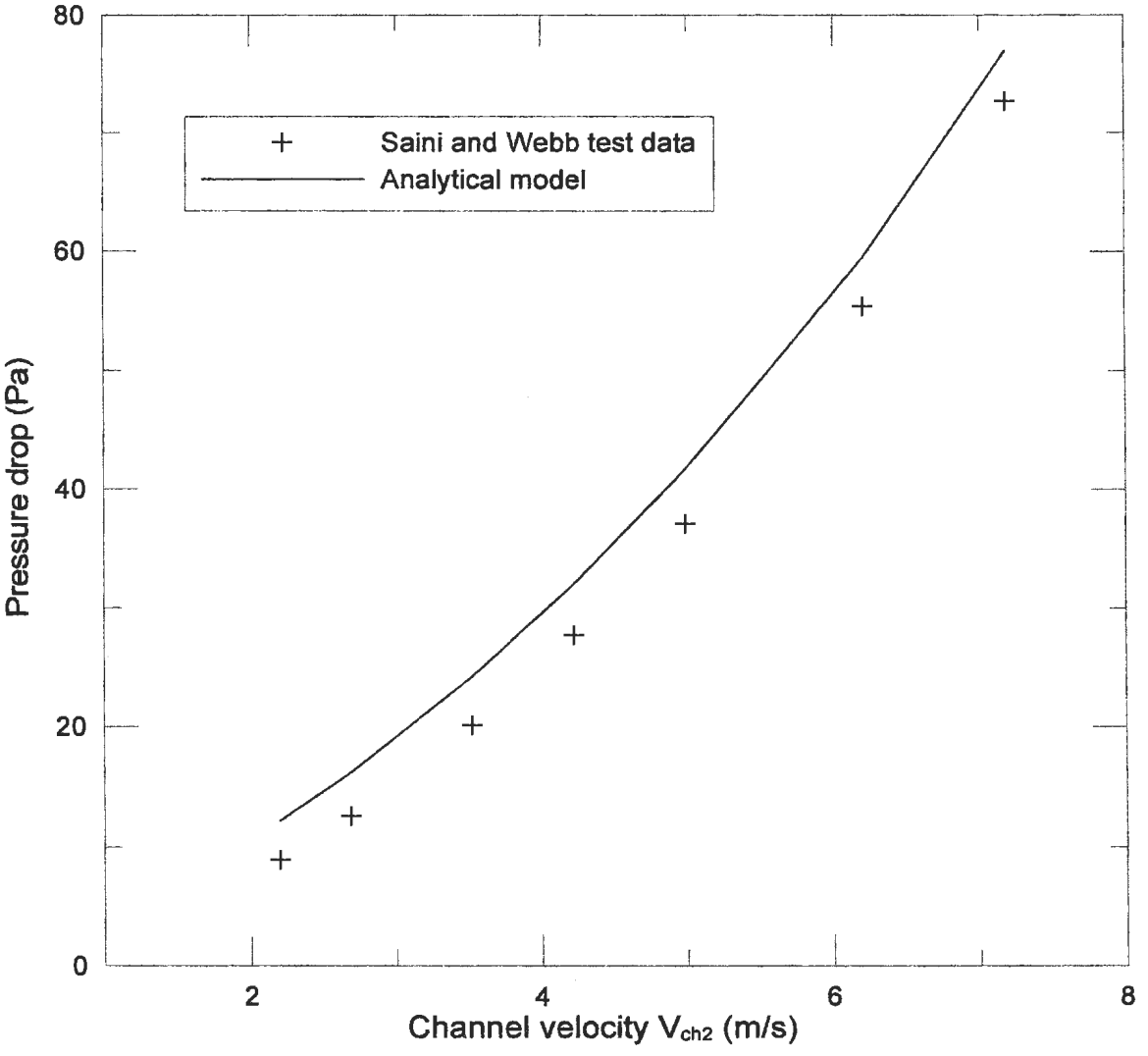

Figure 5.5 Pressure drop comparison for Saini and Webb (2002) test data.

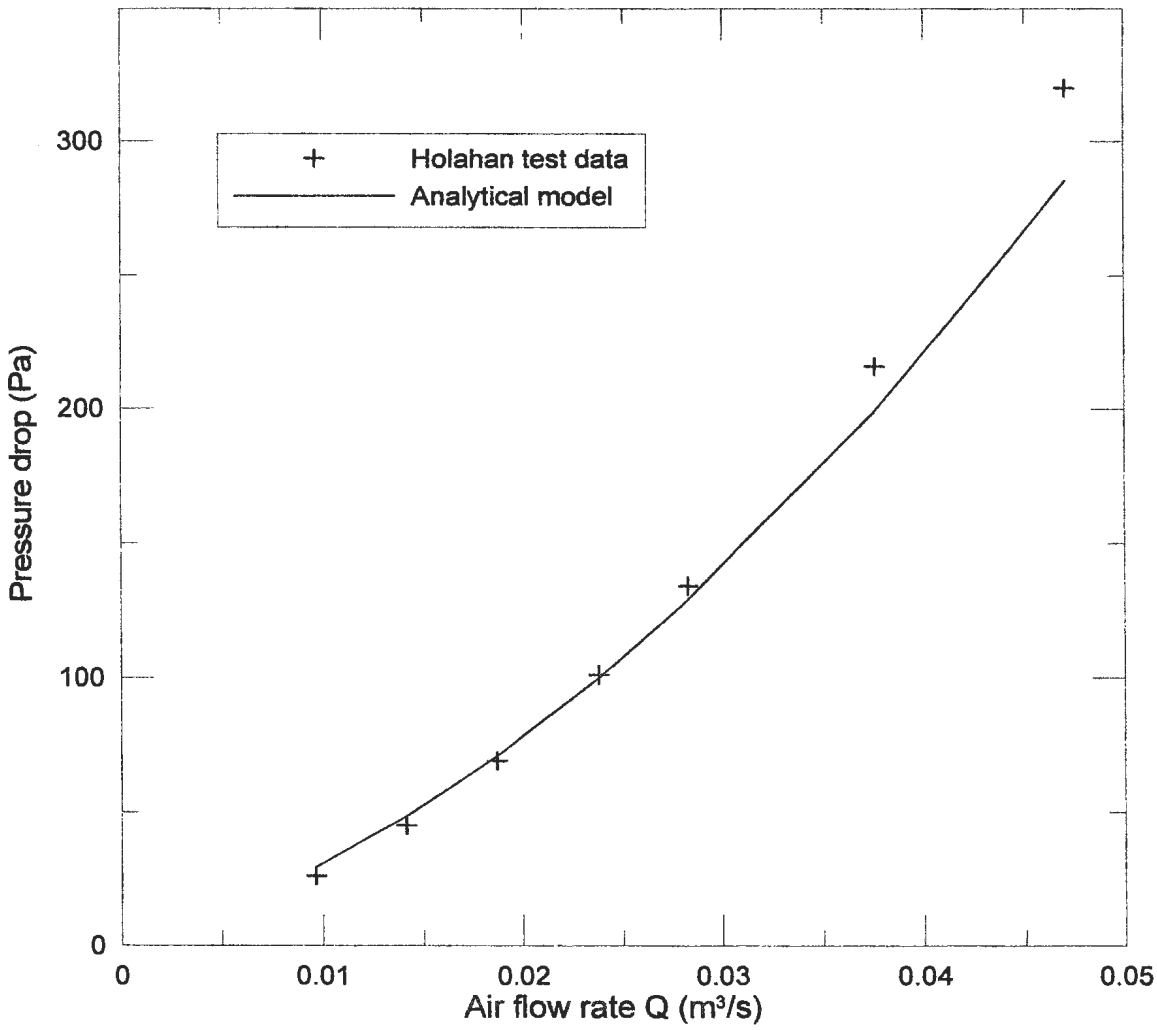

Figure 5.6 Pressure drop comparison for Holahan (1996) test data.

Although the pressure drop prediction algorithm is based on a very simple model, it succeeds in representing the trends of the experimental values fairly well. The test data and predictions are, therefore, in very good agreement after accounting for the combined uncertainties of the predictions and experiments. The agreement is quite satisfying in view of the simplicity of the model. Given the uncertainties of pressure drop measurements, the model is reasonably well validated.

It is noted that fan mounted heat sinks used in electronics cooling typically operate with a Reynolds number between 300 - 1000. Despite the fact that the prediction algorithm for pressure drop used in this thesis is based on an extremely simple model, it was found that the predicted pressure drop agrees with experimental values within about ±20% and 11.5 % RMS for all data in the typical operating range.

5.2.3 Effects of Impingement Inlet Width

The effects of impingement inlet width on pressure drop are shown in Figures 5.1-5.4. Both the predicted and the experimental data illustrate that the total pressure drop increased as the same flow rate was held constant, but the impingement inlet width was decreased. This is due to the fact that the impingement inlet velocity increases when the impingement inlet width becomes small. Thus, the sudden contraction pressure loss increases. When the impingement inlet width surpasses 25% of the heat sink length, the pressure drop changes are relatively insignificant.

5.2.4 Effects of Fin Spacing

The effects of fin spacing on pressure drop are illustrated by the results for Heat Sink #2 and Heat Sink #4, which have the same dimensions except for fin spacing (b). Figure 5.7 shows the experimental values of total pressure drop for Heat Sinks #2 and #4 for impingement inlet widths of 10% and 25%L. Both the predicted and the experimental values increase with a decrease in fin spacing for the same volumetric flow rate. This is due to the fact that channel velocity increases when the fin spacing decreases. Thus, the sudden contraction and expansion pressure losses increase.

When the fin spacing is very small, the surface area of the heat sink increases considerably, the contraction pressure loss at the impingement inlet and the expansion pressure loss at outlet of the heat sink increase, and this effect is significant. When the fin spacing becomes large, the pressure drop decreases and the extended surface area of heat sink also decreases. Moreover, if the performance of the cooling fan is taken into account, the pressure drop will increase and volumetric flow rate will decrease as spacing between the fins becomes small.

5.2.5 Effects of Fin Height

The effects of fin height on pressure drop are illustrated by comparison of the results for Heat Sinks #1 and #2, and Heat Sinks #3 and #4. Heat Sinks #1 and #2 have the same

dimensions except for fin height (H). Heat Sinks #3 and #4 have the same dimensions except for fin height (H). Figure 5.8 depicts the experimental values of total pressure drop for Heat Sinks #1 and #2, and Figure 5.9 demonstrates the experimental values of total pressure drop for Heat Sink #3 and #4. As shown in the figures the total pressure drop increases with a decrease in fin height for the same volumetric flow rate. This is due to the fact that the channel velocity increases when the fin height reduces. Thus, the total pressure loss increases.

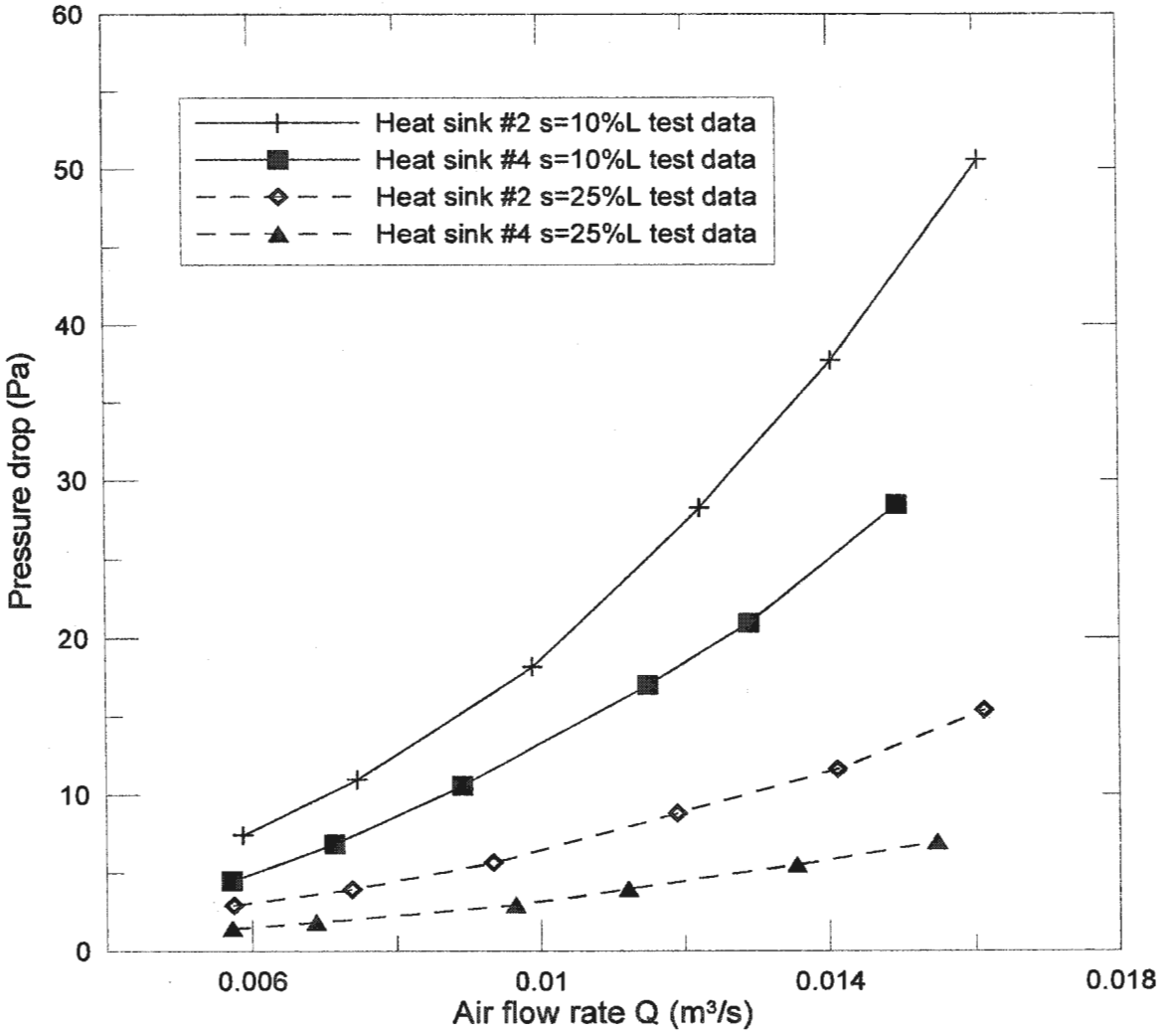

Figure 5.7 Effects of fin spacing on pressure drop.

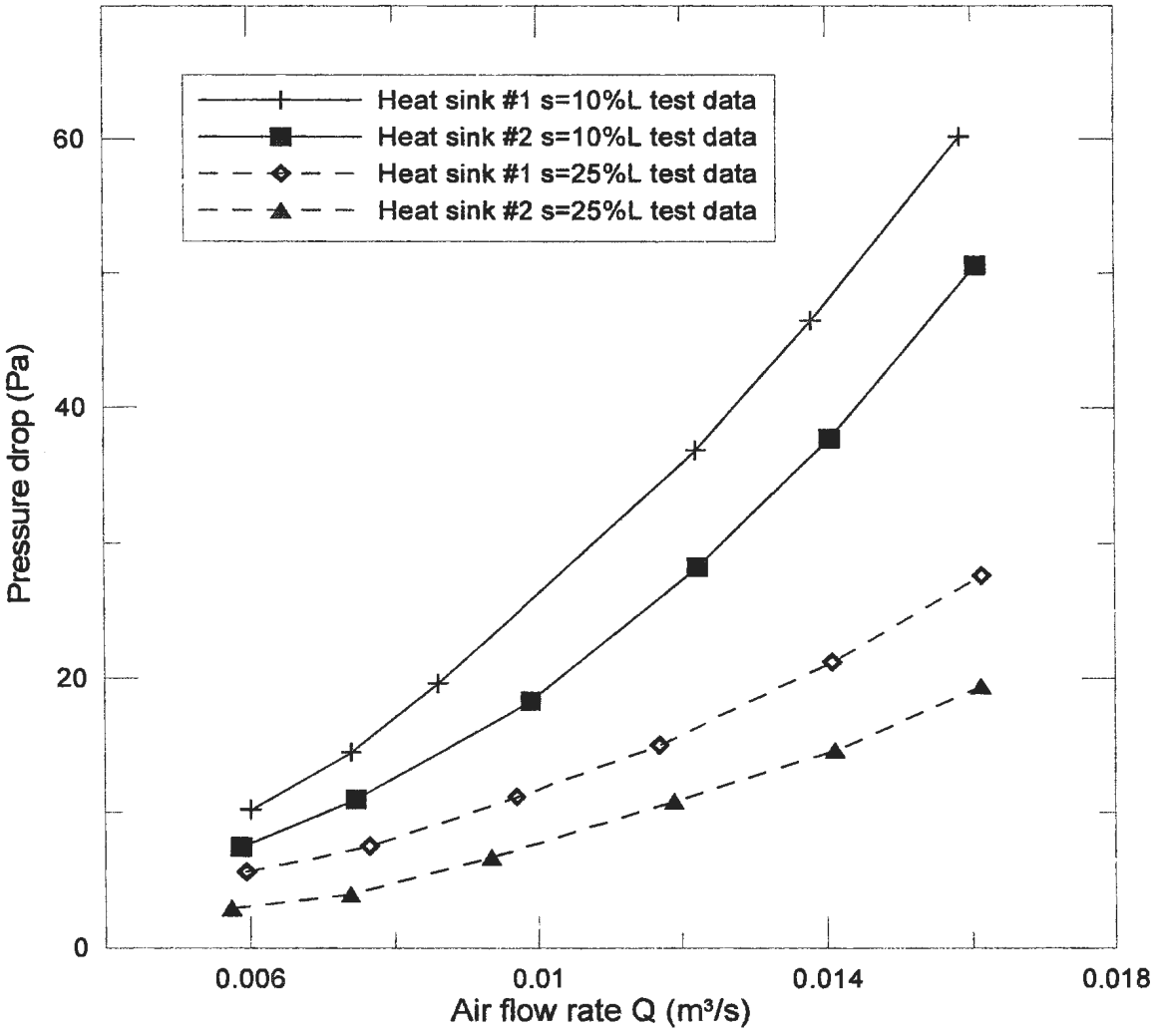

Figure 5.8 Effects of fin height on pressure drop for Heat Sinks #1 and #2.

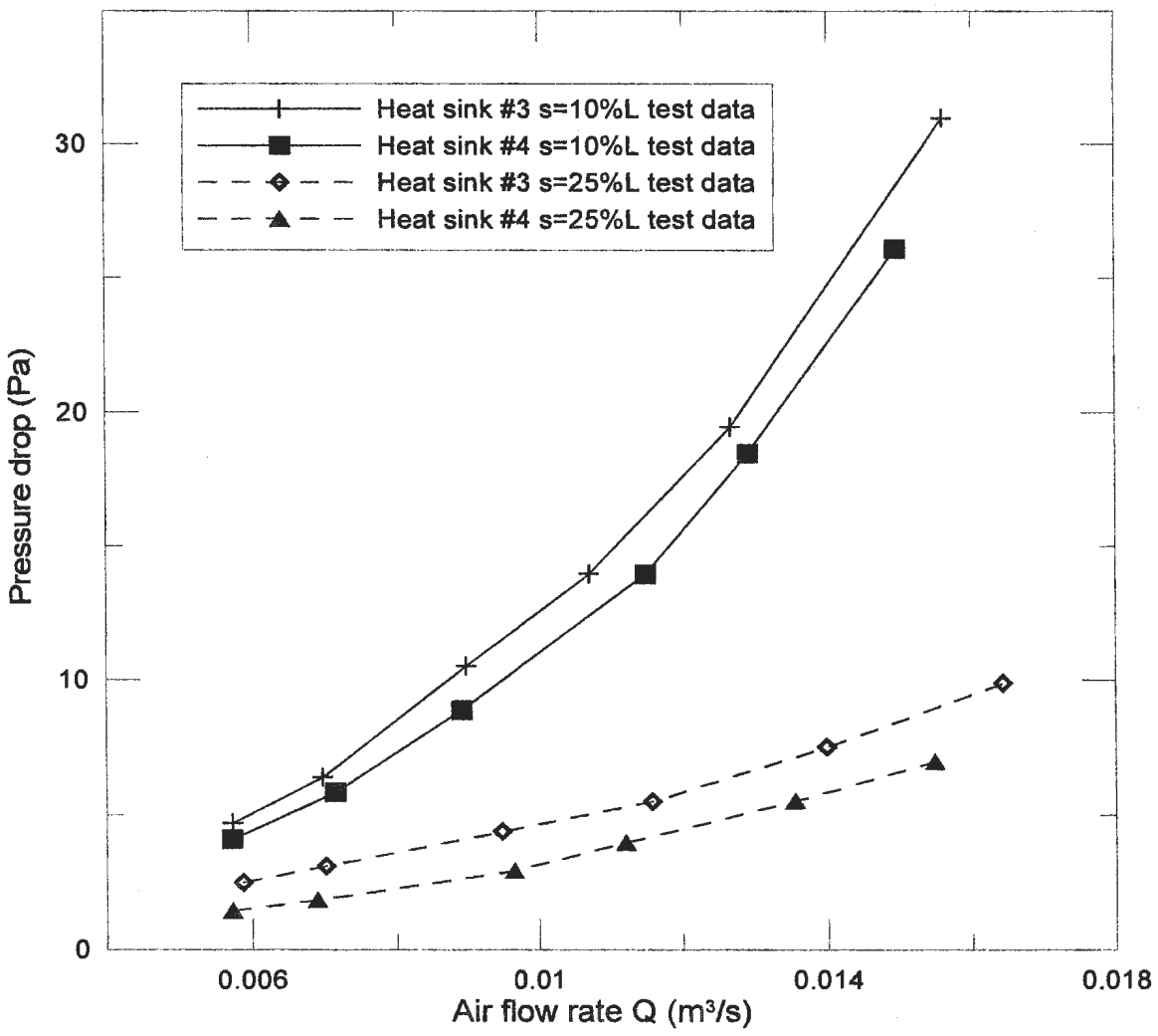

Figure 5.9 Effects of fin height on pressure drop for Heat Sinks #3 and #4.

5.3 Validation of the Thermal Resistance Model

5.3.1 Comparison of the Thermal Resistance Model with the Experimental Data

The analytical thermal resistance model developed in Chapter 3 was evaluated by application to four heat sinks. As was done for the pressure drop model, the experimental results were used to compare with thermal resistance model. Please refer to Table 4.1 for the geometry of the four heat sinks tested.

Figure 5.10 shows the measured and predicted thermal resistance of Heat Sink #1 for different impingement inlet widths. The test data errors between the measured and analytical values are summarized in Table 5.7. The model under predicts measured thermal resistance. The under predictions increase gradually with increasing flow rate.

Figure 5.11 illustrates the measured and predicted thermal resistance of Heat Sink #2 for various impingement inlet widths. The test data errors are presented in Table 5.8. The test data are higher than the predicted values. The differences between predictions and test results increase further with increasing flow rate.

Figure 5.12 demonstrates the measured and predicted thermal resistance of Heat Sink #3 for different impingement inlet widths. The test data errors are summarized in Table 5.9.

The model under predicts measured thermal resistance. The data are increasingly under predicted with increasing flow rate.

Figure 5.13 compares the measured and predicted thermal resistance of Heat Sink #4 for different impingement inlet widths. The test data errors are presented in Table 5.10. The test data are higher than the predicted values. The differences between predictions and test results increase gradually with increasing flow rate.

The thermal test had a small air leakage at the end of the impingement inlet. The average air velocity in the channel will decrease if the leakage is considered and the thermal resistance data will show a slightly better match with predictions.

Table 5.7 The thermal resistance test errors of Heat Sink #1.

s	10% L	25% L	50% L	75% L	100% L
error	3.1-10.7 %	0.2-8.6 %	3.7-14.0 %	5.9-8.1 %	9.3-18.6%
RMS	8.0 %	5.9 %	8.9%	7.1%	14.1%

Table 5.8 The thermal resistance test errors of Heat Sink #2.

s	10% L	25% L	50% L	75% L	100% L
error	3.3-17.2 %	0.5-16.7 %	2.6-20.7 %	1.4-20.3 %	3.3-19.7%
RMS	10.0 %	10.6 %	12.9%	12.5%	13.7%

Table 5.9 The thermal resistance test errors of Heat Sink #3.

s	10% L	25% L	50% L	75% L	100% L
error	7.4-14.1 %	11.6-15.1 %	11.5-18.7 %	12.7-18.8 %	12.6-17.3%
RMS	10.4 %	13.9 %	15.2%	16.1%	15.2%

Table 5.10 The thermal resistance test errors of Heat Sink #4.

s	10% L	25% L	50% L	75% L	100% L
error	1.8-9.2 %	0.7-12.7 %	0.6-15.9 %	3.6-16.1 %	4.8-15.9%
RMS	5.1 %	7.4 %	9.5%	10.1%	10.0%

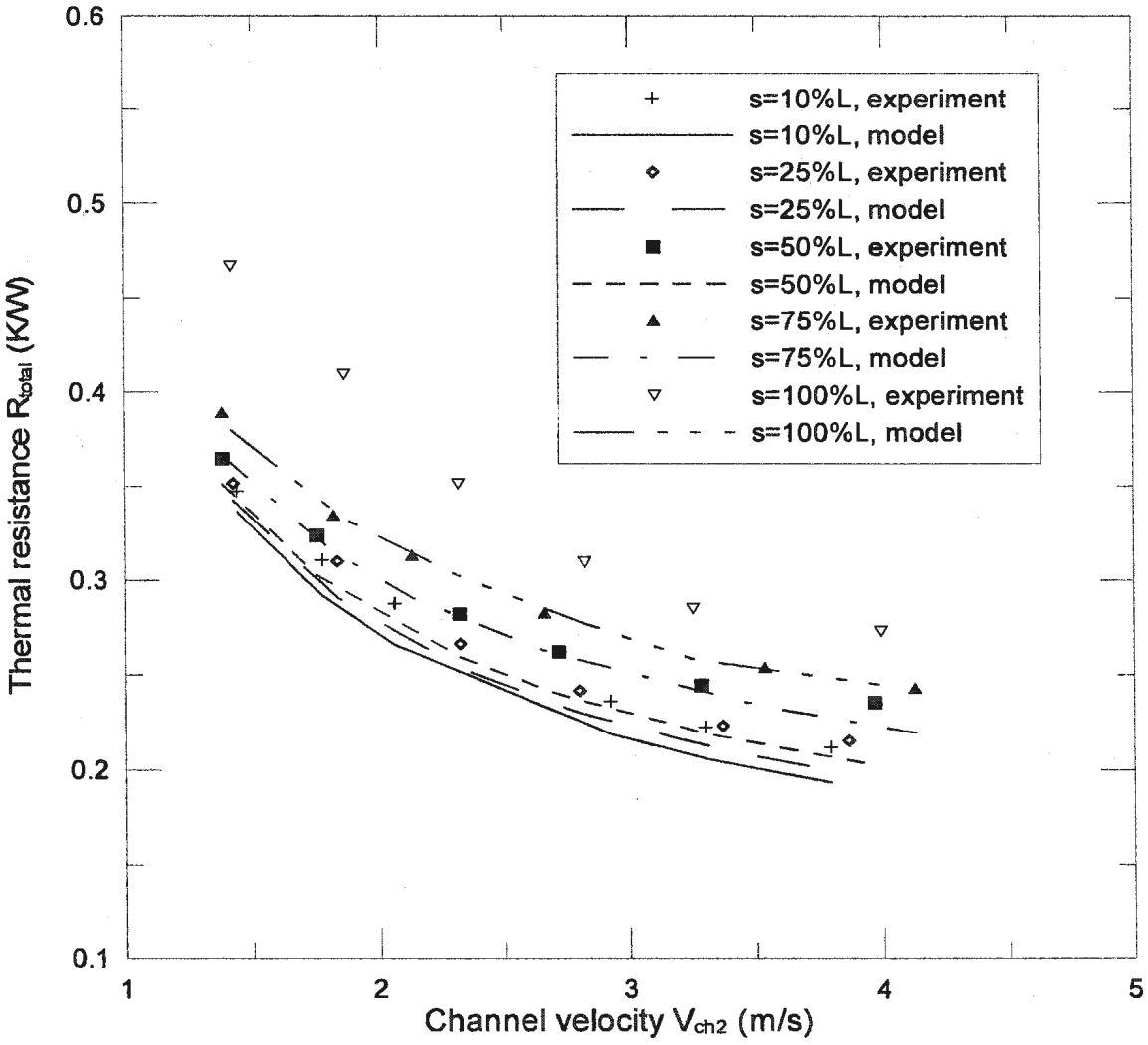

Figure 5.10 Thermal resistance comparison for Heat Sink #1.

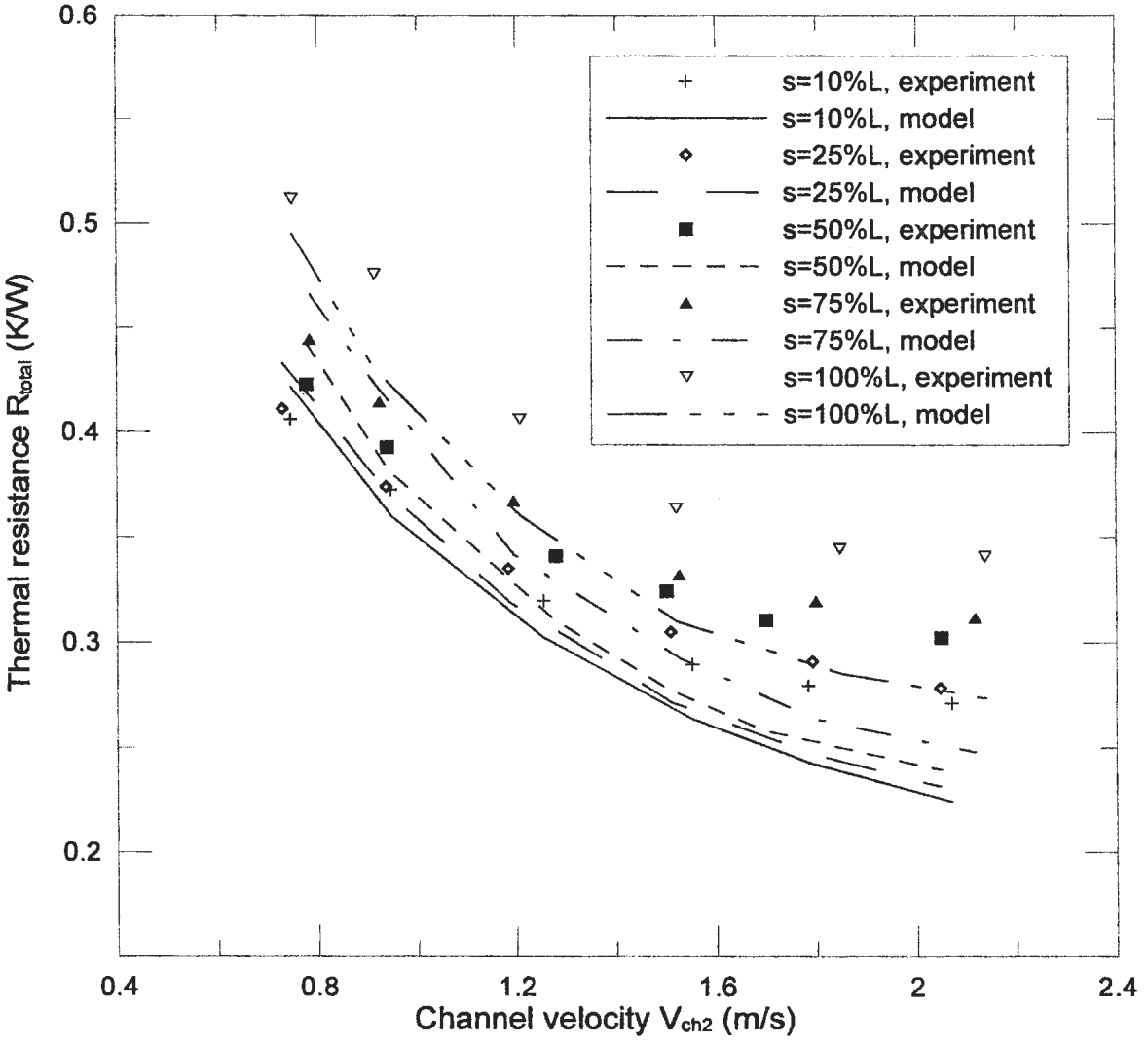

Figure 5.11 Thermal resistance comparison for Heat Sink #2.

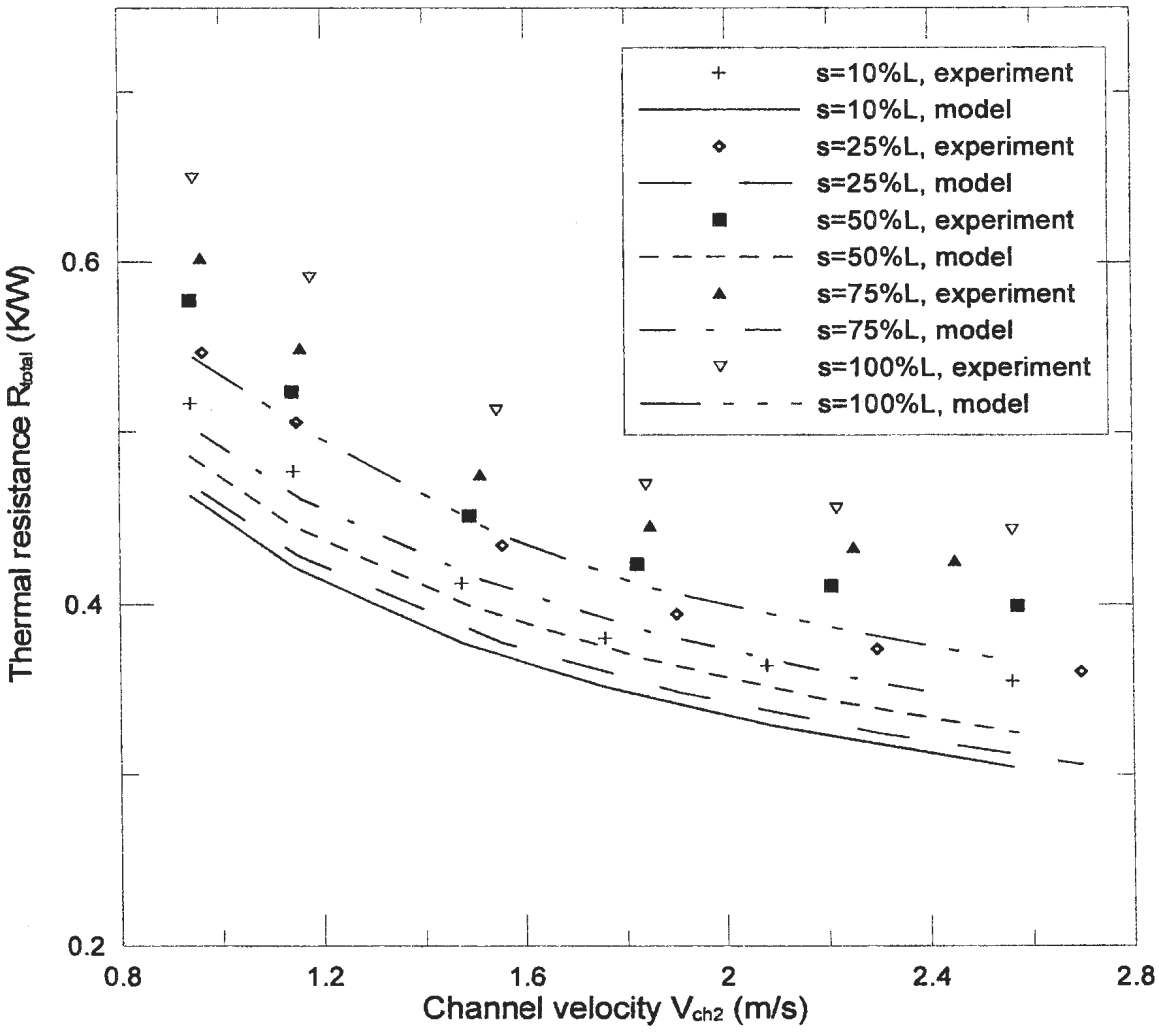

Figure 5.12 Thermal resistance comparison for Heat Sink #3.

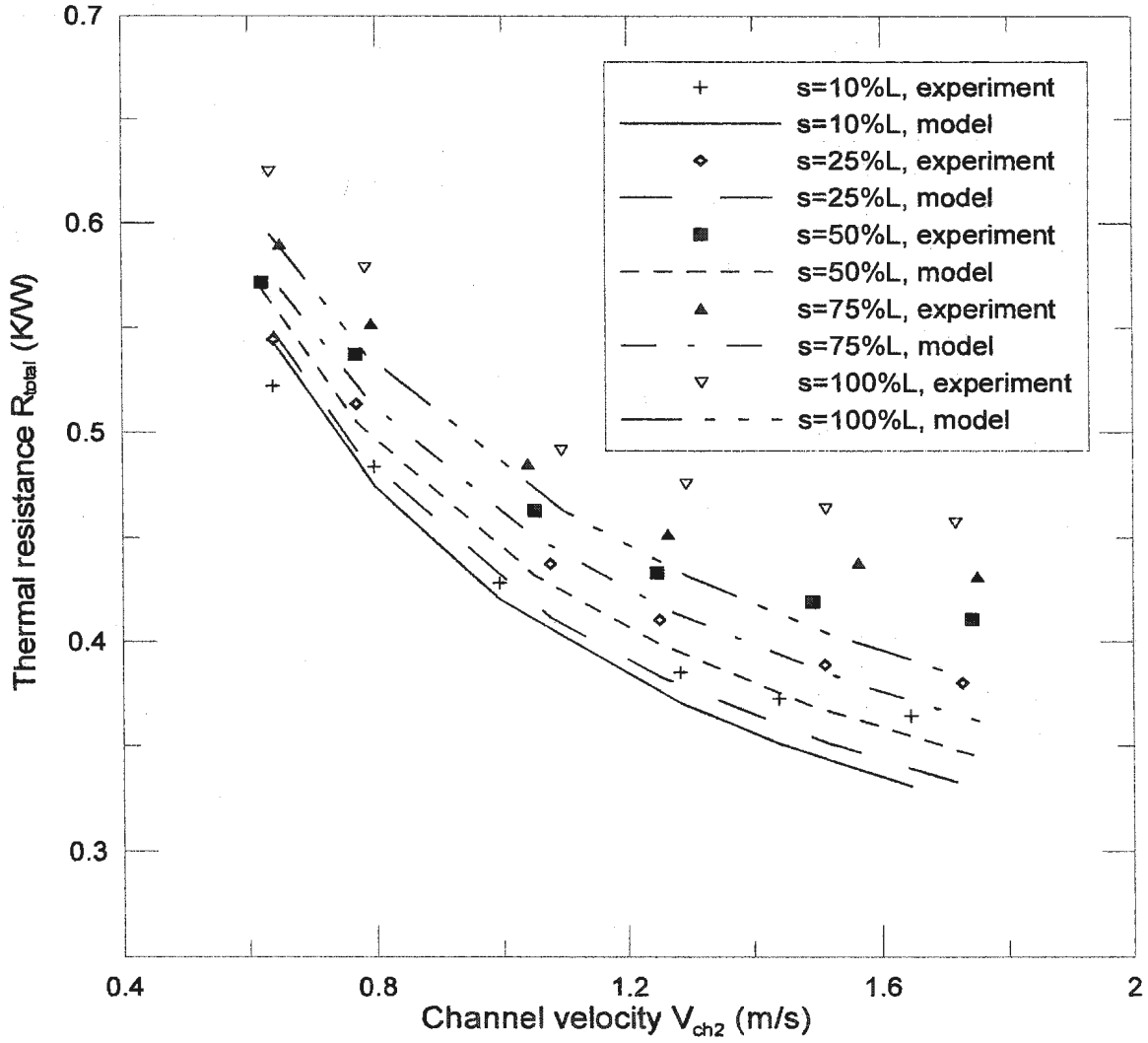

Figure 5.13 Thermal resistance comparison for Heat Sink #4.

5.3.2 Comparison of the Model with Other Test Data

Figure 5.14 shows the comparison between the Saini and Webb (2002) experimental data and the analytical model predictions of total thermal resistance. The details of the heat sink used for the test are summarized in Table 5.5. The test data errors are within 5.1% to 23.2 % with an RMS error of 12.8 %. The experimental data are higher than the predictions at lower flow rate and lower than the predictions at higher flow rate. The over prediction increases with the increasing flow rate.

Figure 5.15 shows the comparison between the Holahan (1996) experimental data and the predictions of total thermal resistance. The geometry of the heat sink used for the test is summarized in Table 5.6. The test data errors are within 0.3 to 4.6 % with an RMS errors of 3.5 %. The experimental data are only a little higher than the predictions, and the experimental data and predictions are in excellent agreement.

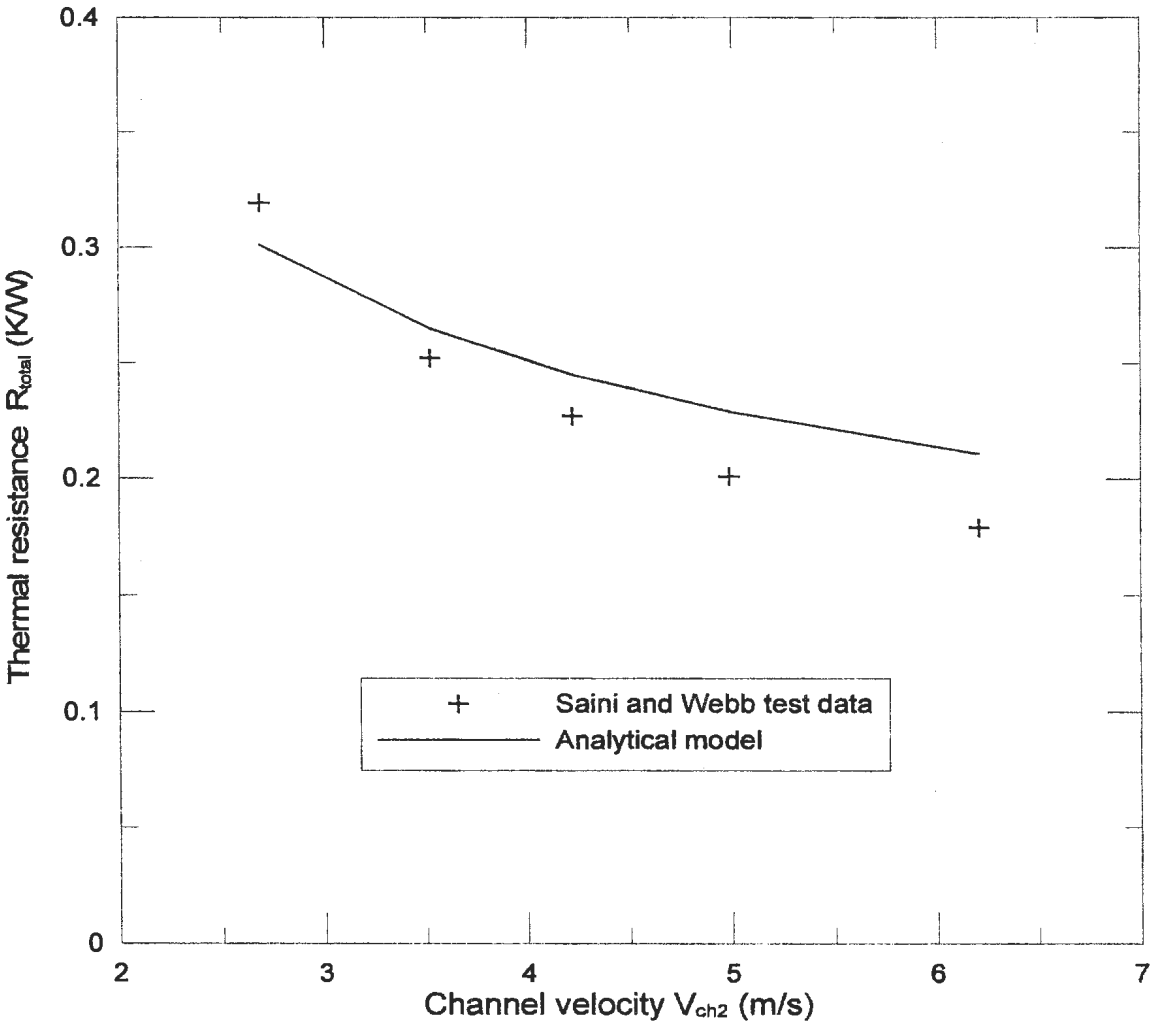

Figure 5.14 Thermal resistance comparison for Saini and Webb (2002) test data.

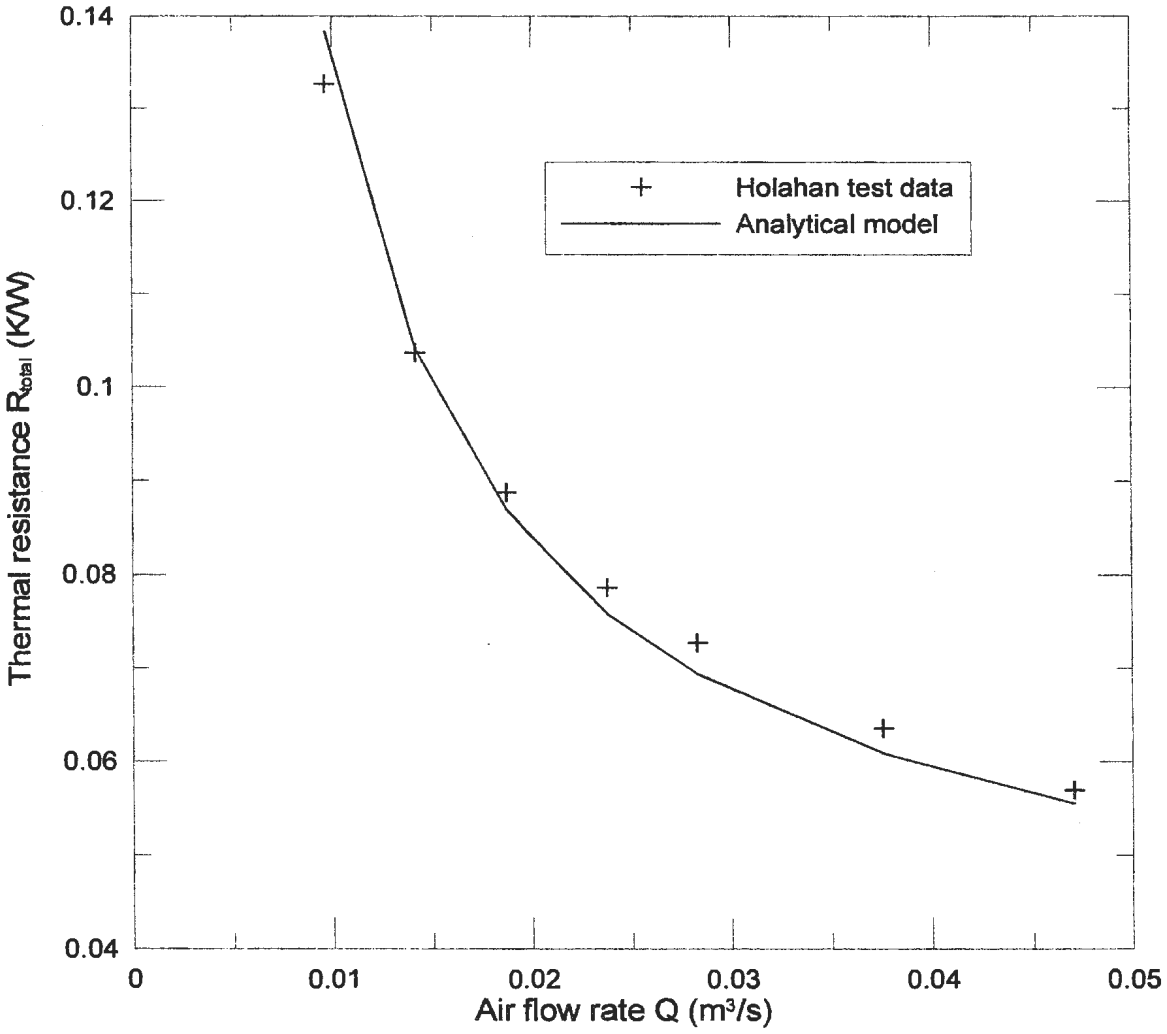

Figure 5.15 Thermal resistance comparison for Holahan (1996) test data.

The accuracy of the predictions of thermal resistance was investigated by comparing them with the experimental measurements. Although the thermal resistance prediction algorithm is based on a very simple model, it succeeds in representing the trends of the experimental values fairly well. The test data and predictions are, therefore, in very good agreement after accounting for the combined uncertainties of the predictions and experiments. The agreement is quite satisfying in view of the simplicity of the model. Given the uncertainties of thermal resistance measurements, the model is reasonably well validated.

It is noted that fan mounted heat sinks used in electronics cooling typically operate with a Reynolds number between 300 - 1000. Despite the fact that the prediction algorithm for thermal resistance used in this thesis is based on an extremely simple model, it was found that the predicted thermal resistance agrees with experimental values within about ±20% and 11.1% RMS for all data in the typical operating range.

The calculated value of fin efficiency was almost constant for the present study; therefore, fin efficiency did not pose a problem in this study. The fin efficiency varies from a high value of 0.97 at low channel velocity (V_{ch2}) to a moderate value of 0.93 at highest channel velocity.

5.3.3 Effects of Impingement Inlet Width

The effects of impingement inlet width on thermal resistance are shown in Figures 5.10-5.13. From these figures it can be seen that, for the same flow rate, the total thermal resistance decreases when the impingement inlet width becomes smaller. This is due to the high impingement channel velocity, which makes the impingement heat transfer coefficient large in the case of small inlet widths. As the heat transfer coefficient increases, however, the total pressure drop also increases, as discussed in section 5.2.3.

5.3.4 Effects of Fin Spacing

The effects of fin spacing on thermal resistance are illustrated by the results for Heat Sink #2 and Heat Sink #4, which have the same dimensions except for fin spacing (b). Figure 5.16 shows the behaviour of the thermal resistance with changes in the spacing between fins. Both the predicted and the experimental values increase with an increase in fin spacing for the same volumetric flow rate. This is due to the fact that channel velocity decreases when the fin spacing increases. Thus, the impingement heat transfer coefficient decreases and thermal resistance increases.

When the fins are closely spaced, the surface area of the heat sink increases, the contraction pressure loss at the impingement inlet and the expansion pressure loss at outlet of the heat sink increase, and this effect dominates. When the fin spacing becomes

larger, although the pressure drop decreases, the surface area of the heat sink also decreases and this makes the rate of heat transfer lower. Furthermore, the pressure drop increases remarkably and volumetric flow rate decreases as the spacing between the fins becomes smaller, if the performance of the cooling fan is taken into account.

As the air is supplied by a cooling fan, the balance between thermal resistance and pressure drop is very important. It is necessary to minimize the thermal resistance, while the pressure drop is maintained at a reasonable level.

5.3.5 Effects of Fin Height

The effects of fin height on thermal resistance are illustrated by comparison of the results for Heat Sinks #1 and #2, and Heat Sinks #3 and #4. Heat Sinks #1 and #2 have the same dimensions except for fin height (H). Heat Sinks #3 and #4 have the same dimensions except for fin height (H). Figure 5.17 depicts the experimental values of thermal resistance for Heat Sinks #1 and #2, and Figure 5.18 demonstrates the experimental values of thermal resistance for Heat Sink #3 and #4. As shown in the figures the thermal resistance increase with an increase in fin height for the same volumetric flow rate. This is due to the fact that the channel velocity decreases when the fin height increases. Thus, the impingement heat transfer coefficient decreases and thermal resistance increases.

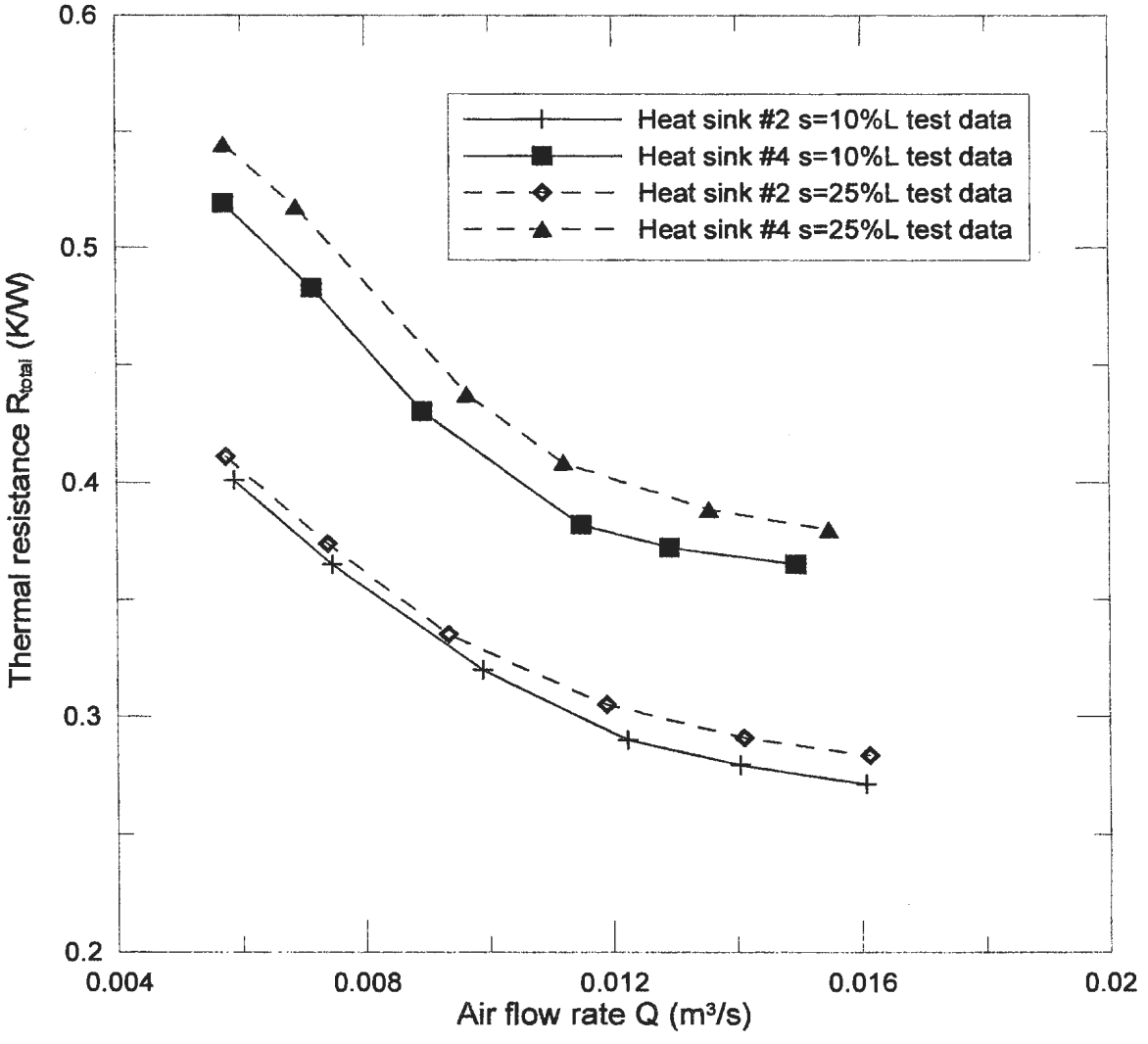

Figure 5.16 Effects of fin spacing on thermal resistance.

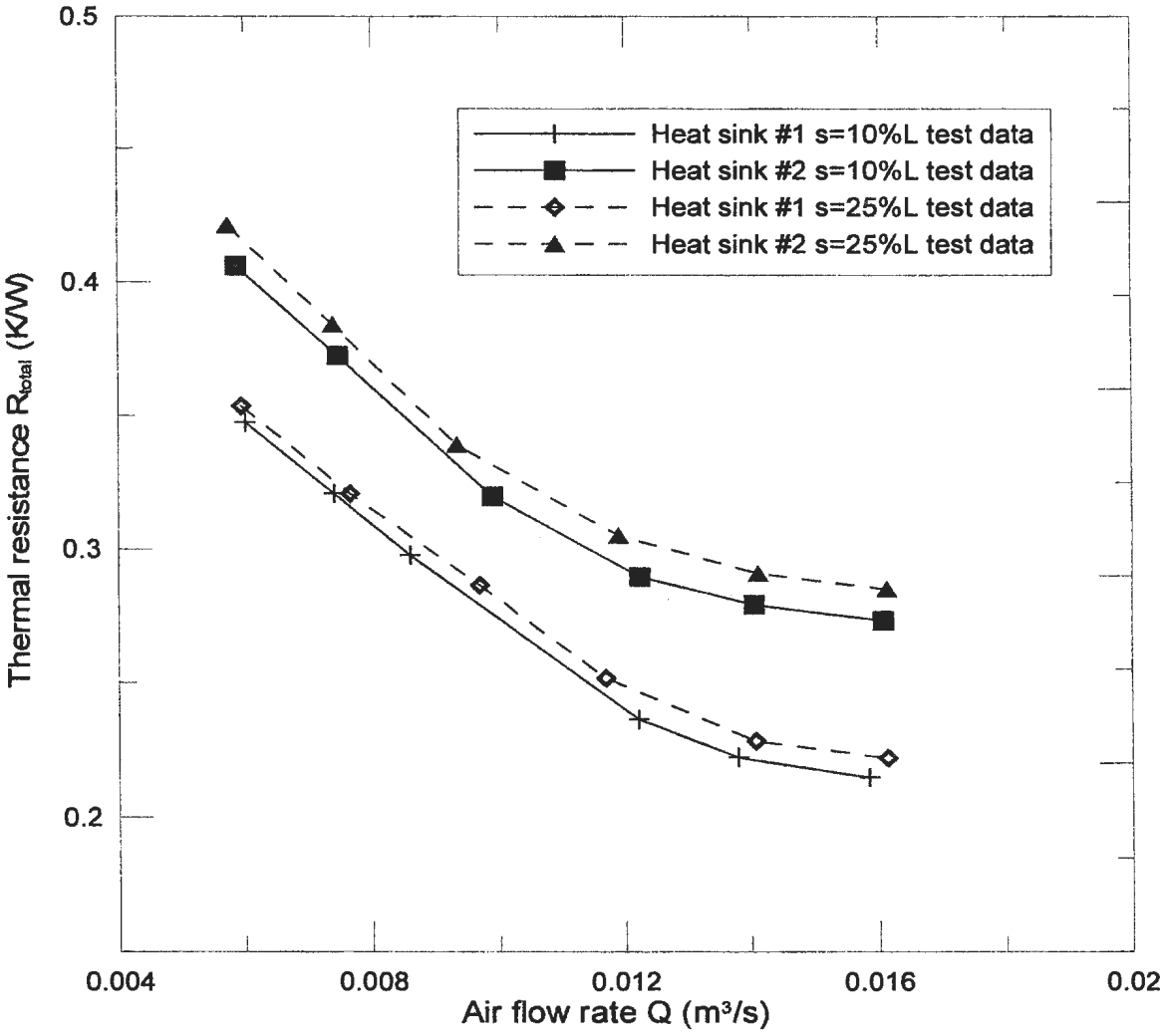

Figure 5.17 Effects of fin height on thermal resistance for Heat Sinks #1 and #2.

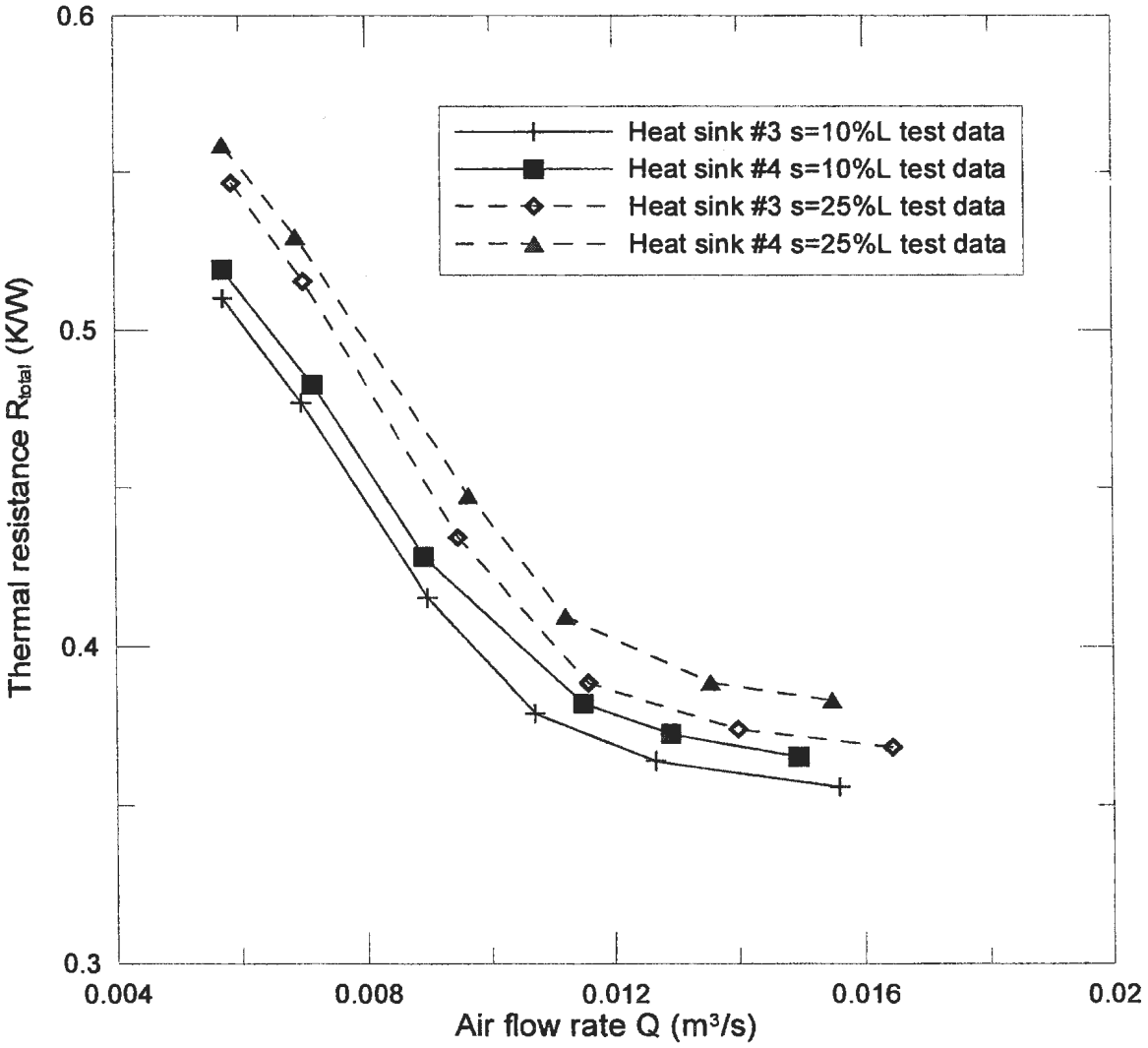

Figure 5.18 Effects of fin height on thermal resistance for Heat Sinks #3 and #4.

5.4 Thermal Resistance Analysis

The thermal resistances for heat flow from the electronic module surface to ambient are shown in Figure 5.19. Each of the thermal resistances will be examined to find how to effectively reduce the total thermal resistance. The thermal resistances from the electronic module surface to ambient are described below:

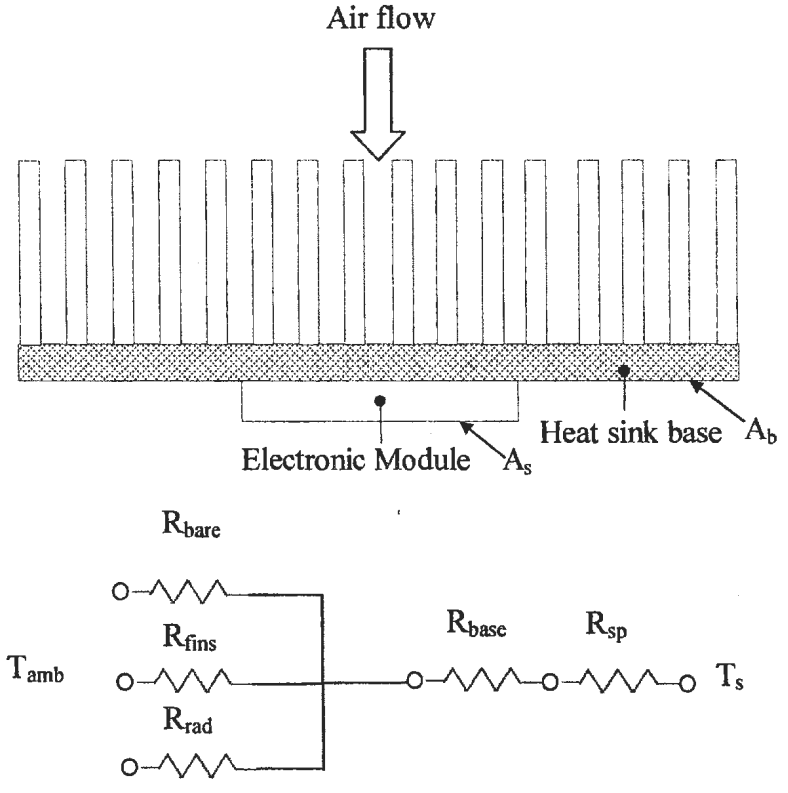

Figure 5.19 Thermal resistance network used to analyze.

R_{sp}: The spreading resistance is calculated using the Eq. (3.41) suggested by Yovanovich, Muzychka and Culham (1999). The values obtained for R_{sp} are from 0.0120 K/W to 0.0129 K/W. The spreading resistance accounts for 2% and 5% of the total thermal resistance at low and high flow rates, respectively.

R_{base}: The heat sink base is a 12.7 mm thick piece of aluminum, to which the fins are attached. A thermal conductivity of 200 W/mK is assumed for aluminum to calculate R_{base}. The conduction thermal resistance amounts for 1% to 2% of the total thermal resistance.

R_{eff}: R_{eff} is an effective resistance that accounts for heat flow paths by conduction, convection and radiation in the fins, and by convection and radiation from the exposed portion area of the base. The effective resistance is taken from results in Section 3.3:

$$\frac{1}{R_{eff}} = \frac{1}{R_{bare}} + \frac{1}{R_{fins}} + \frac{1}{R_{rad}} \tag{5-1}$$

The effective thermal resistance accounts for 97% of the total thermal resistance at low flow rates and 93% of the total thermal resistance at high flow rates. It, therefore, plays a decisive role in the thermal resistance circuit.

R_{fins}: The expression for R_{fins} is given by Eqs. (3.35-3.36). This resistance, which depends on the fin geometry and airflow rate, is the dominant part of the heat sink airside

thermal resistance; $1/R_{fins}$ accounts for over 90% of $1/R_{eff}$ for all four of the tested heat sinks.

R_{bare}: The thermal resistance of the exposed base area, R_{bare}, is given by Eq. (3.33). This resistance accounts for 4%, 3.5%, 6.5% and 6% of $1/R_{eff}$ for Heat Sinks #1, #2, #3 and #4, respectively.

R_{rad}: The radiation thermal resistance, R_{bare}, is given by Eq. (3.37). This resistance accounts for 2%, 3%, 2.5% and 4% of $1/R_{eff}$ for Heat Sinks #1, #2, #3 and #4, respectively.

The major thermal resistance in the thermal circuit is the fin surface heat resistance. This has lead to a need to understand the thermal and hydraulic behaviour of heat sinks. Research on impingement plate fin heat sink modelling was pursued to obtain tools for parametric design studies and optimization of heat sinks.

5.5 Summary

This chapter presented and discussed the experimental results of present research. The models were found to be in agreement with the experimental results within 11.5% RMS and ±20% maximum difference for pressure drop, and 11.1% RMS and ±20% maximum

difference for thermal resistance. The experimental uncertainties were found to be 19%/0.7% in pressure drop, and 2.6% in thermal resistance.

The analytic models developed are for the low Reynolds number laminar flow and heat transfer in the interfin channels of impingement air cooled plate fin heat sinks, since the practical operating range of this type heat sink would be laminar flow. The analytic models are suitable for heat sink parametric design studies and performance optimization.

Chapter 6

Summary and Conclusions

6.1 Summary of the Present Research

This thesis investigated impingement air cooled plate fin heat sinks for a variety of impingement inlet widths, fin spacings and fin heights. The analytic models developed are for the low Reynolds number laminar flow and heat transfer in the interfin channels of impingement plate fin heat sinks. The simple models are suitable for heat sink parametric design studies. The accuracy range of the analytical models was established by comparison with experimental measurements of four actual heat sinks and other obtainable experimental data.

The analytical pressure drop model prediction was within ±20% of experimentally measured values over a Reynolds number range $300<Re<1200$. At higher flow rates, the analytical model appears to underpredict the pressure drop.

The analytically predicted overall thermal resistance for an impinging flow heat sink was found to be within ±20% of experimental values for the range $300<Re<1200$. In general, he thermal resistance model tends to underpredict. The thermal resistance model includes the spreading resistance for a smaller module attached to a larger heat sink.

The pressure drop and thermal resistance models are implemented for laminar flow, since the expected practical operating range of this type of high performance heat sink would typically produce flows in the range of Re <1200. The models can be used as an estimation of pressure drop and thermal resistance for transition and turbulent flow.

Heat sink hydraulic load affects the flow rate and noise output of the fan used to cool it, therefore, heat sink design is crucial to control computer system pressure drop, thermal resistance and acoustical noise level. Fin designs should produce high heat conductance, while the pressure drop is maintained at a reasonable level.

Pressure drop increases with a decrease in impingement inlet width for the same flow rate. When the impingement inlet width goes beyond 25% of heat sink length, changes in pressure drop are relatively insignificant. Thermal resistance decreases when the impingement inlet width becomes smaller for the same flow rate. There exists an optimum impingement inlet width for system operation.

Pressure drop increases significantly with a decrease in fin spacing for the same volumetric flow rate. Thermal resistance increases significantly with an increase in fin spacing for the same volumetric flow rate. Both pressure drop and thermal resistance are very sensitive to changes in fin spacing. There exists an optimum fin spacing for system operation.

Increasing fin height decreases the heat sink pressure drop for the same flow rate. Increasing fin height increases slightly the heat sink thermal resistance for the same flow rate. There also exists an optimum fin height for system operation.

Heat transfer, pressure drop, pumping power, and noise level are usually of interest to find an optimum system operating point.

The fin efficiencies were almost the same for the heat sinks tested, therefore, fin efficiency did not pose a problem in the present study. The fin efficiency varies from a high value of 0.97 at low channel velocity (V_{ch2}) to a moderate value of 0.93 at the highest channel velocity.

6.2 Future Research

The accuracy of the impingement air cooled heat sink thermal resistance model could be improved by using experimental data to develop a correlation for channel Nusselt number:

$$Nu = f\left(L, H, D_h, \mathrm{Re}, s\right)$$

Furthermore, these analytical models will be used for fin geometry optimization of plate fin heat sinks for arbitrary conditions such as specification of cooling fan and available cooling space, using thermal resistance as the objective function.

References

Aranyosi, A., Bolle, L. M. R., and Buyse, H. A., 1997. "Compact Air-Cooled Heat Sinks for Power Packages," *IEEE Transc. On Comp. And Packag. Tech. -Part A*, Vol. 20, No. 4, pp. 442 – 451.

Ashiwake, N., Nakayama, W., Daikoku, T., and Kobayashi, F., 1983. "Forced Convective Heat Transfer from LSI Packages in an Air Cooled Wiring Card Array," *Heat Transfer in Electronic Equipment*, ASME HTD 28, pp. 35-42.

Azar, K., Mcleod, R. S., and Caron, R. E., 1992. "Narrow Channel Heat Sink for Cooling of High Powered Electronic Components," *Proceedings of the Eighth Annual IEEE Semiconductor Thermal Measurement and Management Symposium*, pp. 12-19.

Beavers, G. S., Sparrow, E. M., and Magnuson, R. A., 1970. "Experiments on Hydro - dynamically developing flow in Rectangular Ducts of Arbitrary Aspect Ratio," *Int. J. Heat Mass Transfer*, Vol. 13, pp. 689-702.

Bejan, A, 1995. *Convection Heat Transfer*, 2nd edition, John Wiley & Sons, NY.

Bejan, A, and Sciubba, E., 1992. "The optimal spacing of parallel plates cooled by forced convection," *Int. J. Heat Mass Transfer*, Vol. 35, No. 12, pp. 3259-3264.

Biber, C. R., 1997. "Pressure Drop and Heat Transfer in an Isothermal Channel with Impinging Flow," *IEEE Transc. On Comp. And Packag. Tech. – Part A*, Vol. 20, No. 4, pp. 458 – 462.

Biber, C. R., and Belady, C. L., 1997. "Pressure Drop Prediction for Heat Sinks: What is the Best Method?," *Advances in Electronic Packaging*, Vol 19-2, pp. 1829-1835.

Biber, C. R., and Fijol, S., 1999. "Fan plus Heat Sink Optimization – Mechanical and Thermal Design with Reality," *Proceedings of the International Systems Packaging Symposium*, pp. 285-289.

Biskeborn, R. G., Horvath, J. L., and Hultmark, E. B., 1984. "Integral Cap Heatsink Assembly for IBM 4381 Processor," *Proceedings International Electronics Packaging Conference*, pp. 468-474.

Cohen, A., and Iyengar, M., 2002. "Design and Optimization of air cooled heat sinks for sustainable development," *Proc. of Thermes*, pp. 5-21.

Copeland, D., 1995. "Manifold Microchannel Heat Sinks: Analysis and Optimization," *Thermal Science and Engineering*, Vol. 3, No. 1, pp. 7-12.

Copeland, D., 1995. "Manifold Microchannel Heat Sinks: Numerical Analysis," *ASME HTD. Vol. 319/EEP Vol. 15, "Cooling and Thermal Design of Electronic Systems, ASME* 1995, pp. 111-116.

Copeland, D., 2000. "Optimization of Parallel Plate Heat Sinks for Forced Convection," *Proc. Sixteenth Semi-Therm*, pp. 266-272.

Copeland, D., 2001. "Thermal Design Tradeoffs for Ducted Heat Sinks with Dedicated Fans," *Proc. of Int. Electronic Packaging Technical Conf.*, IPACK2001 – 15795.

Culham, J. R., and Muzychka, Y. S., 2001. "Optimization of Plate Fin Heat Sinks Using Entropy Generation Minimization," *IEEE Transc. On Comp. And Packag. Tech.*, Vol. 24, No. 2, pp. 159-165.

Curr, R. M., Sharma, D., and Tatchell, D. G., 1972. "Numerical Predictions of Some Three Dimensional Boundary Layers in Ducts," *Comp. Meth. in App. Mech. and Eng.*, pp. 143-158.

Goldberg, N., 1984. "Narrow Channel Forced Air Heat Sink," *IEEE Trans. On Components, Hybrids, and Manufacturing Technology*, Vol. CHMT-7, No. 1, pp. 154-159.

Goodman, J. S., 1997. "Microchannel Heat Exchangers – a review," *1993 Society of Photo-Optical Instrumentation Engineers*, Vol. 1, pp. 66-82.

Grimes, R., Davies, M., Punch, J., Dalton, T., and Cole, R., 2001. "Modeling Electronic Cooling Axial Fan Flows," *J. Electronic Packaging*, Vol. 123, pp. 112 – 119.

Hilbert, C., Sommerfeldt, S., Gupta, O., and Herrell, D. J., 1990, "High Performance Micro-Channel Air Cooling", *6th IEEE Semiconductor Thermal and Temperature Measurement Symposium*, Scottsdale Arizona, Feb. 6-8, 1990, pp. 108-113.

Holahan, M. F., Kang, S. S., Bar-Cohen, A. 1996. "A Flowstream Based Analytical Model for Design of Parallel Plate Heatsinks", August 1996, *ASME Proceedings of the 31st National Heat Transfer Conference*, HTD-Vol. 329, Volume 7, pp. 63-71.

Holman, J. P., 1994. *Experimental Methods for Engineers*, 6th edition, McGraw-Hill, NY.

Idelchik, I. E., 1993. *Handbook of Hydraulic Resistance*, 3rd edition, CRC Press.

Incropera, F. P., and Dewitt, D. P., 1996. *Fundamentals of Heat and Mass Transfer*, 4th Edition, John Wiley & Sons Inc.

Intel Corp., 2001. "Pentium 4 Processor Thermal Solution Functional Specifications," Section 4.5, p. 11, http://developer.intel.com/design/Pentium4/guides/.

Iwasaki, H., Sasaki, T., and Ishizuka, M., 1994. "Cooling Performance of Plate Fins for Multichip Modules," *1994 Intersociety Conference on Thermal Phenomena*, pp. 144-147.

Iyengar, M., and Cohen, A. B., 2001. "Design for Manufacturability of SISE Parallel Plate Forced Convection Heat Sinks," *IEEE Transc. On Comp. And Packag. Tech.*, Vol. 24, No. 2, pp. 150 – 158.

Kakac, S., Shah, R. K., and Aung, W., 1987. *Handbook of Single-Phase Convective Heat Transfer*, 2nd edition, Wiley & Sons, New York.

Kang, S. S., and Holahan, M. F., 1995. "Impingement Heat Sinks for Air Cooled High Power Electronic Modules, *ASME HTD-Vol. 303, 1995 National Heat Transfer Conference*-Vol 1, pp. 139-146.

Kays, W. M., and London, A. L., 1984. *Compact Heat Exchangers*, 3rd edition, McGraw Hill.

Knight, R. W., Goodling, J. S., and Gross, B. E., 1992. "Optimal Thermal Design of Air Cooled Forced Convection Finned Heat Sinks-Experimental Verification," *IEEE Intersociety Conference on Thermal Phenomena*, pp. 206-212.

Kondo, Y., Matsuhima, H., 1995. "Prediction Algorithm of Pressure Drop for Impingement Cooling of Heat Sinks with Longitudinal Fins," *Heat Transfer-Japanese Research*, Vol. 24, No. 4, pp. 315-327.

Kondo, Y., Matsuhima, H., and Komatsu, T., 1996. "Experimental Study of Impingement Cooling by Heat Sinks with Thin Longitudinal Fins for LSI Packages," *Heat Transfer-Japanese Research*, Vol. 25, No. 7, pp. 449-459.

Kondo, Y., Matsuhima, H., 1996. "Study of Impingement Cooling of Heat Sinks for LSI Packages with Longiudinal fins," *Heat Transfer-Japanese Research*, Vol. 25, No. 8, pp. 537-553.

Kondo, Y., Matsuhima, H., and Ohashi, S., 1997. "Optimization of Heat Sink Geometries for Impingement Air Cooling of LSI Packages," *Transactions of the Japan Society of Mechanical Engineers, Series B*, Vol. 63, No. 611, pp. 2484-2491.

Kondo, Y., Behnia, M., Nakayama, W., and Matsuhima, H., 1998. "Optimization of Finned Heat Sinks for Impingement Cooling of Electronic Packages," *Journal of Electronic Packaging*, Vol. 120, pp. 259-266.

Kondo, Y., Matsuhima, H., and Komatsu, T., 2000. "Optimization of Pin Fin Heat Sinks for Impingement Cooling of Electronic Packages," *Journal of Electronic Packaging*, Vol. 122, pp. 240-246.

Lee, S., Song, S., Au, V., and Moran, K. P., 1995. "Constriction / Spreading Resistance Model for Electronics Packaging," *Proc. ASME / JSME Thermal Engineering Conference*, Volume 4, pp. 199 – 206.

Lee, S., 1995. "Optimum Design and Selection of Heat Sinks," *IEEE Transc. On Comp. And Packag. Tech. – Part A*, Vol. 18, No. 4, pp. 812 – 817.

Linton, R. L., and Agonaefer, D., 1995. "Coarse and Detailed CFD Modeling of a Finned Heat Sink," *IEEE Transc. On Comp. And Packag. Tech. - Part A*, Vol. 18, No. 3, pp. 517 – 520.

Loh, C.K., Nelson, D. and Chou, D. J., 2002. "Optimization of Heat Sink Design and Fan Selection in Portable Electronics Environment," http://www.enertron-inc.com/PDF/Fan%20Heat%20Sink%20Optimization.pdf.

Mahalingham, M., and Andrew, J., 1987. "High Performance Air Cooling for Microelectronics," *Proceedings of the International Symposium on Cooling Technology for Electronic Equipment*, pp. 608-625.

Mansuria, M. S., and Kamath, V., 1994. "Design Optimization of a High Performance Heat Sink / Fan Assembly," *Proc. Of ASME, HTD*-Vol. 292, pp. 95-103.

Mikic, B. B., and Rohsenow, W. M., 1966. "Thermal Contact Resistance," *Heat Transfer Lab., Pept. 4542-41*, Massachusetts Inst. Of Technology, Cambridge, MA.

Moffat, R. J., 1988. "Describing the uncertainties in experimental results," *Experimental Thermal and Fluid Science*, pp.3-17.

Muzychka, Y. S., and Yovanovich, M.M., 1998. "Modelling Friction Factors in Non-Circular Ducts for Developing Laminar Flow," *AIAA 98-2492, 2nd AIAA Theoretical Fluid Mechanics Meetings, Albuquerque*, NM.

Muzychka, Y. S., 1999. *Analytical and Experimental Study of Fluid Friction and Heat Transfer in Low Reynolds Number Flow Heat Exchangers*, Ph. D. Thesis, University of Waterloo, Waterloo, ON.

Muzychka, Y. S., Culham, J.R., and Yovanovich, M.M., 2000. "Thermal Spreading Resistance of Eccentric Heat Sources on Rectangular Flux Channels," *Proc. of ASME HTD*, Vol. 4, pp. 347-355.

Muzychka, Y. S., and Yovanovich, M.M., 2001. "Forced Convection Heat Transfer in the Combined Entry Region of Non-Circular Ducts," *Presented at the 2001 International Mechanical Engineering Congress and Exposition*, New York, NY.

Muzychka, Y. S., and Yovanovich, M.M., 2002. "Laminar Flow Friction and Heat Transfer in Non-Circular Ducts and Channels: Part I-Hydrodynamic Problem," *Compact Heat Exchangers*, A Festschrift on the 60th Birthday of Ramesh K. Shah, Grenoble, France, August 24, pp. 123-130.

Muzychka, Y. S., and Yovanovich, M.M., 2002. "Laminar Flow Friction and Heat Transfer in Non-Circular Ducts and Channels: Part I-Thermal Problem," *Compact Heat Exchangers*, A Festschrift on the 60th Birthday of Ramesh K. Shah, Grenoble, France, August 24, pp. 131-139.

Nottage, H. B., 1945, in discussion of Gardner, K. A., 1945. "Efficiency of Extended Surface," *Transaction of the ASME*, Vol. 67, pp. 621-631.

Saini, M., and Webb, R. L., 2002. "Heat Rejection Limits of Plane Fin Heat Sinks used in Computer Cooling," *Proc. of I Therm.* pp. 1-8.

Saini, M., and Webb, R. L., 2002. "Validation of Models for Air Cooled Plane Fin Heat Sinks used in Computer Cooling," *Proc. of I Therm.* pp. 243-250.

Sasao, K., Honma, M., Nishihara, A., and Atarashi, T., 2001. "Numerical Analysis of Impinging Air Flow And Heat Transfer in Plate Fin Type Heat Sinks," *Journal of Electronic Packaging*, Vol. 123, pp. 315-318.

Sasao, K., Honma, M., Nishihara, A., and Atarashi, T., 1999. "Numerical Analysis of Impinging Air Flow And Heat Transfer in Plate Fin Type Heat Sinks," *Advances in Electronic Packaging*, Vol. 26-1, pp. 493-499.

Sasao, K., Honma, M., and Nishihara, A., 1997. "Numerical Analysis for Fluid Flow and Heat Transfer with Plate Fin Type Heat Sinks," *Advances in Electronic Packaging*, Vol. 19, pp. 1813-1819.

Sathe, S. B., Sammakia, B. G., Wong, A. C., and Mahaney, H. V., 1995. " A Numerical Study of A High Performance Air Cooled Impingement Heat Sink," *Proceedings 30th 1995 National Heat Transfer Conference*, Portland, OR, Aug. 1995, Vol. 1, pp.43-54.

Sathe, S. B., Kelkar, K. M., Karki, K. C., Tai, C., Lami, C., and Patankar, S. V., 1997. "Numerical Prediction of Flow and Heat Transfer in an Impingement Heat Sink," *Journal of Electronic Packaging*, Vol. 119, No. 1, pp. 58-63.

Schlichting, H. S., 1979. *Boundary-Layer Theory*, 7th edition, McGraw Hill, NY.

Shah, R. K., and London A. L., 1978. *Laminar Flow Forced Convection in Ducts*, Academic Press, NY.

Soodphakdee, D., Copeland, D. W., Take, K., Behnia, M., and Furukawa, Y., 2001. "Comparison of TISE and SITE Heat Sinks – A Numerical Study," *Proc. Of Int. Electronic Packaging Technical Conf.*, IPACK2001 – 15745.

Sparrow, E. M., Stryker, P. C., and Altemani, A. C., 1985. "Heat transfer and pressure drop in flow passages that are open along their lateral edges," *International Journal of Heat Mass Transfer*, Vol. 28, No. 4, pp.731-740.

Tanaka, T., Matsushima, H., Ueki, A., and Atarashi, T., 1997. "Numerical Simulation of Impingement Air Cooling from LSI Packages with Large Plate Fins by the Penalty Finite Element Method," *Journal of Electronic Packaging*, Vol. 119, No. 1, pp. 73-77.

Tasaka, M., Aihara, T, and Hayashi, C., 1995, "Air-Impingement Cooling and Pressure Loss Characteristics of Very Compact Heat Sinks," *ASME/JSME Thermal Engineering Conference*, Vol. 5, ASME, 1995, pp. 223-230.

Teertstra, P., Yovanovich, M.M, Culham, J. R., and Lemczyk, T., 1999. "Analytical Forced Convection Modeling of Plate Fin Heat Sinks," *Proc. Fifteenth Semi-Therm Symposium*, pp. 34-41.

Tuckerman, D. B. and Pease R. F. W., 1981 "High-Performance Heat Sinking for VLSI," *IEEE Electron Device Letters*, Vol.2, No. 5, pp. 126-129.

White, F. M., 1986. *Fluid Mechanics*, 2nd edition, McGraw Hill, NY.

Yovanovich, M.M., Culham, J. R., and Teertstra, P, 1998. "Analytical Modeling of Spreading Resistance in Flux Tubes, Half Spaces, and Compound Disks," *IEEE Transc. On Comp. And Packag. Tech.-Part A*, Vol. 21, No. 1, pp. 168 – 176.

Yovanovich, M.M., Muzychka, Y. S ., and Culham, J. R., 1999. "Spreading Resistance of Isoflux Rectangles and Strips on Compound Flux Channels," *Journal of Thermophysics and Heat Transfer*, Vol. 13, No. 4, pp. 495-500.

Appendix A

Experimental Data

A.1 Heat Sink #1

Table A.1.1 Experimental data for Heat Sink #1 (s=10%L).

Channel Velocity V_{ch2} (m/s)	Pressure Drop ΔP (Pa)	Thermal Resistance R (K/W)
1.440	10.17	0.3474
1.772	14.44	0.3108
2.059	19.61	0.2877
2.924	36.82	0.2362
3.303	46.46	0.2222
3.795	60.18	0.2118

Table A.1.2 Experimental data for Heat Sink #1 (s=25%L).

Channel Velocity V_{ch2} (m/s)	Pressure Drop ΔP (Pa)	Thermal Resistance R (K/W)
1.425	5.60	0.3516
1.832	7.49	0.3102
2.320	11.14	0.2665
2.799	14.99	0.2416
3.370	21.23	0.2233
3.863	27.63	0.2155

Table A.1.3 Experimental data for Heat Sink #1 (s=50%L).

Channel Velocity V_{ch2} (m/s)	Pressure Drop ΔP (Pa)	Thermal Resistance R (K/W)
1.383	4.81	0.3646
1.754	6.27	0.3238
2.317	10.26	0.2820
2.717	13.89	0.2620
3.287	18.82	0.2443
3.968	26.78	0.2355

Table A.1.4 Experimental data for Heat Sink #1 (s=75%L).

Channel Velocity V_{ch2} (m/s)	Pressure Drop ΔP (Pa)	Thermal Resistance R (K/W)
1.384	4.19	0.3895
1.818	5.45	0.3348
2.130	7.51	0.3133
2.662	10.58	0.2826
3.536	17.70	0.2538
4.125	24.38	0.2429

Table A.1.5 Experimental data for Heat Sink #1 (s=100%L).

Channel Velocity V_{ch2} (m/s)	Pressure Drop ΔP (Pa)	Thermal Resistance R (K/W)
1.419	3.51	0.4668
1.861	4.13	0.4092
2.315	5.81	0.3515
2.821	9.10	0.3097
3.255	11.66	0.2851
3.992	17.68	0.2730

A.2 Heat Sink #2

Table A.2.1 Experimental data for Heat Sink #2 (s=10%L).

Channel Velocity V_{ch2} (m/s)	Pressure Drop ΔP (Pa)	Thermal Resistance R (K/W)
0.746	7.42	0.4060
0.947	10.95	0.3724
1.256	17.68	0.3198
1.552	28.25	0.2896
1.782	37.70	0.2793
2.069	50.57	0.2712

Table A.2.2 Experimental data for Heat Sink #2 (s=25%L).

Channel Velocity V_{ch2} (m/s)	Pressure Drop ΔP (Pa)	Thermal Resistance R (K/W)
0.730	2.92	0.4110
0.937	3.95	0.3740
1.184	5.67	0.3350
1.510	8.80	0.3051
1.791	11.62	0.2909
2.046	15.40	0.2784

Table A.2.3 Experimental data for Heat Sink #2 (s=50%L).

Channel Velocity V_{ch2} (m/s)	Pressure Drop ΔP (Pa)	Thermal Resistance R (K/W)
0.778	2.21	0.4228
0.940	2.95	0.3927
1.280	4.64	0.3411
1.501	5.97	0.3243
1.698	7.56	0.3105
2.048	11.04	0.3021

Table A.2.4 Experimental data for Heat Sink #2 (s=75%L).

Channel Velocity V_{ch2} (m/s)	Pressure Drop ΔP (Pa)	Thermal Resistance R (K/W)
0.784	1.96	0.4444
0.925	2.61	0.4142
1.196	3.55	0.3671
1.528	5.60	0.3320
1.799	7.72	0.3196
2.116	10.26	0.3114

Table A.2.5 Experimental data for Heat Sink #2 (s=100%L).

Channel Velocity V_{ch2} (m/s)	Pressure Drop ΔP (Pa)	Thermal Resistance R (K/W)
0.749	1.73	0.5119
0.915	2.38	0.4758
1.209	2.96	0.4063
1.521	4.65	0.3638
1.847	6.10	0.3444
2.137	8.06	0.3409

A.3 Heat Sink #3

Table A.3.1 Experimental data for Heat Sink #3(s=10%L).

Channel Velocity V_{ch2} (m/s)	Pressure Drop ΔP (Pa)	Thermal Resistance R (K/W)
0.941	4.40	0.5165
1.143	6.39	0.4769
1.473	10.51	0.4123
1.758	13.56	0.3799
2.079	19.45	0.3639
2.560	29.85	0.3547

Table A.3.2 Experimental data for Heat Sink #3 (s=25%L).

Channel Velocity V_{ch2} (m/s)	Pressure Drop ΔP (Pa)	Thermal Resistance R (K/W)
0.964	2.50	0.5465
1.149	3.11	0.5055
1.554	4.39	0.4343
1.899	6.10	0.3946
2.295	8.31	0.3740
2.697	10.79	0.3603

Table A.3.3 Experimental data for Heat Sink #3 (s=50%L).

Channel Velocity V_{ch2} (m/s)	Pressure Drop ΔP (Pa)	Thermal Resistance R (K/W)
0.940	1.66	0.5773
1.140	2.10	0.5235
1.489	3.49	0.4515
1.822	4.74	0.4236
2.206	6.44	0.4110
2.570	8.70	0.3994

Table A.3.4 Experimental data for Heat Sink #3 (s=75%L).

Channel Velocity V_{ch2} (m/s)	Pressure Drop ΔP (Pa)	Thermal Resistance R (K/W)
0.962	1.55	0.6022
1.157	1.98	0.5488
1.511	2.76	0.4753
1.848	4.06	0.4459
2.250	5.38	0.4332
2.448	6.33	0.4257

Table A.3.5 Experimental data for Heat Sink #3 (s=100%L).

Channel Velocity V_{ch2} (m/s)	Pressure Drop ΔP (Pa)	Thermal Resistance R (K/W)
0.947	1.39	0.6493
1.177	1.51	0.5906
1.544	2.28	0.5127
1.839	3.29	0.4696
2.217	4.65	0.4558
2.561	6.09	0.4405

A.4 Heat Sink #4

Table A.4.1 Experimental data for Heat Sink #4 (s=10%L).

Channel Velocity V_{ch2} (m/s)	Pressure Drop ΔP (Pa)	Thermal Resistance R (K/W)
0.639	4.49	0.5222
0.797	6.84	0.4837
0.995	10.18	0.4283
1.283	16.65	0.3851
1.440	20.97	0.3725
1.645	28.47	0.3643

Table A.4.2 Experimental data for Heat Sink #4 (s=25%L).

Channel Velocity V_{ch2} (m/s)	Pressure Drop ΔP (Pa)	Thermal Resistance R (K/W)
0.639	1.45	0.5544
0.769	1.85	0.5235
1.076	3.14	0.4474
1.251	3.98	0.4105
1.512	5.52	0.3887
1.727	6.97	0.3801

Table A.4.3 Experimental data for Heat Sink #4 (s=50%L).

Channel Velocity V_{ch2} (m/s)	Pressure Drop ΔP (Pa)	Thermal Resistance R (K/W)
0.621	1.35	0.5718
0.768	1.61	0.5373
1.051	2.49	0.4629
1.247	3.21	0.4333
1.493	4.15	0.4193
1.742	4.99	0.4107

Table A.4.4 Experimental data for Heat Sink #4 (s=75%L).

Channel Velocity V_{ch2} (m/s)	Pressure Drop ΔP (Pa)	Thermal Resistance R (K/W)
0.650	1.30	0.5899
0.793	1.46	0.5519
1.041	1.75	0.4852
1.263	2.56	0.4516
1.565	3.88	0.4378
1.752	4.69	0.4315

Table A.4.5 Experimental data for Heat Sink #4 (s=100%L).

Channel Velocity V_{ch2} (m/s)	Pressure Drop ΔP (Pa)	Thermal Resistance R (K/W)
0.634	1.28	0.6244
0.784	1.36	0.5785
1.094	1.65	0.4915
1.293	2.31	0.4755
1.513	3.20	0.4637
1.717	4.21	0.4570

Appendix B

Zonal Model

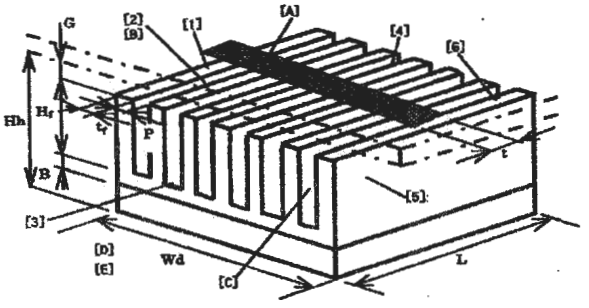

Thermal Resistance Correlations.

$R_{co} = (T_c - T_\infty)/W = 1/(A_f \cdot h_f)$.

- $A_f = A_1 + A_2 + A_3 + A_{4f} + A_{4pr} + A_5 + A_6$ (subscripts indicate areas in Fig. 1)
  - $A_1 = N_f \cdot t_f \cdot t$
  - $A_2 = 2 \cdot (N_f - 1) \cdot H_f \cdot t$
  - $A_3 = (N_f - 1) \cdot P \cdot L$
  - $A_{4f} = 2 \cdot (N_f - 1) \cdot H_f \cdot (L - t)$
  - $A_{4pr} = 2 \cdot (Wd \cdot B + N_f \cdot t_f \cdot H_f)$
  - $A_5 = 2 \cdot (H_f + B) \cdot L$
  - $A_6 = N_f \cdot t_f \cdot (L - t)$
- $h_f = \sum_i (A_i \cdot h_i)/A_f \quad (i = 1\text{–}6$, Fig. 1)
- $h_f = \{A_1 \cdot h_1 + (A_2 + A_{4f} - 2 \cdot H_f \cdot L) \cdot h_{24f} \cdot Fr_{24} + A_3 \cdot h_3 + A_{4pr} \cdot h_{4pr} + 2 \cdot H_f \cdot L \cdot (h_{24f} + h_5) \times Fr_{245} + 2 \cdot B \cdot L \cdot h_5 + A_6 \cdot h_6\}/A_f$
  - $h_1 = \lambda_{air}/t_f \cdot 0.6 \cdot \mathrm{Re}_1^{0.5}$
    $\mathrm{Re}_1 = U_1 \cdot t_f/\nu_{air}$
    $U_1 = Q/60/(t \cdot Wd)$
  - $h_{2m} = \lambda_{air}/(2 \cdot P) \times [7.55 + \{(0.024 \cdot \mathrm{Co}_2^{1.14})/(1 + 0.358 \cdot \mathrm{Co}_2^{0.64} \cdot \mathrm{Pr}^{0.17})\}] \quad (\mathrm{Re}_2 \leqq 3 \times 10^3)$
    - $h_{2m} = \{\lambda_{air}/(2 \cdot P)\} \cdot [1 + C_2'/\{H_f/(2 \cdot P)\}] \times 0.022 \cdot \mathrm{Re}_2^{0.8} \cdot \mathrm{Pr}^{0.5} \quad (\mathrm{Re}_2 > 3 \times 10^3)$
      $\mathrm{Co}_2 = (2 \cdot P) \cdot \mathrm{Re}_2 \cdot \mathrm{Pr}/H_f$
      $C_2' = 2$
      $\mathrm{Re}_2 = U_2 \cdot (2 \cdot P)/\nu_{air}$
      $U_2 = Q/60/(Wd \cdot t - N_f \cdot t_f \cdot t)$
  - $h_3 = \{\lambda_{air}/(2 \cdot t)\} \cdot J\{x_3/(2 \cdot t), (G + H_f)/(2 \cdot t)\} \cdot \mathrm{Re}_3^{m3} \cdot \mathrm{Pr}^{0.42} \quad (2 \leqq x_3/(2 \cdot t) \leqq 25,\ 2 \leqq (G + H_f)/(2 \cdot t) \leqq 10)$
    $\mathrm{Re}_3 = U_3 \cdot (2 \cdot t)/\nu_{air}$
    $U_3 = Q/60/\{Wd \cdot t - (N_f - 1) \cdot t_f\}$
    $J = 1.53/\{x_3/(2 \cdot t) + (G + H_f)/(2 \cdot t) + 1.39\}$
    $m3 = 0.695 - [x_3/(2 \cdot t) + \{(G + H_f)/(2 \cdot t)\}^{1.33} + 3.06]^{-1}$
  - $h_3 = \{\lambda_{air}/(2 \cdot t)\} \cdot 0.26 \cdot \mathrm{Re}_3^{0.59} \quad (x_3/(2 \cdot t) < 2,\ (G + H_f)/(2 \cdot t) < 2)$
  - $h_{4m} = \{\lambda_{air}/(2 \cdot P)\} \times [7.55 + \{0.024 \cdot \mathrm{Co}_4^{1.14}/(1 + 0.0358 \cdot \mathrm{Co}_4^{0.64} \cdot \mathrm{Pr}^{0.17})\}] \quad (\mathrm{Re}_4 \leqq 3 \times 10^3)$
  - $h_{4m} = \{\lambda_{air}/(2 \cdot P)\} \cdot [1 + C_4'/\{(L/2)/(2 \cdot P)\}] \times 0.022 \cdot \mathrm{Re}_4^{0.8} \cdot \mathrm{Pr}^{0.5} \quad (\mathrm{Re}_4 > 3 \times 10^3)$
  - $h_{4pr} = \{\lambda_{air}/(2 \cdot B)\} \cdot 0.1 \cdot (2)^{1/3} \times (3 \cdot U_4 \cdot B/\nu_{air})^{2/3}$
    $\mathrm{Co}_4 = (2 \cdot P) \cdot \mathrm{Re}_4 \cdot \mathrm{Pr}/(L/2)$
    $C_4' = 2$
    $\mathrm{Re}_4 = U_4 \cdot (2 \cdot P)/\nu_{air}$
    $U_4 = Q/60/[2 \cdot \{G \cdot Wd + (N_f - 1) \cdot P \cdot H_f\}]$
- $h_{24f} = (1 - e^{-\xi}) \cdot h_{24m}/\xi$
  - $h_{24m} = (A_2 \cdot h_{2m} + A_{4f} \cdot h_{4m})/(A_2 + A_{4f})$
    $\xi = (A_2 + A_{4f}) \cdot h_{24m}/(\rho_{air} \cdot Cp \cdot Q/60)$
- $h_5 = h_{5co} + h_{5ra}$
  - $h_{5co} = \{\lambda_{air}/(H_f + B)\} \cdot (4/3) \cdot C_5 \cdot \mathrm{Ra}^{1/4}$
  - $h_{5ra} = \varepsilon \cdot \sigma \cdot \{(273 + T_w) + (273 + T_\infty)\} \cdot \{(273 + T_w)^2 + (273 + T_\infty)^2\}$
    $C_5 = (3/4) \cdot \{\mathrm{Pr}/(2.4 + 4.9 \cdot \mathrm{Pr}^{1/2} + 5 \cdot \mathrm{Pr})\}$
    $\mathrm{Ra}_5 = \mathrm{Gr}_5 \cdot \mathrm{Pr}$
    $\mathrm{Gr}_5 = g \cdot \beta \cdot (T_w - T_\infty) \cdot (H_f + B)/\nu_{air}^2$
    $T_w = T_\infty + W \cdot R_{co}$
    $\beta = 1/(273 + T_\infty)$
    $\varepsilon = 0.2$
- $h_6 = h_{6co} + h_{6ra}$
  - $h_{6co} = (\lambda_{air}/t_f) \cdot (4/3) \cdot C_6 \cdot \mathrm{Ra}_6^{1/4}$
  - $h_{6ra} = h_{5ra}$
    $C_6 = C_5$
    $\mathrm{Ra}_6 = \mathrm{Gr}_6 \cdot \mathrm{Pr}$
    $\mathrm{Gr}_6 = g \cdot \beta \cdot (T_w - T_\infty) \cdot t_f^3/\nu_{air}^2$
- $Fr = Th/Ud$
  $Th = (e^{Ud} - e^{-Ud})/(e^{Ud} + e^{-Ud})$
  $Ud = \{h'/\lambda_{fin}/(t_f/2)\}^{0.5} \cdot H_f$

Pressure Drop Correlations.

$\Delta P = \sum_i \Delta Pi$ ($i = A\text{–}E$, Fig. 1).

- $\Delta P_A = \rho_{air} \cdot U_A^2/2 \cdot (1 + \zeta)$
  $U_A = Q/(60 \cdot Wd \cdot t)$
  $\zeta = 0.5$
- $\Delta P_B = \{\rho_{air}/(G + H_f)\} \cdot [(U_B^2/2) \cdot (t/2) \cdot \{(Kc_B + 1 - \sigma_B^2) + f_B/4 \cdot A_B/Ac_B\} + (1/2) \cdot \{(U_B + U_c)/2\}^2 \cdot H_f \cdot \xi + Uc^2 \cdot H_f \cdot \{1 - (2 \cdot H_f)/t\}]$
  $U_B = Q/(60 \cdot Ac_B)$
  $\mathrm{Re}_B = U_B \cdot (2 \cdot P)/\nu_{air}$
  $A_B = 2 \cdot H_f \cdot N_f \cdot t$
  $Ac_B = (Wd - N_f \cdot t_f) \cdot t$
  $P = (Wd - t_f)/(N_f - 1) - t_f$
  $\sigma_B = (Wd - N_f \cdot t_f)/Wd$
  $Kc_B = 0.4 \cdot (1 - \sigma_B^2) + \beta_B$

$$\beta_B = \begin{cases} 0.4 & (\mathrm{Re}_B < 2 \times 10^3) \\ 0.1 & (2 \times 10^3 \leqq \mathrm{Re}_B < 1 \times 10^4) \\ 0.06 & (1 \times 10^4 \leqq \mathrm{Re}_B < 2 \times 10^4) \\ 0 & (\mathrm{Re}_B \geqq 2 \times 10^4) \end{cases}$$

$$f_B = \begin{cases} 96/\mathrm{Re}_B & (\mathrm{Re}_B \leqq 2 \times 10^3) \\ 0.3164/\mathrm{Re}_B^{1/4} & (\mathrm{Re}_B > 2 \times 10^3) \end{cases}$$

- $\Delta Pc = \rho_{air} \cdot U_C^2/2 \cdot \{H_f/(H_f + G)\} \times f_C/4 \cdot Ac/Ac_C$
  $U_c = Q/\{60 \cdot 2 \cdot H_f \cdot (Wd - N_f \cdot t_f)\}$
  $\mathrm{Re}_C = U_C \cdot 4 \cdot H_f \cdot P/(2 \cdot H_f + P)/\nu_{air}$
  $A_C = (L - t) \cdot (N_f - 1) \cdot (H_f + P)$
  $Ac_C = (N_f - 1) \cdot H_f \cdot P$

$$f_C = \begin{cases} 96/\mathrm{Re}_C & (\mathrm{Re}_C \leqq 2 \times 10^3) \\ 0.3164/\mathrm{Re}_C^{1/4} & (\mathrm{Re}_C > 2 \times 10^3) \end{cases}$$

- $\Delta P_D = -\rho_{air} \cdot U_D^2/2 \cdot \{H_f/(H_f + G)\} \times (1 - \sigma_D^2 - Ke_D)$
  $U_D = U_C$
  $\mathrm{Re}_D = \mathrm{Re}_C$
  $\sigma_D = Ac_C/(H_f \cdot Wd)$
  $Ke_D = (1 - \sigma_D)^2 - \beta_D \cdot \sigma_D$

$$\beta_D = \begin{cases} 0.4 & (\mathrm{Re}_D < 2 \times 10^3) \\ 0.1 & (2 \times 10^3 \leqq \mathrm{Re}_D < 1 \times 10^4) \\ 0.06 & (1 \times 10^4 \leqq \mathrm{Re}_D < 2 \times 10^4) \\ 0 & (\mathrm{Re}_D \geqq 2 \times 10^4) \end{cases}$$

- $\Delta P_E = -\rho_{air} \cdot U_{E-1} \cdot (U_{E-0} - U_{E-1})$
  $U_{E-0} = Q/(60 \cdot 2 \cdot Wd \cdot H_f)$
  $U_{E-1} = Q/\{60 \cdot 2 \cdot Wd \cdot (G + H_f + B + B_0)\}$